Wind-Tunnel Investigation of a Full-Scale Canard-Configured General Aviation Airplane

Long P. Yip

NASA

Wind-Tunnel Investigation of a Full-Scale Canard-Configured General Aviation Airplane

Long P. Yip

*Langley Research Center
Hampton, Virginia*

Summary

An investigation was conducted in the Langley 30-by 60-Foot Tunnel to determine the aerodynamic characteristics of a powered, full-scale model of a general aviation airplane employing a canard. Although primary emphasis of the investigation was placed on evaluating the aerodynamic performance and the stability and control characteristics of the basic configuration, tests were also conducted to study the following effects of varying the basic configuration: effect of Reynolds number; effect of canard; effect of outboard wing leading-edge droop; effect of center-of-gravity location; effect of elevator trim; effect of landing gear; effect of lateral-directional controls; effect of power; effect of fixed transition; effect of water spray; effects of canard incidence, canard airfoil section, and canard position; and effects of winglets and upper winglet size. Additional aspects of the study were to determine the boundary-layer transition characteristics of the airfoil surfaces and the effect of fixing the boundary layer to be turbulent by means of a transition strip near the leading edge. The tests were conducted at Reynolds numbers from 0.60×10^6 to 2.25×10^6, based on the wing mean aerodynamic chord, at angles of attack from $-4.5°$ to $41.5°$, and at angles of sideslip from $-15°$ to $15°$.

The investigation indicated that employing the canard on this configuration was effective in providing increased stall departure resistance because the canard stalled before the wing stalled. Influence of the canard flow field on the wing decreased the inboard loading of the wing as the outboard loading of the wing increased. The increased outboard loading and spanwise flow development on the wing caused wing tip stall. The addition of a wing outboard leading-edge droop increased stall angle of attack and increased pitch stability at low to moderate angles of attack. From tests using a chemical sublimation technique, the natural boundary-layer transition was found to be at 55 percent chord of the canard. Fixing transition near the leading edge of the canard resulted in a significant reduction of lift due to flow separation near the trailing edge of the canard and, subsequently, a nose-down trim change and loss of elevator effectiveness. Variations in the canard airfoil showed that the canard airfoil-section characteristics can strongly affect the airplane stall and poststall characteristics. Moving the canard to a lower position had little effect on the static longitudinal and lateral-directional aerodynamic characteristics of this configuration. The lateral-directional stability was generally satisfactory, but the directional stability became weak at high angles of attack. Larger upper winglets provided significant increases in directional stability of the configuration.

Introduction

As part of the aeronautics program in the area of stall/spin research at the Langley Research Center, wind-tunnel tests were conducted to assess and document the aerodynamic characteristics of a canard configuration designed for general aviation use. In the mid-1970's, a new homebuilt airplane design, the VariEze (ref. 1), made a significant impact on the general aviation community because of its canard design and other advanced features. These advanced features included use of composite construction for lighter weight and for smoother surface contours to improve aerodynamic performance, use of winglets on the main wing for directional stability and, at the same time, for reducing drag, and use of a canard surface to increase pitch stability near stall so that the maximum trim angle of attack was less than wing stall angle of attack.

This report presents results of a full-scale research model of the VariEze design tested in the Langley 30-by 60-Foot Tunnel for which preliminary results were reported in reference 2. Test data obtained included measurements of aerodynamic forces and moments of the total configuration, isolated loads on the canard, pressure distributions, propeller torque-thrust loads, and flow visualization using tufts and sublimating chemicals. Also included in the study were effect of Reynolds number; effect of canard; effect of outboard wing leading-edge droop; effect of center-of-gravity location; effect of elevator trim; effect of landing gear; effect of lateral-directional controls; effect of power; effect of fixed transition; effect of water spray; effects of canard incidence, canard airfoil section, and canard position; and effects of winglets and upper winglet size. _____

Symbols

All longitudinal forces and moments are referred to the wind axis system, and all lateral-directional forces and moments are referred to the body axis system. Unless otherwise noted, total-airplane and canard moments are presented with respect to a center-of-gravity location at fuselage station 99, which was $0.71\bar{c}$ ahead of the leading edge of the wing mean aerodynamic chord $\bar{c}$, and at a vertical location on waterline 16. Also, unless otherwise noted, total-airplane and canard aerodynamic coefficients were reduced by using a wing reference area based on the trapezoidal planform of the wing projected to the fuselage centerline.

b wing span, 22.17 ft

b_w upper winglet span, ft

C_D total airplane drag coefficient, $\frac{\text{Drag}}{qS}$

$C_{D,c}$ canard drag coefficient, $\frac{\text{Canard balance drag}}{qS}$

$C_{D,f}$ skin-friction drag coefficient, $\frac{\text{Skin-friction drag}}{qS}$

C_L total-airplane lift coefficient, $\frac{\text{Lift}}{qS}$

$C_{L,c}$ canard lift coefficient based on wing reference area, $\frac{\text{Canard balance lift}}{qS}$ (C_{Lc} in computer-generated figures)

$C'_{L,c}$ canard lift coefficient based on canard planform area, $\frac{\text{Canard balance lift}}{qS'}$

$C_{L,o}$ lift coefficient at zero angle of attack

C_{L_α} lift-curve slope, per degree

C_l rolling-moment coefficient, $\frac{\text{Rolling moment}}{qSb}$

C_{l_β} rolling moment due to sideslip, per degree

C_m total-airplane pitching-moment coefficient, $\frac{\text{Pitching moment}}{qS\bar{c}}$

$C_{m,c}$ canard pitching-moment coefficient relative to airplane c.g., $\frac{\text{Canard balance pitching moment}}{qS\bar{c}}$

$C_{m,o}$ pitching-moment coefficient at zero angle of attack

C_{m_α} slope of pitching-moment curve with respect to angle of attack, per degree

C_n yawing-moment coefficient, $\frac{\text{Yawing moment}}{qSb}$

C_{n_β} yawing moment due to sideslip, per degree

C_p pressure coefficient, $\frac{p-p_\infty}{q}$

C_T thrust coefficient, $\frac{\text{Thrust}}{qS}$

C_Y total-airplane side-force coefficient, $\frac{\text{Side force}}{qS}$

C_{Y_β} side force due to sideslip, per degree

c local chord, ft

$\bar{c}$ reference wing mean aerodynamic chord, 2.58 ft

c_n section normal-force coefficient obtained from integration of pressure measurements

i_c incidence angle of canard relative to WL, positive trailing edge down, deg

L/D lift-drag ratio

p local static pressure, lb/ft^2

p_∞ free-stream static pressure, lb/ft^2

q free-stream dynamic pressure, lb/ft^2

R Reynolds number based on $\bar{c}$

S reference wing area, 53.60 ft^2

S' exposed canard area, ft^2

V free-stream velocity, ft/sec

V/nd propeller advance ratio, $V/$(Propeller rotation speed $\times$ Propeller diameter)

x chordwise distance from leading edge, ft

$(x/c)_T$ boundary-layer transition location

y spanwise distance from plane of symmetry, ft

y' distance along winglet span, ft

α angle of attack relative to WL, deg

β angle of sideslip, deg

ΔC_D incremental drag coefficient

ΔC_l incremental rolling-moment coefficient

ΔC_n incremental yawing-moment coefficient

ΔC_Y incremental side-force coefficient

δ_a aileron deflection based on a setting of equal and opposite deflection, positive when right aileron is down, deg

δ_e elevator deflection, positive trailing edge down, deg

δ_r rudder deflection based on setting one rudder in an outward deflection for directional control, positive left rudder deflected, deg

η propeller efficiency

Subscripts:

c canard

l lower surface

max maximum

u upper surface

w winglet

Abbreviations:

BL butt line, in.

c.g. center of gravity

FS fuselage station, in.

L.E. leading edge

WL waterline, in.

Model Description and Test Apparatus

The configuration used in the study was a powered full-scale model of an airplane intended for the home-built market (ref. 1). The model was constructed of

foam covered with fiberglass and epoxy. Body putty was applied to the wing and canard to attain the desired airfoil-section contours. Geometric characteristics of the model are given in table I and shown in figure 1. A total of 322 pressure orifices were installed in the wing, canard, and winglet. The pressure orifice locations are given in table II. Photographs showing the model installed in the Langley 30- by 60-Foot Tunnel are presented in figures 2 and 3.

The basic model configuration is defined as follows:

> Outboard wing leading-edge
>   droop off
> Center of gravity located at FS 99
> Nose gear removed
> Main wheel pants off
> Propeller removed, spinner on
> Inlet faired, exit area sealed
> High canard position with
> $i_c = 0°$
> Canard with GU 25-5(11)8
>   airfoil section (ref. 3)
> Small upper and lower winglets

Variations to the basic configuration include the following:

> Adding a discontinuous outboard wing
>   leading-edge droop
> Removing canard
> Moving center of gravity to forward and
>   aft locations
> Varying landing-gear arrangements
> Adding power effects
> Varying canard incidence
> Changing canard airfoil section
> Changing from high canard position to
>   low canard position
> Removing winglets
> Increasing upper winglet size

Range of control settings tested were $\delta_e = -20°$ to $24°$, $\delta_a = -20°$ to $20°$, and $\delta_r = -40°$ to $40°$. Pitch control was obtained with elevator deflections at a fixed canard incidence setting. Canard incidences of $-4°$, $0°$, and $4°$ were tested. A low canard position (fig. 1(a)) was also tested because of interest in improving pilot visibility. Since earlier studies (refs. 4 and 5) indicated that the droop was effective in delaying tip stall, tests were conducted with the leading-edge droop installed. (See fig. 1(d).) Upper winglets with 50 percent more area (figs. 1(b) and 1(c)) were also tested.

Powered tests were conducted with a 200-HP electric motor to turn a fixed-pitch, 4.83-ft-diameter, two-bladed propeller. The propeller is a Hendrickson H58G64 propeller designed for climb. The majority of the tests was conducted with the propeller removed, and

the engine inlet and exit areas were sealed and faired for a no-flow-through condition. No attempt was made to simulate the internal duct flow due to a reciprocating internal combustion engine.

Overall aerodynamic forces and moments acting on the model were measured on the external scale balance system of the Langley 30- by 60-Foot Tunnel. (See ref. 6.) In addition, the model was instrumented with internal strain-gauge balances to measure isolated loads on the canard and the propeller and with scannivalve transducers to measure the surface pressures. Small cotton tufts were used in conjunction with fluorescent photography to provide flow visualization of the model. (See ref. 7.) Tufts were used in flow visualization studies to examine areas of flow separation and other surface flow conditions at angles of attack up to complete wing stall. Initially, tufts were installed on the upper surfaces of the wing, upper winglet, and canard. However, the tufts on the canard resulted in premature transition of the boundary layer; thus, there was a large decrement in the lift performance of the canard. Therefore, canard tufts were not installed in later tests because of their adverse effect on the flow patterns of the canard. A chemical sublimation technique (ref. 8) was used to provide information on the extent of laminar flow on the canard, wing, and winglet.

Test Conditions and Corrections

Test conditions included a range of α from $-4.5°$ to $41.5°$ and a range of β from $-15°$ to $15°$. Aerodynamic data were obtained at free-stream tunnel velocities of 26, 68, and 94 mph that correspond to Reynolds numbers based on $\bar{c}$ of 0.60×10^6, 1.60×10^6, and 2.25×10^6, respectively. Most of the tests, however, were conducted at a nominal free-stream velocity of 68 mph.

The model was tested upright and inverted to evaluate the flow angularity and strut tare corrections. An extensive wind-tunnel calibration was made prior to model installation to determine the horizontal buoyancy correction, and flow-field surveys ahead of the model were made in the manner of reference 9 to determine the flow-blockage correction. These corrections have been applied to the data. Jet-boundary corrections were made in accordance with the method of reference 10. Since an electric motor, rather than a reciprocating engine, was used to power the model and no attempt was made to simulate the internal duct flow, no corrections were made for cooling drag due to a reciprocating engine.

Presentation of Results

The test results are presented in figures 4 to 44, which are grouped in the order of discussion as follows:

Discussion of Results

Effect of Reynolds Number

In order to assess the sensitivity of the configuration to Reynolds number effects, data were compared at Reynolds numbers based on $\bar{c}$ of 0.60×10^6, 1.60×10^6, and 2.25×10^6. These data are shown in figure 4. The lift and pitching-moment characteristics of the basic configuration and, also, the isolated lift characteristics of the canard obtained from the canard balance indicate that at the low Reynolds number this configuration exhibited significantly different lift and pitching-moment characteristics from those at higher Reynolds numbers.

The canard data for low Reynolds number exhibited significantly lower lift than the lift obtained at the higher Reynolds numbers and were a primary factor in the lower lift level of the total airplane. Also, lift-curve slope of the canard for the low value of R was lower for angles of attack less than 6° and increased with increasing angle of attack. The ineffectiveness of the canard to generate lift is probably caused by laminar separation of the boundary layer due to the effect of low Reynolds number, whereas the increase in the lift-curve slope is probably caused by turbulent reattachment at the higher angles of attack. Since the canard is located well ahead of the airplane center of gravity, changes in the lift and lift-curve slope of the canard significantly affected $C_{m,o}$ and C_{m_α} of the total airplane, as shown in figure 4. At the low Reynolds number, the loss in canard lift shifted $C_{m,o}$ to a more negative value, whereas near $\alpha = 6°$, the increased canard lift-curve slope caused C_{m_α} to be unstable. Although this Reynolds number is low compared to flight conditions, the data are presented here to illustrate the sensitivity of total-airplane lift and pitching moments of canard configurations to subcritical Reynolds number.

The data at mid and high Reynolds numbers indicated much better agreement on the lift and pitching-moment curves. The data at mid Reynolds number are representative of landing approach speed of the airplane at higher angles of attack. The remaining analysis in this report is based on the data obtained at this mid Reynolds number.

Pressure Distributions

Presented in figure 5 are the chordwise pressure distributions and section normal-force coefficients of the

wing, upper winglet, and canard. The data of figure 5 are presented graphically with the pressure distributions on the configuration so that they could be related to the spanwise distribution of section normal-force coefficients. The data are presented for an angle-of-attack range from $-2.5°$ to $31.5°$ for the basic configuration.

The data of figure 5 indicate that strong favorable pressure gradients, conducive to boundary-layer stability for laminar flow, were obtained on the canard upper surface from the leading edge to about 50 percent chord at angles of attack up to about 10°. Favorable pressure gradients were also found on the wing upper surface at angles of attack less than 5.5° and on the upper surface of the upper winglet throughout the angle-of-attack range presented.

The chordwise pressure distributions were integrated to obtain section normal-force coefficients for the wing, upper winglet, and canard. The data of figure 5 indicate that the canard operates at a higher section loading than does the wing at angles of attack up to 13.5°. The higher canard section loading promotes canard stall before wing stall; thus, airplane stall resistance is provided.

The section normal-force coefficients c_n of the wing and upper winglet are shown in figure 6 for the canard-on and canard-off conditions. Figure 6 illustrates the influence of the canard downwash/upwash flow field on the wing and winglet. On the inboard part of the wing, lower levels of c_n were caused by the downwash of the canard, while higher levels of c_n on the outboard part of the wing were caused by the upwash outboard of the canard tip. From a design point of view, the effect of downwash on longitudinal stability and the effect of upwash on wing tip stall must be considered. The impact of the canard downwash/upwash flow field on the aerodynamics of this configuration is discussed in later sections.

Effect of Outboard Leading-Edge Droop

Based on the design philosophy of references 4 and 5 on wing leading-edge droop design, an outboard wing leading-edge droop was installed on the VariEze airplane to increase stall resistance and reduce the wing rock tendency of the configuration. As reported in references 4 and 5, the outboard leading-edge droop provided attached flow near the wing tip to a higher angle of attack and reduced the autorotative moments in the poststall region. Wing tip stall was more prevalent for the present configuration because of higher wing loading outboard, due to the canard, and from the wing sweep effect. Wing tuft patterns of the droop-off and droop-on configurations are shown in figures 7 and 8, respectively. Without leading-edge droop, the tuft patterns on the wing show the spread of spanwise flow near the trailing edge of the wing and the development of tip

stall. The tuft patterns of the wing with the L.E. droop on show that the leading-edge droop reduced spanwise flow, kept the flow attached at the wing tip region, and thereby delayed wing tip stall to a higher angle of attack. The significance of these flow patterns is indicated by the lift and pitching-moment data of figure 9, which indicate that the leading-edge droop increased $C_{L,max}$ and increased the pitch stability near $\alpha = 4°$ which made the pitching-moment curve more linear in the mid angle-of-attack range. The effect of leading-edge droop on elevator deflection required for trim is shown in figure 10 for forward, mid, and aft center-of-gravity locations. The leading-edge droop provided a larger stall margin between the maximum trimmed C_L and $C_{L,max}$.

The effect of leading-edge droop on the trimmed drag characteristics of the configuration is shown in figure 11. A drag penalty, $\Delta C_D = 0.0040$, at cruise condition of $C_L = 0.25$ was incurred due to the addition of the leading-edge droop. This drag penalty probably would not be as large on an airplane with leading-edge droop integrated into the construction of the wing because the test model leading-edge droop was made removable and was not fastened to the wing surface as smoothly as the original construction surface. At higher lift coefficients corresponding to climb, there was no significant drag penalty associated with the leading-edge droop modification.

The lateral-directional stability derivatives C_{Y_β}, C_{n_β}, and C_{l_β} were obtained from tests conducted at $\beta = -5°$ and 5° and are shown in figure 12. The addition of the leading-edge droop increased directional stability C_{n_β} at angles of attack up to wing stall. Rolling moments due to sideslip increased with angle of attack typical of configurations with wing sweep. The addition of the droop reduced the magnitude of dihedral effect $-C_{l_\beta}$ of the configuration for angles of attack up to about 20°. At low angles of attack near 2°, this reduction in dihedral effect made the configuration marginally stable in C_{l_β}. However, at higher angles of attack, the reduction in dihedral effect may be beneficial in reducing the amount of lateral control required to trim the configuration in sideslip, such as in a crosswind landing situation.

Lift and Pitching-Moment Characteristics

Canard configurations require that the center of gravity be located between the canard center of lift and wing center of lift for both positive stability and control. If the canard stalls before the wing stalls, longitudinal stability and airplane stall resistance are increased. However, as pointed out in reference 11, many factors must be considered in order to make the configuration stable and controllable as well as stall resistant. These factors, including airfoil-section characteristics, power

effects, and center-of-gravity location, are discussed in later sections of this report.

Figure 13 presents data for the canard-on and canard-off conditions and incremental data obtained by subtracting canard balance data from the total-airplane data. Analysis of the data indicates that the wing lift is influenced by the presence of the canard because of its downwash effect. This downwash effect caused the wing to experience less lift than would be predicted by adding the interference-free contributions of wing and canard individually. A beneficial effect of canard downwash is that it delays the stall of the wing; thus, the angle of attack margin between canard stall and wing stall is increased. The data of figure 13(a) indicate that canard stall occurred at about $\alpha = 13°$, whereas wing stall occurred at about 21°. With the canard off, the wing stall occurred at about 19° which is 2° less than with the canard on.

Examination of the pitching-moment data of figure 13(b) showed three significant changes in pitch stability throughout the test angle-of-attack range. The first change occurred at about $\alpha = 4°$ where there was a decrease in the lift-curve slope of the wing. This decrease in C_{L_α} caused a reduction in total-airplane pitch stability since the aerodynamic center of the wing is located aft of the center of gravity. The decrease in C_{L_α} of the wing is caused by the development of spanwise flow due to wing sweep. This development of spanwise flow is shown by the tuft photographs of figure 7. This decrease in pitch stability at $\alpha = 4°$ can also be found in the canard-off configuration. The second change in pitch stability occurred at about $\alpha = 13°$ where canard stall resulted in a nose-down pitching-moment increment to provide a large increase in pitch stability. This increase in pitch stability would require more elevator deflection to trim the configuration. The third change in pitch stability occurred at about $\alpha = 21°$ where wing stall occurred. Because the wing is located aft of the center of gravity, a destabilizing pitching-moment increment occurred when the wing stalled. This pitch-up tendency would not normally be encountered in flight as long as the canard provides enough stall resistance to limit the airplane angle of attack to that below the wing stall angle of attack. Although the canard does provide beneficial increment to stall resistance of this configuration, several factors, including elevator control authority, center-of-gravity location, airfoil section, power effects, and surface roughness could adversely affect the configuration stability and cause the configuration to trim at angles of attack higher than wing stall. Effects of elevator control and center-of-gravity location are examined in the following discussion, and the effects of airfoil section, power, and surface roughness are discussed in a subsequent section.

The effect of canard elevator deflection on lift and pitching-moment coefficients for three center-of-gravity locations is presented in figure 14 for the basic configuration with the L.E. droop on. As expected, the lift data of figure 14 indicate that increasing the elevator deflection in the positive direction (trailing-edge down) increases the overall lift. Thus, this canard configuration does provide a positive increment in trimmed lift as opposed to a conventional tail arrangement which would normally provide a decrement in trimmed lift. However, analysis of the canard balance lift data indicates that the canard lift is not directly additive to the total lift because of the increasing downwash due to elevator deflection of the canard on the wing. This increasing downwash caused a destabilizing effect on the total airplane pitching moment at angles of attack below canard stall.

Since changes in the center-of-gravity location would not alter the lift curves of figure 14(a), only pitching-moment data are presented in figures 14(b) and 14(c) for the forward and aft center-of-gravity locations. The data of figure 14 indicate that canard stall reduced the effectiveness of the elevator at high angles of attack; thus, the maximum trim angle of attack was limited. The maximum trim angle of attack for the aft center-of-gravity configuration was obtained with an elevator setting of $\delta_e = 15°$. A plot of elevator deflection required for trim, shown in figure 15, indicates that increasing elevator deflection beyond 15° actually trimmed the configuration at slightly lower values of lift coefficients. In all test conditions, the trimmed lift coefficient was less than the maximum lift for the configuration; thus, stall resistance to the configuration was provided.

Drag Characteristics

The effect of elevator deflection on drag characteristics of the basic configuration with L.E. droop on is shown in figure 16. The drag of this canard configuration increases with increasing elevator deflection for a given lift coefficient which indicates a drag penalty associated with trim. A trimmed lift-drag polar for a mid center-of-gravity location is indicated by the dashed line of figure 16. Values of the trimmed lift-drag ratio are plotted in figure 17, and a maximum value of 12.6 was obtained for this configuration. Incremental values of drag for the nose gear, main landing gear, and wheel pants of the main gear are presented in figure 18. As shown in figure 19, these increments were incorporated into the drag curve of the basic configuration to obtain new values of trimmed lift-drag values. The maximum lift-drag ratio of this configuration was improved by moving the center of gravity aft by $0.10\bar{c}$ $((L/D)_{max} = 13.1)$, by adding wheel pants $((L/D)_{max} = 14.1)$, by removing leading-edge droop $((L/D)_{max} = 15.4)$, and by removing the main landing gear $((L/D)_{max} = 17.1)$.

Lateral-Directional Characteristics

The lateral-directional stability derivatives C_{Y_β}, C_{n_β}, and C_{l_β} were obtained from tests conducted at $\beta = -5°$ and $5°$ and are shown in figure 20 for the basic configuration with L.E. droop on. This configuration was directionally stable at low angles of attack; however, the directional stability decreased to zero at about $\alpha = 19°$. This configuration exhibited stable dihedral effect that increased with angle of attack up to wing stall. The effect of deflecting the elevator on lateral-directional stability of this configuration is also shown in figure 20. Over the test angle-of-attack range up to the stall, deflecting the elevator caused the directional stability to decrease and the lateral stability to become more stable. The decrease in directional stability is probably due to the increase in canard drag ahead of the center of gravity. The increase in the dihedral effect is probably due to the asymmetric canard downwash on the wing with sideslip angle, which causes an incremental increase in rolling-moment contribution due to sideslip.

The aileron and rudder control authorities of the basic configuration are shown in figures 21 and 22, respectively. Both positive and negative control inputs were tested; results were averaged to reduce effects of model asymmetries and tunnel flow angularity; data are presented for a right roll input ($\delta_a < 0$) and right yaw input ($\delta_r < 0$). The data of these figures indicate that both aileron and rudder control authorities decreased at higher angles of attack. Also, aileron deflections produced favorable yawing moments in the normal operational angle-of-attack range ($\alpha = 2°$ to $18°$).

Power Effects

Propeller thrust and torque were measured by means of a balance mounted between the motor and the propeller. The data shown in figure 23 indicate that a maximum propeller efficiency of 0.75 was obtained. This value of propeller efficiency is relatively low compared with that for more optimized arrangements. The propeller used in the tests was of low pitch for maximum climb performance and was therefore not properly matched for cruise conditions. The low value of effectiveness in the tests is consistent with that obtained in reference 12 for low propeller blade angle settings. The low value of efficiency may also be associated to some degree with the pusher arrangement at the rear of the fuselage. Improved shaping of the aft fuselage and engine nacelle and careful matching of the propeller geometry with the fuselage flow field could provide increased propeller efficiency.

Effects of propeller thrust on the longitudinal aerodynamic characteristics of the configuration are shown in figure 24. The data of figure 24 indicate that for most conditions a nose-down increment of pitching moment is associated with increasing power setting. Although the thrust line of the propeller is slightly above the center of gravity, the moments produced by this offset do not account for the nose-down increment of pitching moment due to power. This increment probably comes from the power-induced flow cleanup of the wing trailing edge and from increased suction pressures acting on the base area of the cowling. The data of figure 24 also indicate that there is a slight increase in pitch stability due to the propeller except for $C_T = 0.11$ at $\alpha < 6°$. This stabilizing effect is probably due to the rotating propeller disk developing a propeller normal force (ref. 11), which on a pusher configuration produces a nose-down moment because the propeller is located behind the center of gravity. Conversely, a propeller located ahead of the center of gravity would have a destabilizing effect, especially if the propeller slipstream immerses the canard and provides increased lift.

Boundary-Layer Transition Study

Several pilots have reported that while flying their homebuilt version of this configuration in rain conditions, the airplane exhibited a pitch trim change. This pitch trim characteristic seemed to indicate an effect caused by changes in the boundary-layer properties of the canard or wing. In order to investigate the boundary-layer characteristics, tests were conducted to determine the extent to which laminar flow existed on the configuration and to determine the effect of a loss in laminar flow which might occur when the airfoil surfaces become contaminated by insect or rain-drop accumulations on the leading edges.

A chemical sublimation technique (ref. 8) was used to locate the boundary-layer transition on the canard, wing, and winglets. The technique involved spraying a coat of chemical film on the model surface, starting the wind-tunnel airflow, and observing the sublimating process of the chemicals. Since the surface chemicals sublimate at a higher rate in a turbulent boundary layer than in a laminar boundary layer, a definite pattern of chemical residue is observed on the wing which denotes transition. Tests were conducted on the upper surface only at an angle of attack of 1.5° and at a Reynolds number based on $\bar{c}$ of 1.60×10^6. Test results, shown by the photographs of figure 25, indicate that transition was located at 55 percent chord of the canard, 65 percent chord of the wing, and 60 percent chord of the winglet. These transition results were confirmed by flight tests as reported in reference 8. The large amount of laminar flow on the configuration can be attributed to the composite construction of the aircraft which allowed for smooth airfoil contour.

In order to simulate conditions in which laminar flow would be lost, such as in rain conditions or with insect

accumulations, a transition strip of No. 60 carborundum grit was applied at the 5-percent-chord location of the canard and wing in accordance with the method of reference 13. Results of the transition grit tests are shown in figure 26 for test conditions of transition free (no grit applied), transition grit at 5 percent chord of the canard, and transition grit at 5 percent chord of both the canard and wing. The data of figure 26 indicate that fixed transition at 5 percent chord of the canard caused a decrease in the lift-curve slope of the canard by about 30 percent. This decrease in the canard lift-curve slope resulted in an increase in pitch stability and a large nose-down pitching-moment increment at the higher angles of attack. With transition grit on the wing and canard, the data of figure 26 indicate that the configuration exhibited a slight increase in nose-up pitching moments at angles of attack of 4° or below. This effect of fixed transition at low angles of attack is probably due to the nature of the boundary layer on the wing which is indicated by pressure distributions as highly laminar at low angles of attack but quickly become turbulent near the leading edge at angles of attack above 4°. Thus, fixed transition would only affect the laminar flow nature of the wing at low angles of attack.

Presented in figure 27 are canard balance lift-drag polars. The data of figure 27 indicate significant drag increases due to fixed transition on the canard. An examination of the chordwise pressure distribution on the canard, shown in figure 28, indicates that the loss of lift due to a fixed transition is a result of trailing-edge separation which was probably caused by the thickened turbulent boundary layer having to overcome a sharp pressure recovery near the trailing edge. This separated flow condition also resulted in a decreased elevator control authority as indicated by the data of figure 29. This decreased control authority could become significant when flying in rain where loss of laminar flow could require sudden changes in elevator settings to trim the pitching-moment changes encountered.

In other tests without transition grit, water spray from a horizontal boom fixture in the wind tunnel was used to study effects of surface water on transition. The water-spray boom, shown schematically in figure 30, was located approximately 4 canard chord lengths in front of the canard and covered only one side. The spray rate was approximately 1 gal/min. Results from water-spray tests of the canard, shown in figure 31, are similar to results of fixed transition on the canard, that is, a reduction in the canard lift-curve slope and an increase in drag. It should be noted that only about one-half of the canard was immersed in water spray for these tests. If the canard were fully immersed in water spray, the data would be in closer agreement with the data obtained with fixed transition.

Effect of Canard Incidence

In order to obtain an inherently stall-proof airplane that employs a canard, it is important that the canard incidence be set so that it will stall at an angle of attack below the wing stall angle of attack. Canard incidences of 0°, −4°, and 4° were tested to determine the effect of canard incidence on the longitudinal aerodynamic characteristics of this configuration. The data from these tests, presented in figure 32, show the expected changes in $C_{m,o}$ and stall angle of attack where positive incidence produced increased $C_{m,o}$ and reduced angle of attack for canard stall. At an incidence angle of −4°, the canard stall angle occurred at about 18° which is below the wing stall angle of 23°. At a canard incidence angle of 4°, the pitching-moment curve was more linear in the mid angle-of-attack range ($\alpha = 4°$ to 10°). This effect was probably caused by the combination of an increased downwash on the wing which delayed the angle of attack where the pitch stability changed near $\alpha = 4°$ and an increase in pitch stability caused by early canard stall. Elevator settings required to trim the configuration with canard incidence settings of −4°, 0°, and 4° are presented in figure 33 through the trim-lift-coefficient range. The data of figure 33 indicate that the effectiveness of the elevator with canard incidence at $i_c = 4°$ decreased and was probably caused by the elevator operating in a separated flow region above $\alpha = 8°$. (See the data for C_{Lc} of fig. 32.)

Effect of Canard Airfoil Section

The canard is an important factor in the configuration's trim capability and stall characteristics. To determine the effects of the canard airfoil section on the configuration, an NACA 0012 airfoil section was tested on the configuration. The NACA 0012 section is typical of airfoil sections used on conventional general aviation airplane horizontal tails. The basic canard airfoil section, GU 25-5(11)8, was designed for high lift and low drag at low speeds. (See ref. 3.) This airfoil was relatively thick and highly cambered, and a comparison between it and the NACA 0012 airfoil is shown in figure 34. As discussed earlier, the basic airfoil section is characterized by large amounts of laminar flow. Test data comparing the effect of canard airfoil on the total-airplane lift and pitching moments are shown in figure 35. The data of figure 35 show the change in $C_{m,o}$ of the total airplane which is primarily due to the change in $C_{L,o}$ of the canard with uncambered NACA 0012 airfoil section. Changing to the NACA 0012 canard also lowers $C_{L,max}$. The poststall lift characteristics, which are significant to the total-airplane pitch stability, are examined in more detail in figure 36. A comparison of the canard lift obtained from the canard balance is shown in figure 36 based on the canard area. The data

of figure 36 indicate that the GU 25-5(11)8 airfoil section had significantly higher maximum lift coefficient at the test Reynolds number of 1.60×10^6. In addition, the GU 25-5(11)8 airfoil exhibited a relatively flat-top lift curve with an abrupt decrease in lift at about $\alpha = 25°$ while the NACA 0012 airfoil showed an abrupt loss in lift at a lower stall angle of attack. In the poststall angle-of-attack range, $\alpha > 15°$, the lift of the NACA 0012 airfoil section increased while the lift of the GU 25-5(11)8 airfoil section leveled off before it decreased at about $\alpha = 25°$. The positive poststall lift-curve slope of the NACA 0012 section could contribute to an undesirable poststall pitch-up tendency.

Effect of Canard Position

On the VariEze airplane design, the canard was placed in a high position in order to minimize the aerodynamic interference effects from the canard downwash on the wing and from the trailing tip vortices of the canard which could impinge on the wing. The canard was placed in a low position on the model in order to examine its effect on the aerodynamic characteristics of the configuration. A photograph showing the model with the canard in the low position is presented in figure 37.

Tuft patterns in figure 8(c) for a high canard and in figure 38(b) for the low canard indicate an impingement of canard tip vortex on the wing as indicated by the disturbance of the tufts on the wing at $\alpha = -0.5°$ for the high canard and $\alpha = 5.5°$ for the low canard. A comparison of the longitudinal characteristics of the low-canard configuration and the high-canard configuration, shown in figure 39, indicates that placing the canard in the low position had little effect on lift, pitching moment, and trimmed drag. A comparison of the lateral-directional characteristics of the low-canard and high-canard configurations, as shown in figure 40, indicates that moving the canard to a low position had little effect on lateral-directional stability characteristics. Although the static aerodynamic effects of moving the canard to a low position are small for this configuration, the dynamic effects of the canard tip vortex impingement may be significant in terms of handling characteristics.

Effect of Winglets

The basic configuration was designed to make use of winglets (described in ref. 14) in lieu of a vertical tail to provide directional stability while at the same time reducing wing induced drag. The effect of winglets on the drag characteristics is shown in figure 41 in terms of incremental drag due to the winglets. Winglets provided overall drag reduction at lift coefficients above 1.0. An estimate of skin-friction drag coefficient, determined from the wetted area of the upper winglets, of

0.0018 would imply that winglets were reducing wing induced drag at lift coefficients above 0.5.

The effect of winglets on the lateral-directional stability characteristics of the basic configuration with the leading-edge droop on is shown by the data of figure 42. As expected, the winglets-off configuration was directionally unstable. The addition of the upper and lower winglets made the configuration directionally stable up to $\alpha = 19°$. In an effort to increase the directional stability, 50-percent-larger winglets were "gloved" onto existing upper winglets. (See fig. 1(b).) The data of figure 43 indicate that the directional stability was increased, and stable values of directional stability were provided over most of the test angle-of-attack range. The enlarged upper winglet did not significantly alter the dihedral effect.

Chordwise pressure distributions measured at $y'/b_w = 0.60$ are shown in figure 44 for the upper winglet on the right wing at sideslip angles of $-10°$ and $10°$. The pressure distribution at $\beta = 10°$ is representative of the leading winglet, while at $\beta = -10°$, the pressure distributions are representative of the trailing winglet. The magnitude of normal force of the leading winglet, as determined by the integration of the chordwise pressures, was approximately twice the magnitude of the trailing winglet. Examination of the chordwise pressures of the trailing winglet indicates that the outboard surface of the winglet has stalled out. This stalled flow region, indicated by the flat-top pressure distribution, is probably a result of the flat-bottom airfoil section. Thus, the trailing winglet was not as effective in providing directional stability as was the leading winglet at a sideslip angle of $10°$.

Summary of Results

A full-scale wind-tunnel investigation has been conducted to determine the static longitudinal and lateral-directional aerodynamic characteristics of a canard-configured general aviation airplane. The significant results of this investigation are as follows:

1. The canard on this configuration was effective in providing airplane stall resistance since the canard stalled before the wing stalled.

2. Downwash from the canard decreased loading of the main wing inboard of the canard tip; upwash from the canard tip increased main wing loading outboard of the canard tip.

3. The discontinuous outboard wing leading-edge droop increased wing-tip-stall angle of attack and increased pitch stability at low to moderate angles of attack.

4. For the three center-of-gravity locations studied, the maximum trimmed lift coefficient was less than the maximum lift coefficient. Thus, the limited elevator

control authority contributed to the stall resistance of the configuration.

5. Trimming this canard-configured airplane produced increments in drag similar to conventional aft-tail configurations.

6. Power effects on this configuration provided a stabilizing effect on longitudinal stability.

7. Natural boundary-layer transition occurred at the 55-percent-chord location of the canard. Fixing canard transition at 5 percent chord caused flow separation near the trailing edge of the canard, significantly reduced canard lift, and, subsequently, caused a nose-down airplane pitch trim change and a loss of elevator effectiveness.

8. The canard-airfoil-section characteristics strongly affected the stall and poststall characteristics of the airplane.

9. Moving the canard to a lower position had little effect on the static longitudinal and lateral-directional aerodynamic characteristics of this configuration.

10. Increasing the area of the upper winglets by 50 percent significantly increased directional stability.

Langley Research Center
National Aeronautics and Space Administration
Hampton, VA 23665
October 11, 1984

References

1. Rutan, Burt: Development of a Small High-Aspect-Ratio Canard Aircraft. 1976 Report to the Aerospace Profession, *Tech. Rev.*, vol. 13, no. 2, Soc. Exp. Test Pilots, 1976, pp. 93–101.

2. Yip, Long P.; and Coy, Paul F.: Wind-Tunnel Investigation of a Full-Scale Canard-Configured General Aviation Aircraft. ICAS Paper No. 82-6.8.2, Aug. 1982.

3. Kelling, F. H.: *Experimental Investigation of a High-Lift Low-Drag Aerofoil.* C.P. No. 1187, British A.R.C., 1971.

4. Staff of Langley Research Center: *Exploratory Study of the Effects of Wing-Leading-Edge Modifications on the Stall/Spin Behavior of a Light General Aviation Airplane.* NASA TP-1589, 1979.

5. Newsom, William A., Jr.; Satran, Dale R.; and Johnson, Joseph L., Jr.: *Effects of Wing-Leading-Edge Modifications of a Full-Scale, Low-Wing General Aviation Airplane—Wind-Tunnel Investigation of High-Angle-of-Attack Aerodynamic Characteristics.* NASA TP-2011, 1982.

6. DeFrance, Smith J.: *The NACA Full-Scale Tunnel.* NACA Rep. 459, 1933.

7. Crowder, J. P.: *Fluorescent Mini-Tufts for Non-Intrusive Flow Visualization.* MDC J7374, McDonnell Douglas Corp., Feb. 1, 1977.

8. Holmes, Bruce J.; Obara, Clifford J.; and Yip, Long P.: *Natural Laminar Flow Experiments on Modern Airplane Surfaces.* NASA TP-2256, 1984.

9. Theodorsen, Theodore; and Silverstein, Abe: *Experimental Verification of the Theory of Wind-Tunnel Boundary Interference.* NACA Rep. 478, 1934.

10. Heyson, Harry H.: *Use of Superposition in Digital Computers To Obtain Wind-Tunnel Interference Factors for Arbitrary Configurations, With Particular Reference to V/STOL Models.* NASA TR R-302, 1969.

11. Foa, Joseph V.: Proportioning the "Canard" Airplane for Longitudinal Stability and Safety Against Stall. *J. Aeronaut. Sci.*, vol. 9, no. 14, Dec. 1942, pp. 523–528.

12. Hassell, James L., Jr.; Newsom, William A., Jr.; and Yip, Long P.: *Full-Scale Wind-Tunnel Investigation of the Advanced Technology Light Twin-Engine Airplane (ATLIT).* NASA TP-1591, 1980.

13. Braslow, Albert L.; and Knox, Eugene C.: *Simplified Method for Determination of Critical Height of Distributed Roughness Particles for Boundary-Layer Transition at Mach Numbers From 0 to 5.* NACA TN 4363, 1958.

14. Whitcomb, Richard T.: *A Design Approach and Selected Wind-Tunnel Results at High Subsonic Speeds for Wing-Tip Mounted Winglets.* NASA TN D-8260, 1976.

TABLE I. GEOMETRIC CHARACTERISTICS OF MODEL

Reference dimensions:
- S, ft² . . . .
- b, ft 53.60
- $\bar{c}$, ft 22.17

Wing: 2.58
- Area, ft² . . . .
- Span, ft 53.60
- Aspect ratio 22.17
- Root chord at centerline, ft 9.17
- Tip chord, ft 3.47
- Taper ratio 1.33
- Sweep angle (25-percent-chord line), deg 0.38
- Dihedral, deg 25.7
- Root incidence at BL 32, deg . . . . −4
- Tip incidence, deg 1.2
- Airfoil section . . . . −1.8
- Aileron: . . . . GA(W)-1 (modified)
  - Total area, ft² . . . .
  - Span, per side, ft 4.0
  - Chord, percent wing chord 3.33
  20

Canard:
- Area, ft² . . . .
- Span, ft 12.82
- Aspect ratio 11.83
- Chord, ft 10.92
- Taper ratio 1.08
- Sweep angle, deg 1.00
- Airfoil section 0
- Incidence, deg . . . . GU 25-5(11)8
- Elevator hinge-line location, percent chord 0

Winglets: 70

	Upper	Lower
Total area, ft²		
Span, per side, ft	6.96	0.39
Root chord, ft	3.09	0.58
Tip chord, ft	1.67	0.42
Sweep angle (25-percent-chord line), deg	0.58	0.25
Dihedral, deg	26.3	12
	86	−60

Propeller:
- Designation . . . .
- Diameter, ft . . . . Hendrickson H58G64
- Thrust-line inclination relative to WL (looking forward), deg 4.83
- WL at FS 157 . . . . −2
. . . . 21.3

TABLE II. PRESSURE ORIFICE LOCATIONS

WING		CANARD		WINGLET		L. E. DROOP	
$(x/c)_u$	$(x/c)_l$	$(x/c)_u$	$(x/c)_l$	$(x/c)_u$	$(x/c)_l$	$(x/c)_u$	$(x/c)_l$
0	.02	0	.01	0	.02	-.065	.050
.005	.05	.005	.05	.02	.10	-.060	.020
.02	.10	.02	.15	.05	.30	-.045	.030
.05	.25	.05	.35	.10	.50	-.015	
.10	.40	.10	.50	.30	.70	.030	
.175	.55	.175	.625	.50	.90		
.25	.65	.25	.65	.75			
.40	.75	.40	.75	.90			
.55	.85	.50	.85	.95			
.65	.95	.65	.95				
.75		.75					
.85		.85					
.95		.95					

$$\frac{2y}{b_c}$$

0.26
0.53
0.79
0.95

0.15
0.25
0.40
0.55
0.75
0.85
0.95

$$\frac{2y}{b}$$

$$\frac{y'}{b_W}$$

0.85
0.60
0.25

12
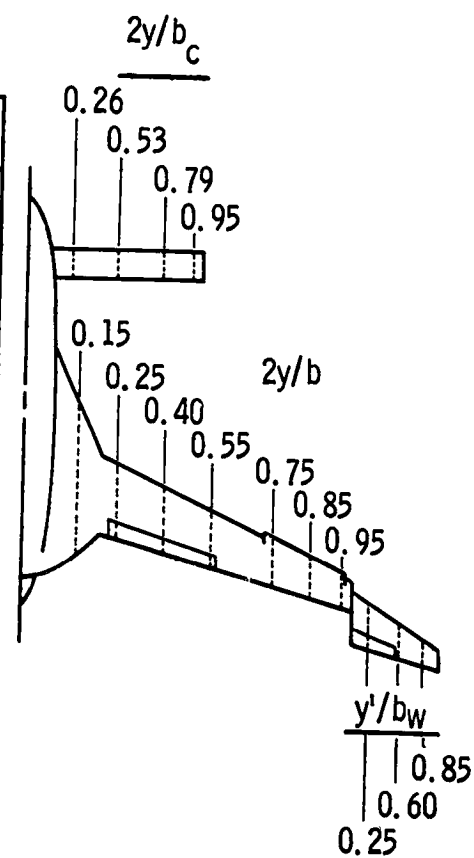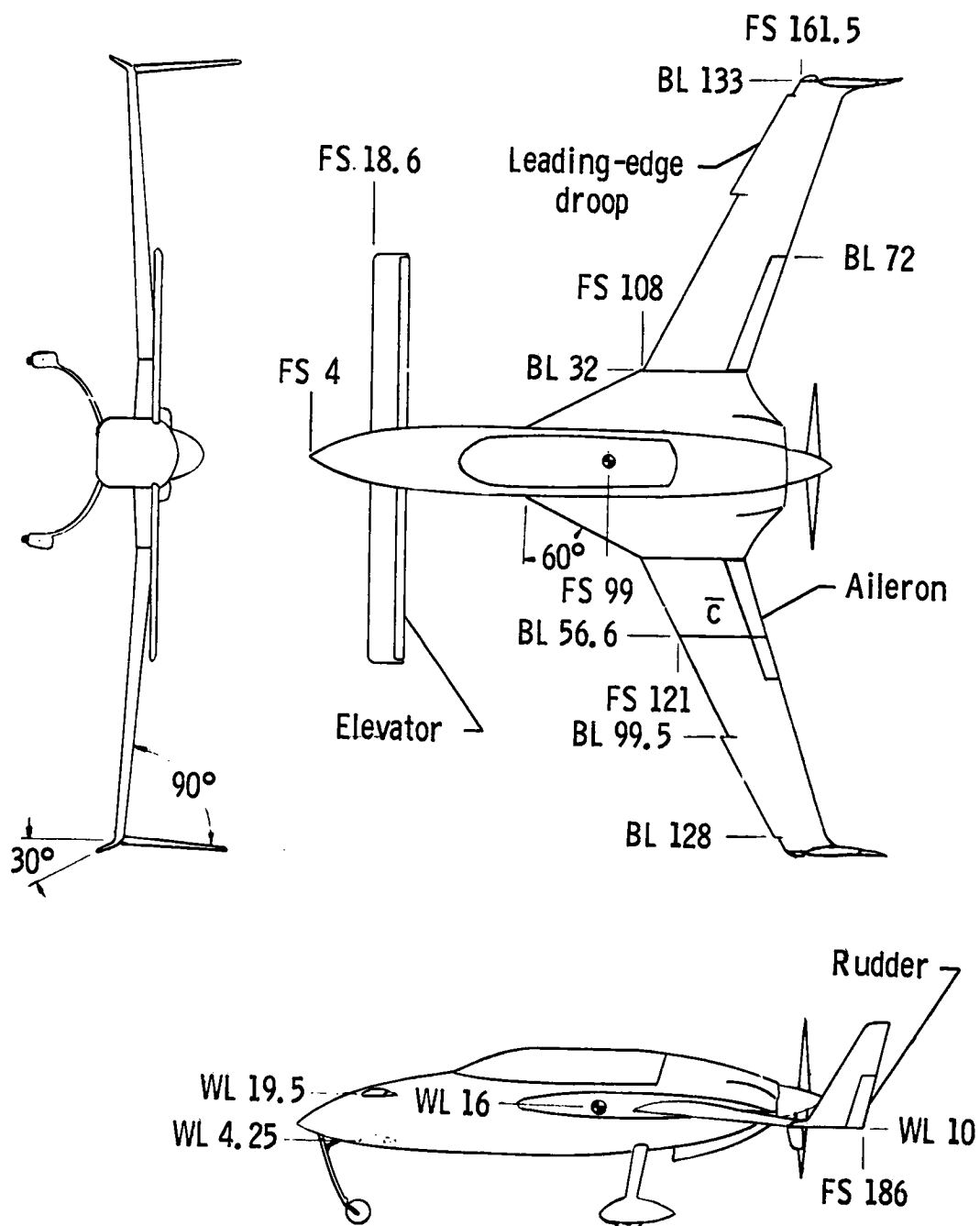
(a) Three-view drawing.

Figure 1. Geometric characteristics of model. Linear dimensions are in inches.

(b) Upper winglet planform.

WINGLET

——— ORIGINAL

– – – – ENLARGED

(c) Upper winglet section contour.

Figure 1. Continued.

14
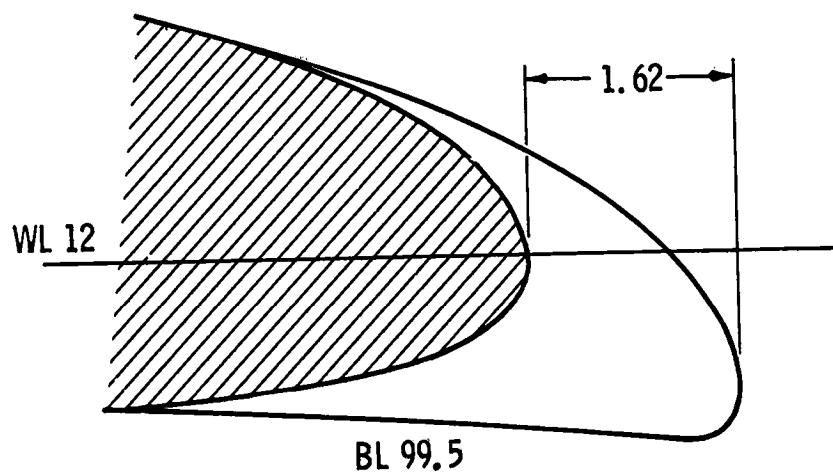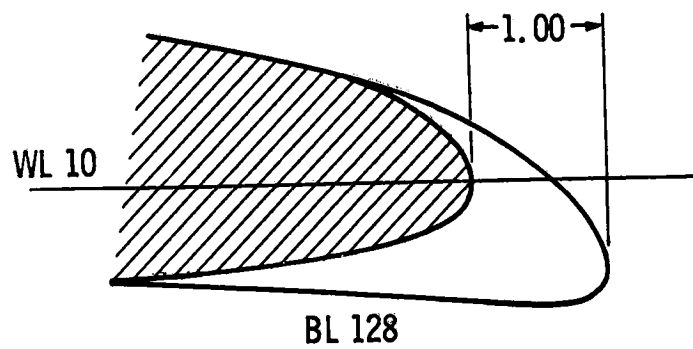
(d) Leading-edge droop.

Figure 1. Concluded.

Figure 2. Model installed in Langley 30- by 60-Foot Tunnel.

L-81-6300
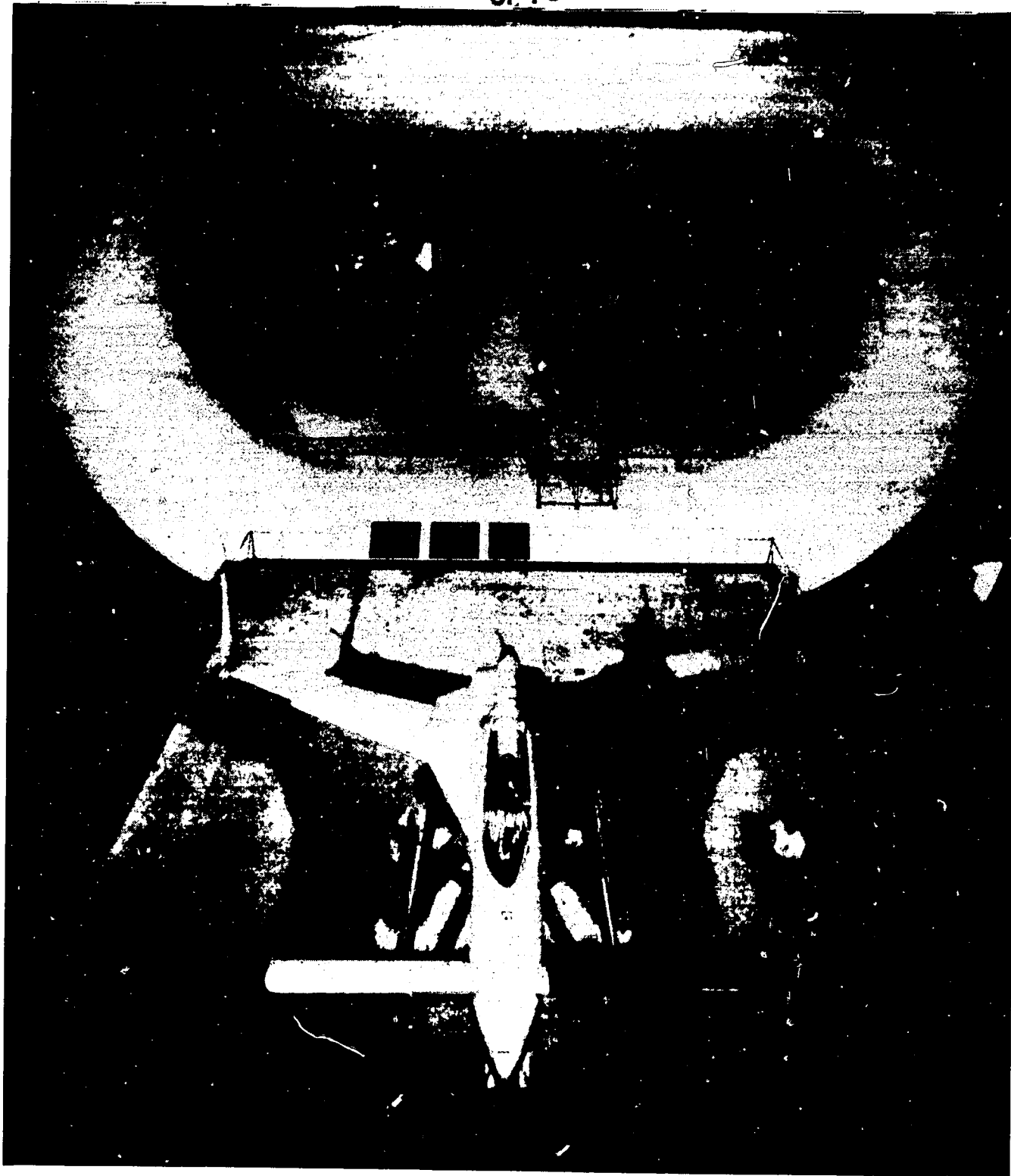
L-81-7334

Figure 3. Top-front view of model.
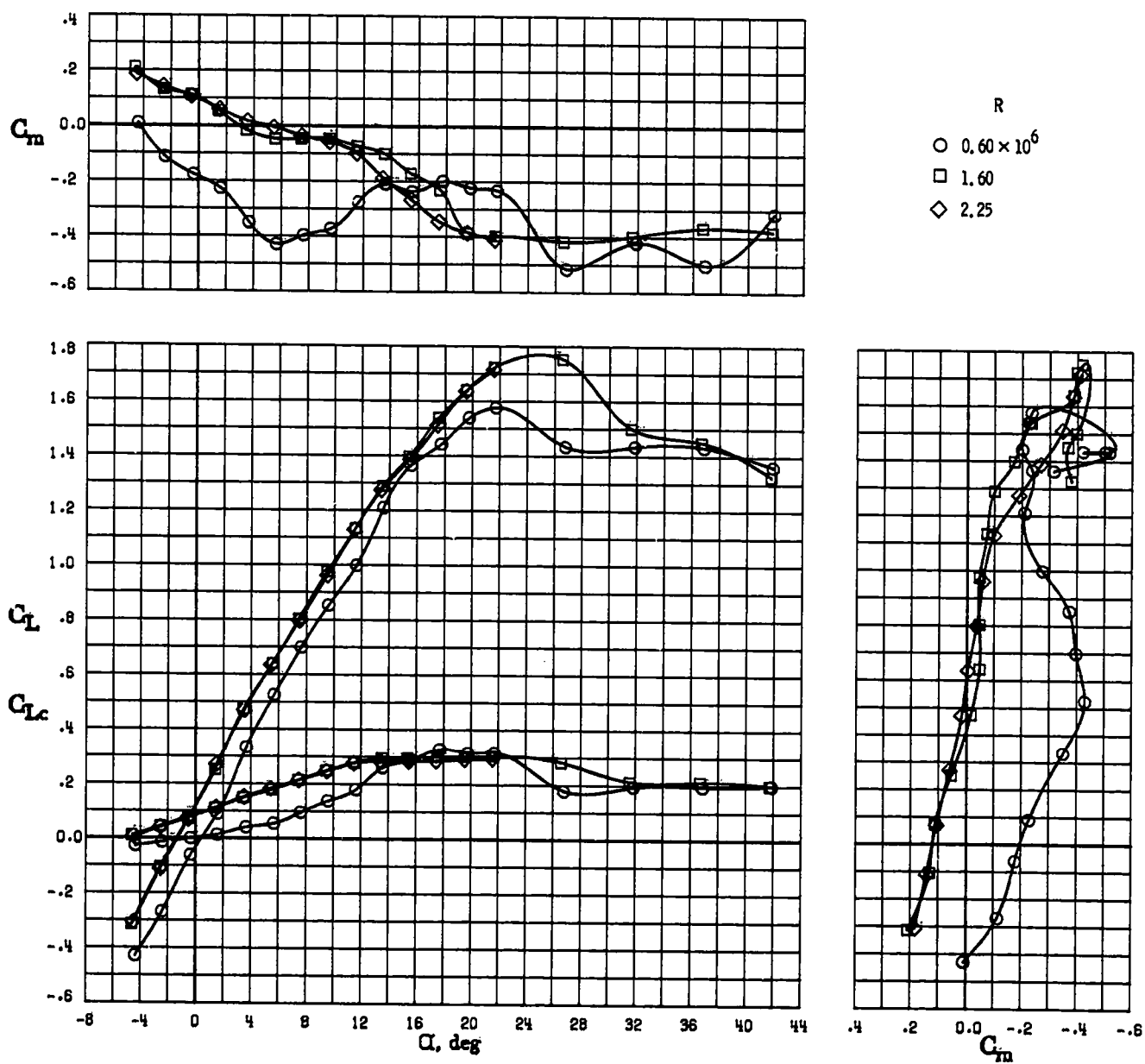
Figure 4. Effect of Reynolds number on longitudinal aerodynamic characteristics of basic configuration.

18

(a) $\alpha = -2.5°$.
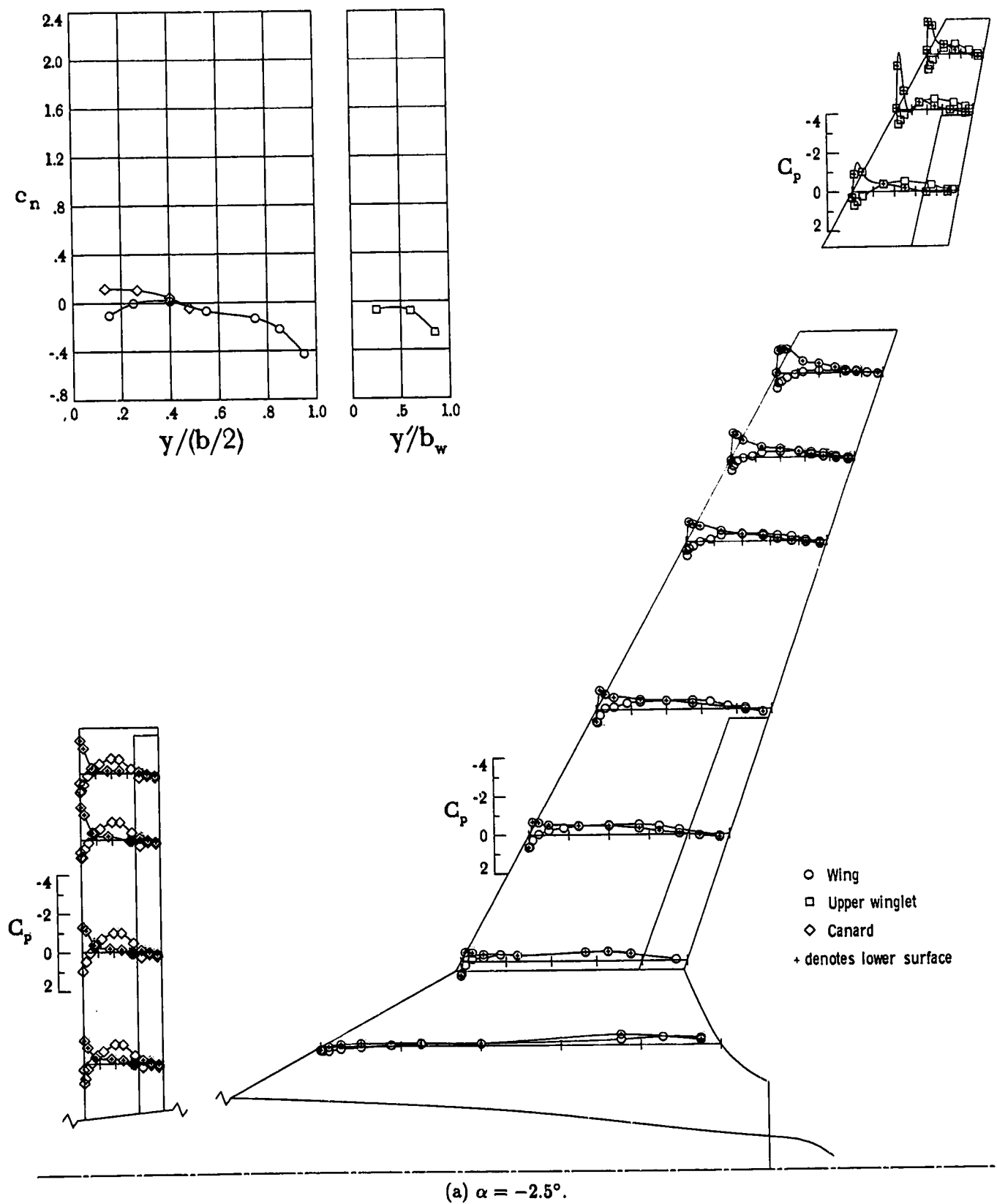
Figure 5. Chordwise pressure distributions and section normal-force coefficients of basic configuration. Controls neutral; $\beta = 0°$.
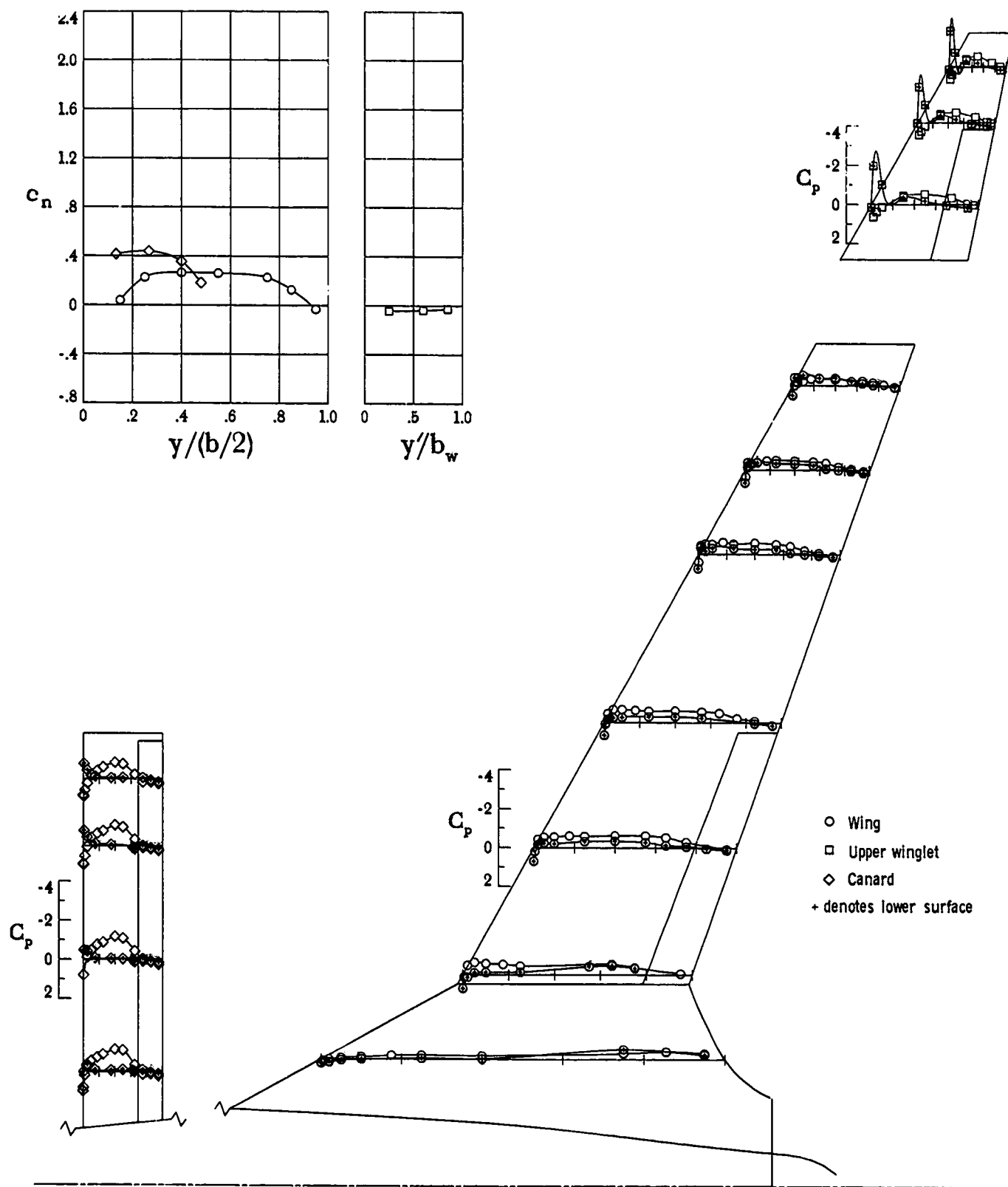
(b) $\alpha = 1.5°$.

Figure 5. Continued.

(c) $\alpha = 5.5°$.

Figure 5. Continued.

Legend:
○ Wing
□ Upper winglet
◇ Canard
+ denotes lower surface
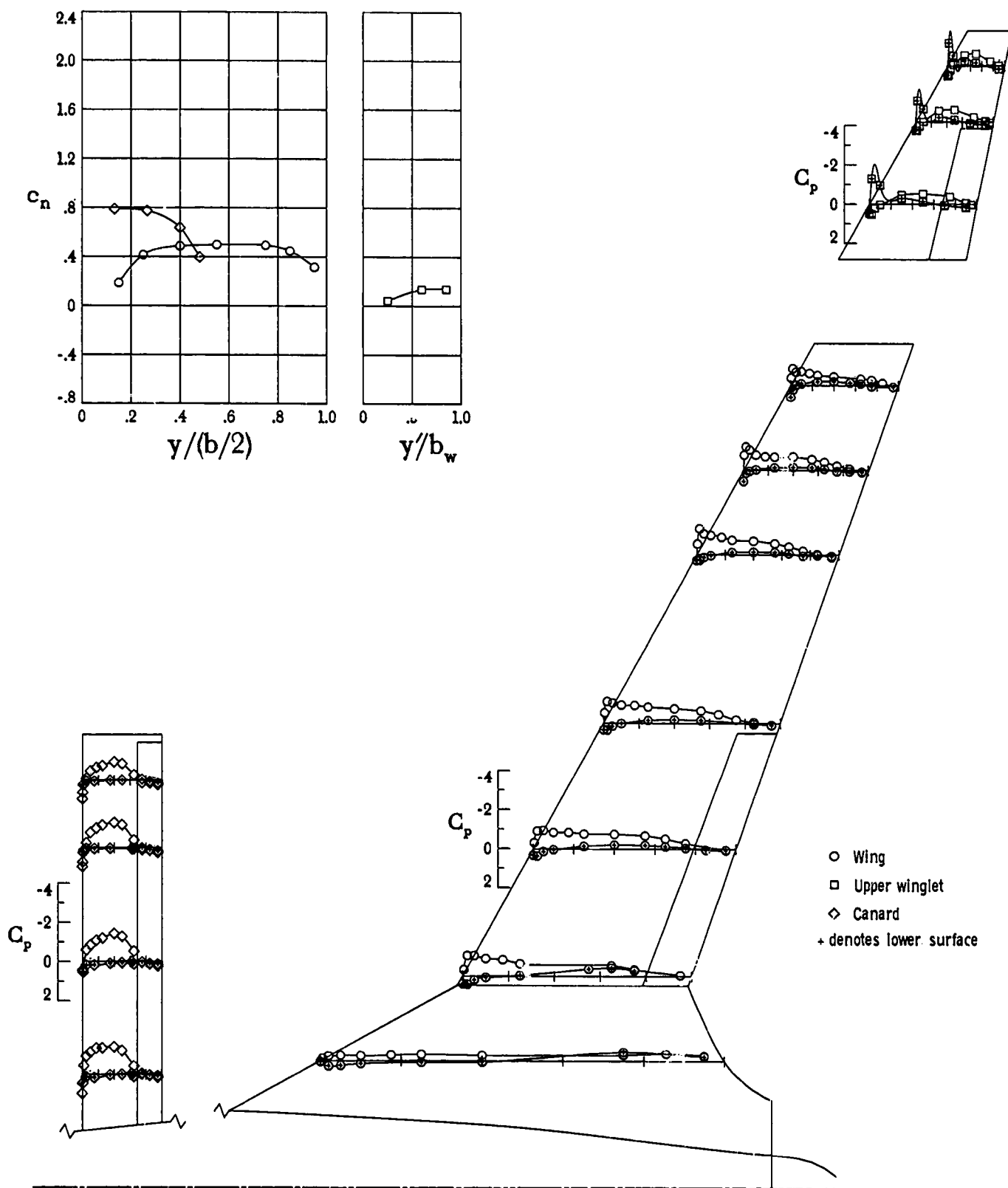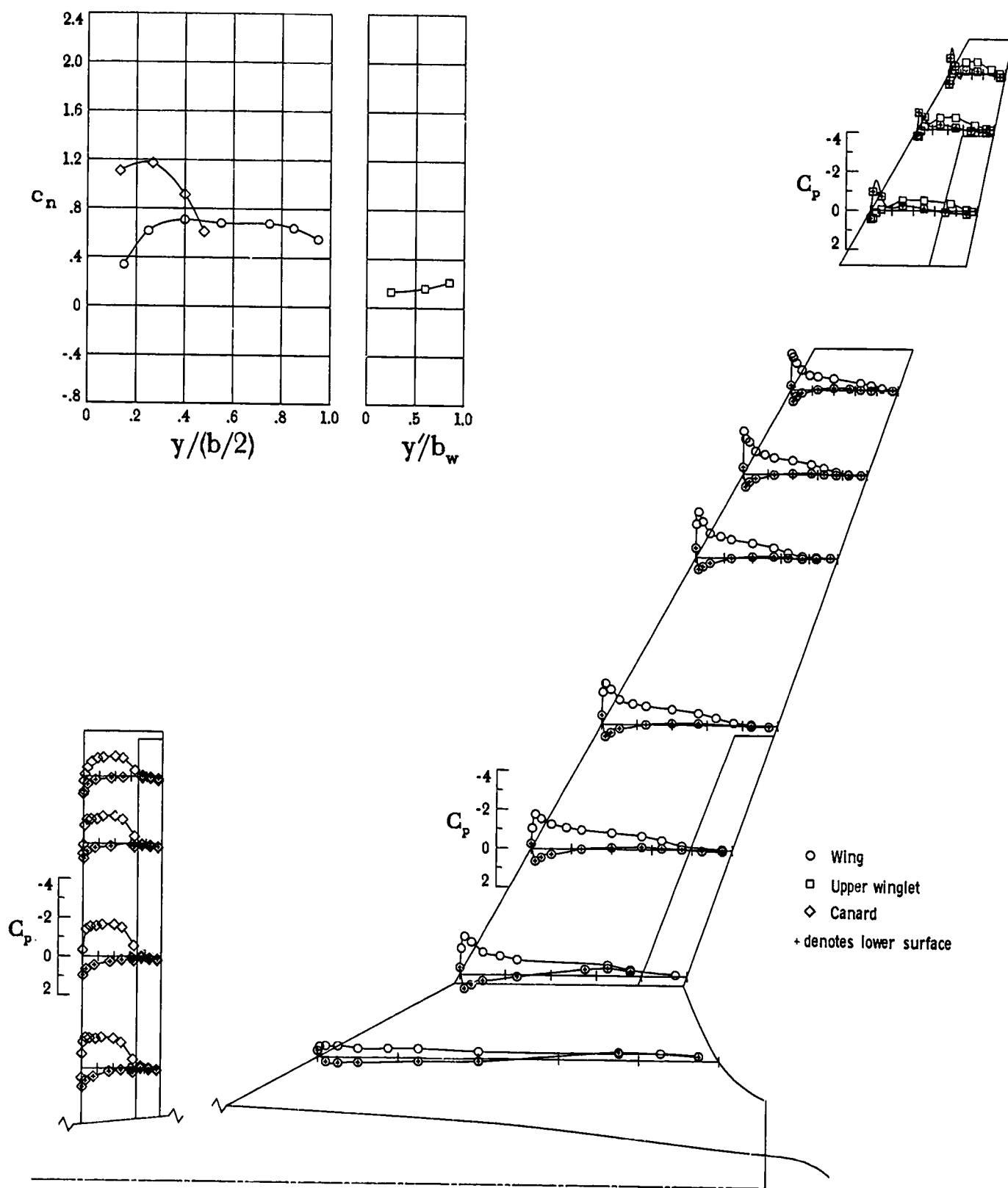
(d) $\alpha = 9.5°$.

Figure 5. Continued.

(e) $\alpha = 13.5°$.

Figure 5. Continued.

Legend:
○ Wing
□ Upper winglet
◇ Canard
+ denotes lower surface
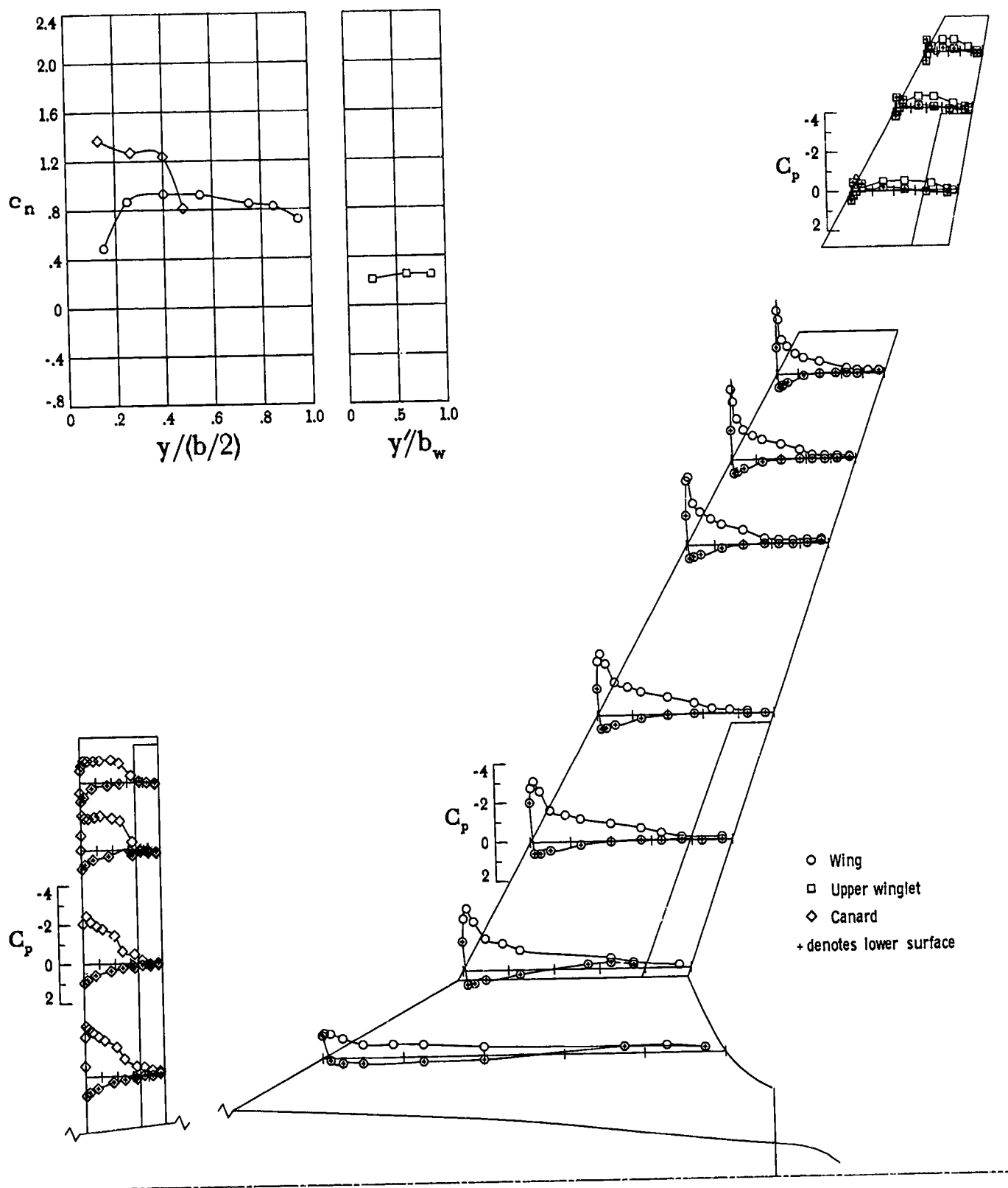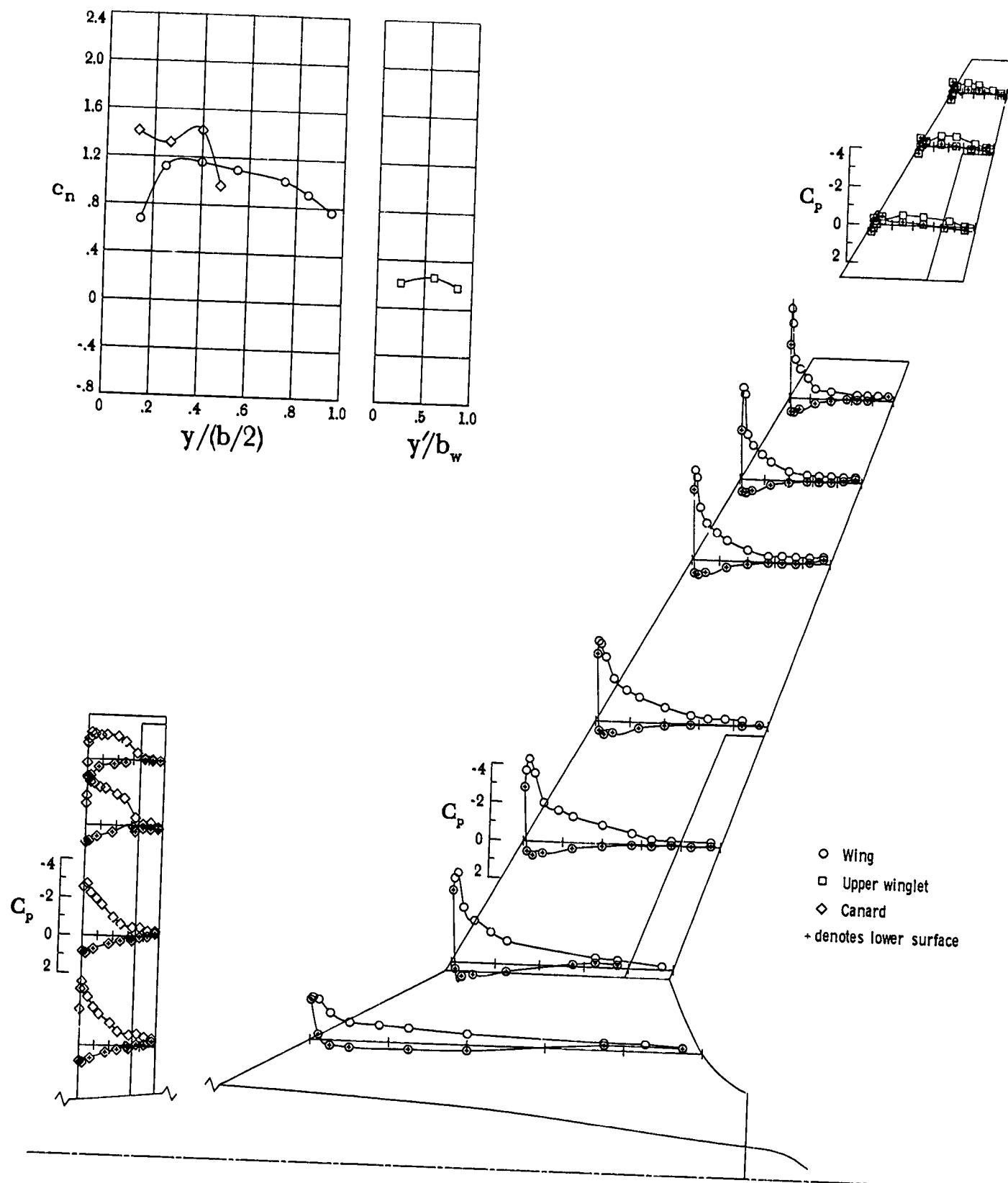
(f) $\alpha = 17.5°$.

Figure 5. Continued.

Legend:
- ○ Wing
- □ Upper winglet
- ◇ Canard
- + denotes lower surface
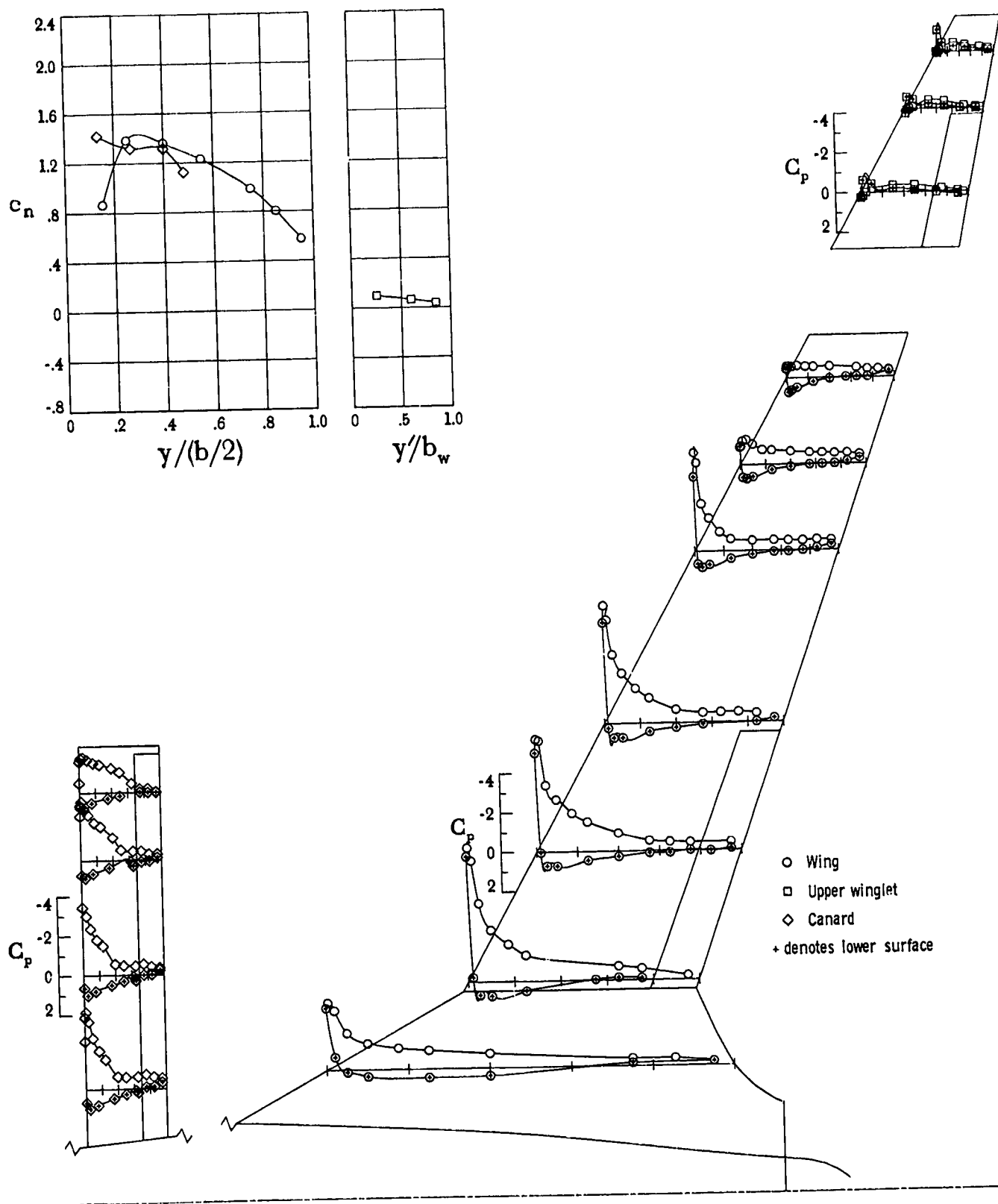
(g) $\alpha = 21.5°$.
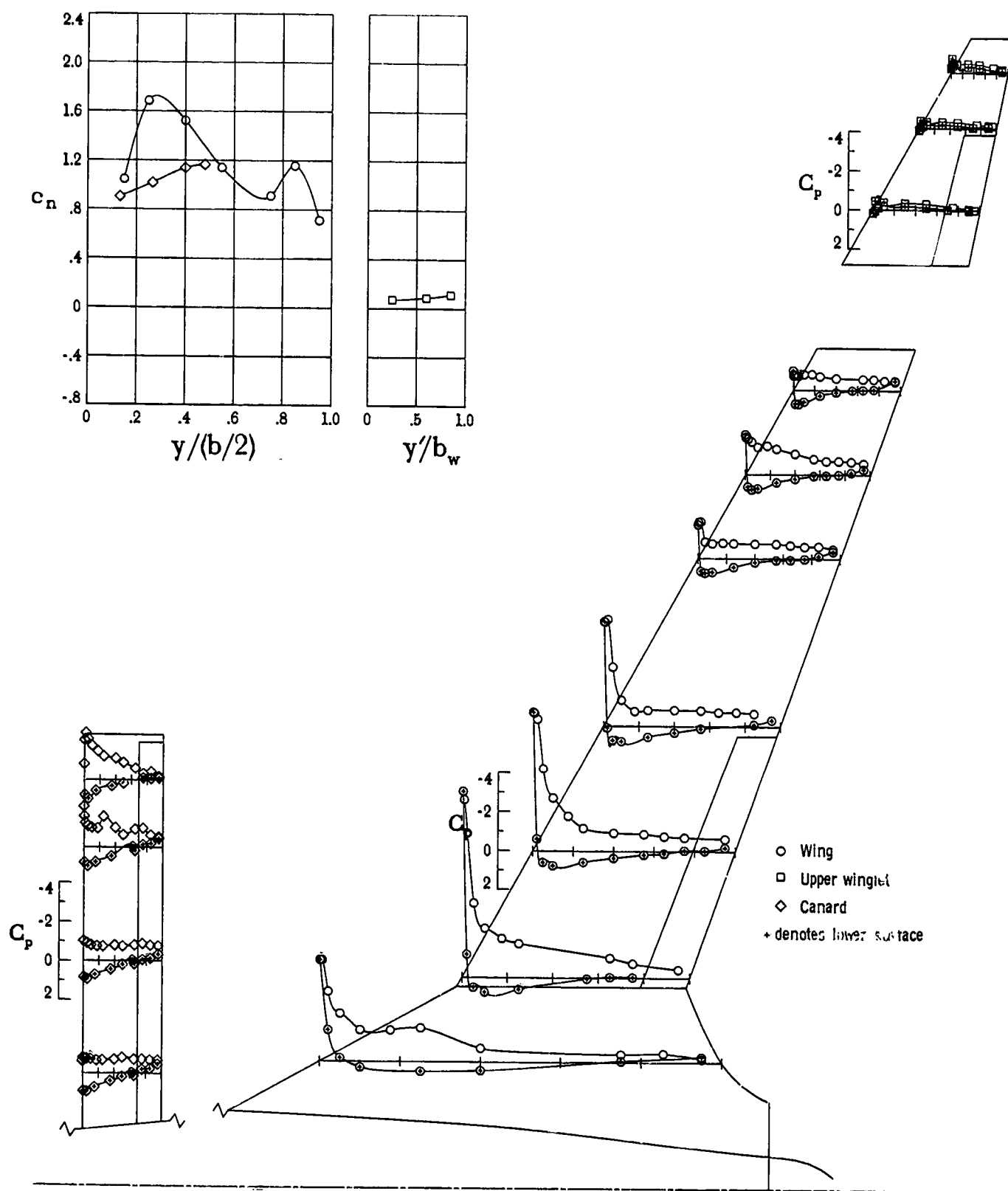
Figure 5. Continued.

(h) $\alpha = 26.5°$.

Figure 5. Continued.
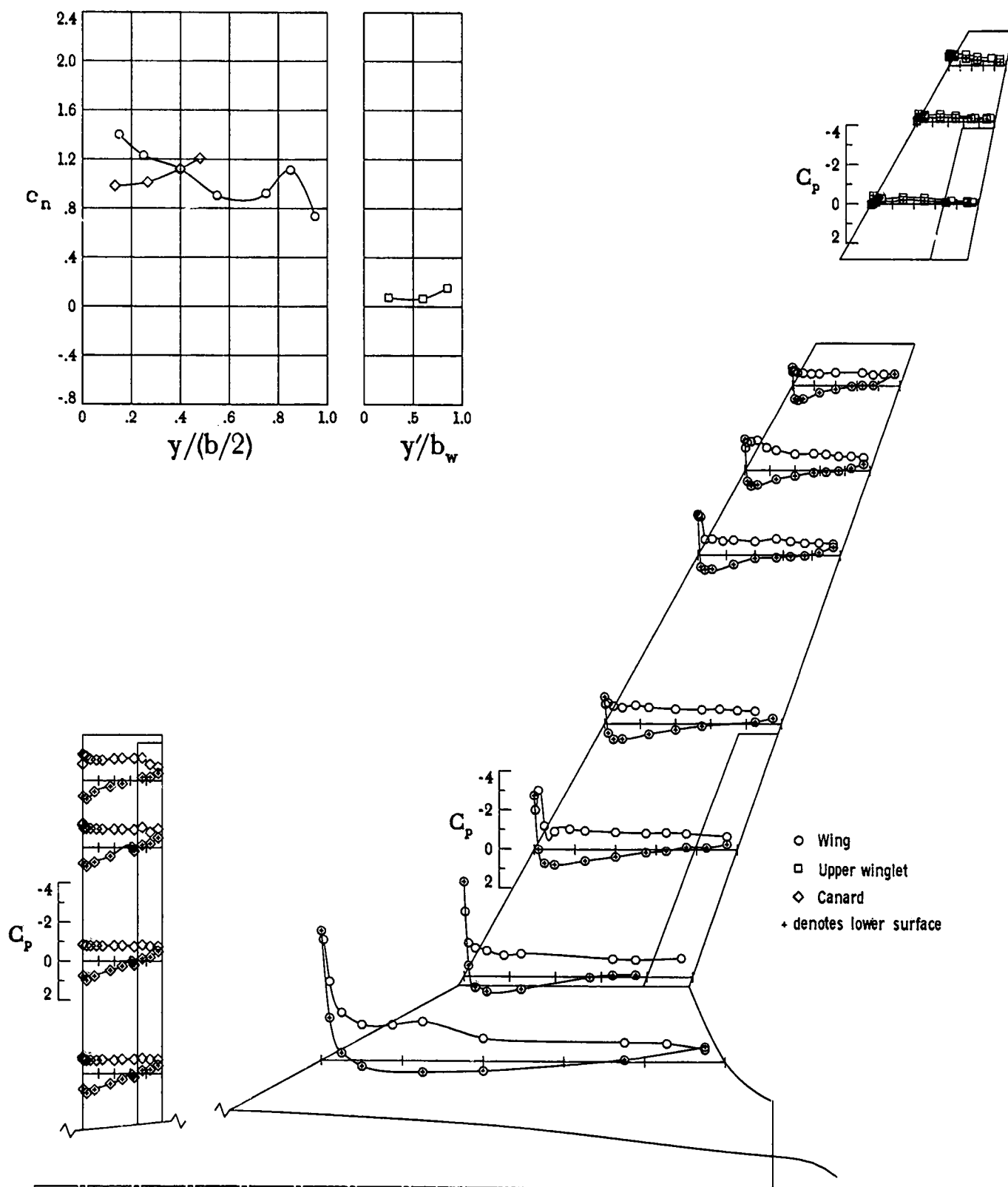
(i) $\alpha = 31.5°$.

Figure 5. Concluded.
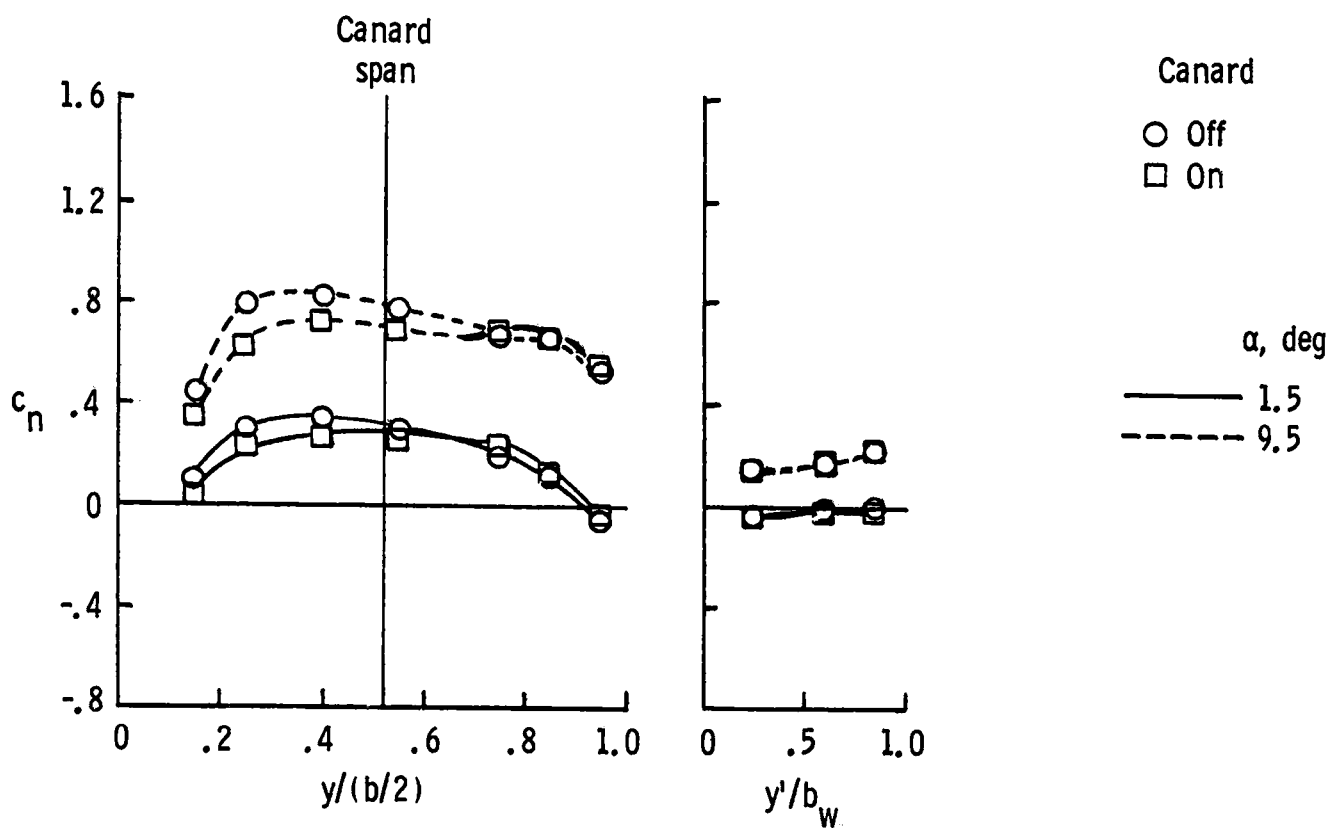
Figure 6. Effect of canard on section normal-force coefficient of wing and upper winglet.

L-84-10,657

(a) $\alpha = -0.5°$.

L-84-10,658

(b) $\alpha = 1.5°$.

Figure 7. Effect of angle of attack on wing surface flow patterns of basic configuration with leading-edge droop off.

29
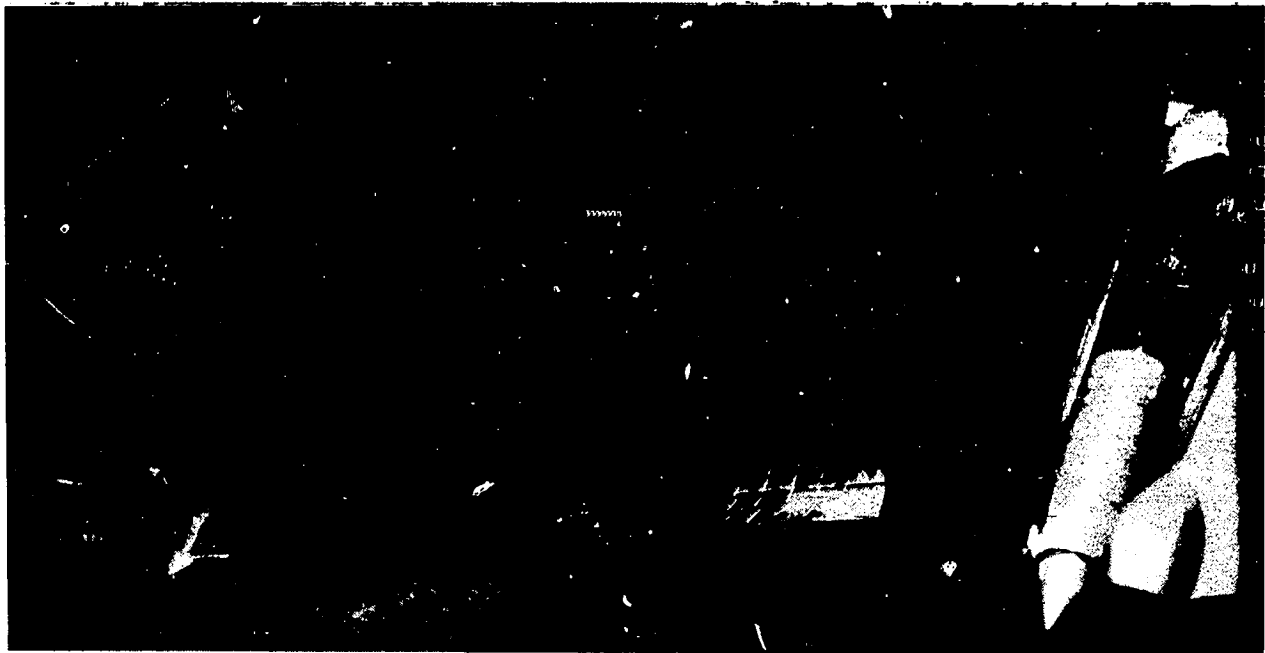
L-84-10,659

(c) $\alpha = 3.5°$.

L-84-10,660

(d) $\alpha = 5.5°$.

Figure 7. Continued.

L-84-10,661

(e) $\alpha = 7.5°$.

L-84-10,662

(f) $\alpha = 9.5°$.

Figure 7. Continued.

31
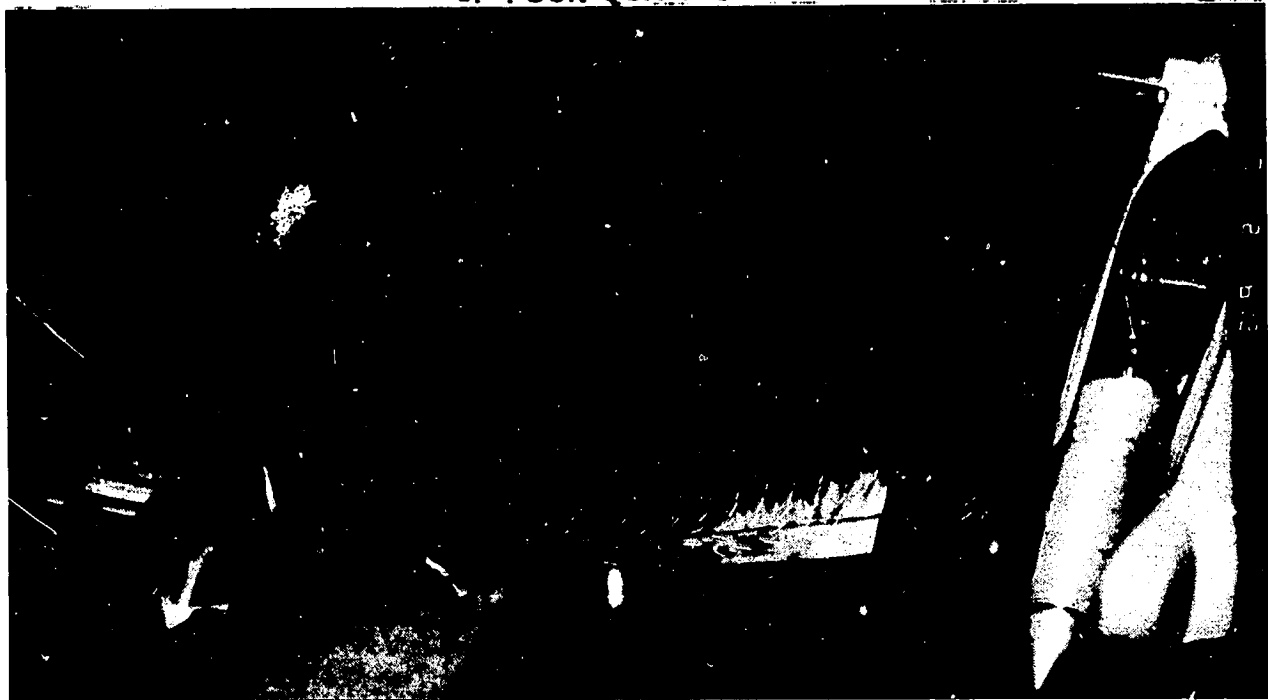
L-84-10,663

(g) $\alpha = 11.5°$.

L-84-10,664

(h) $\alpha = 13.5°$.

Figure 7. Continued.

L-84-10,665

(i) $\alpha = 15.5°$.

L-84-10,666

(j) $\alpha = 17.5°$.

Figure 7. Continued.

33

L-84-10,667

(k) $\alpha = 19.5°$.

L-84-10,668

(l) $\alpha = 21.5°$.

Figure 7. Continued.
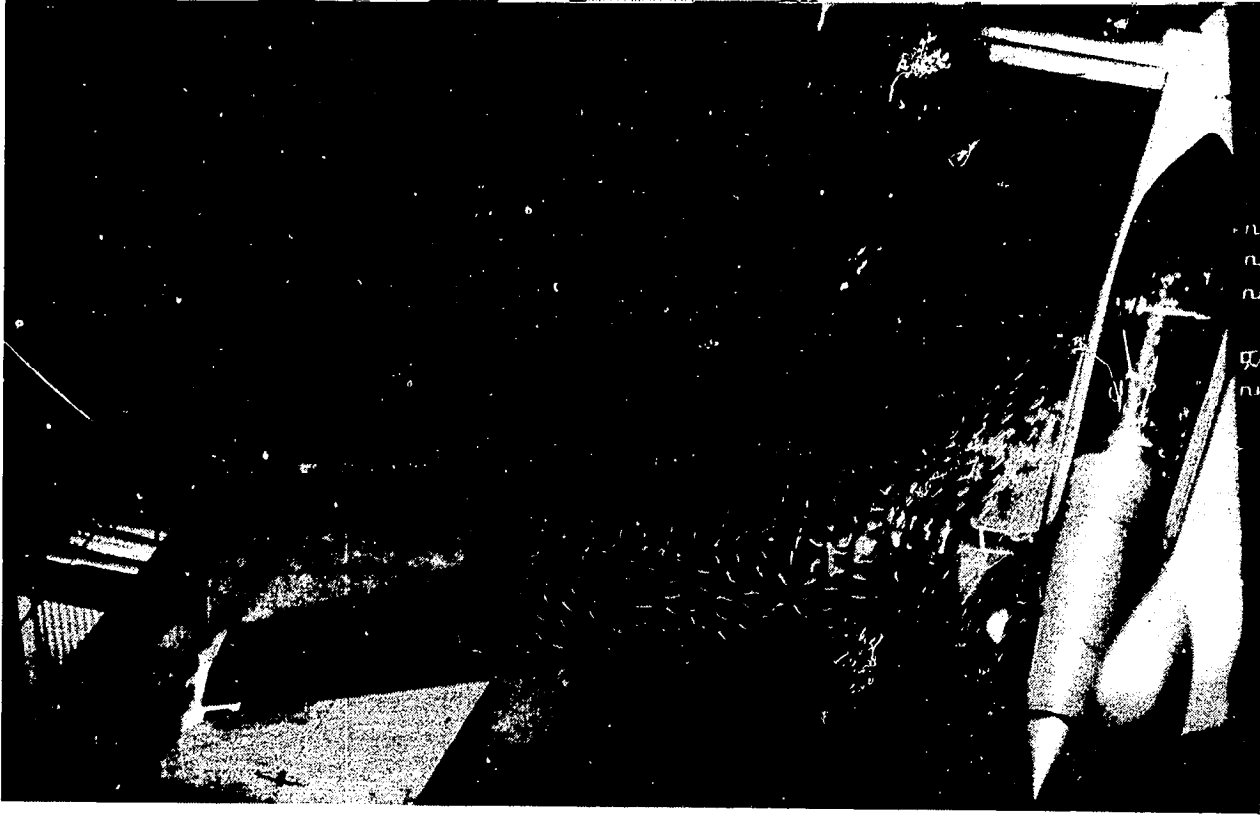
(m) $\alpha = 23.5°$.

L-84-10,669

(n) $\alpha = 25.5°$.

L-84-10,670

Figure 7. Concluded.

L-84-10,671

(a) $\alpha = -4.5°$.
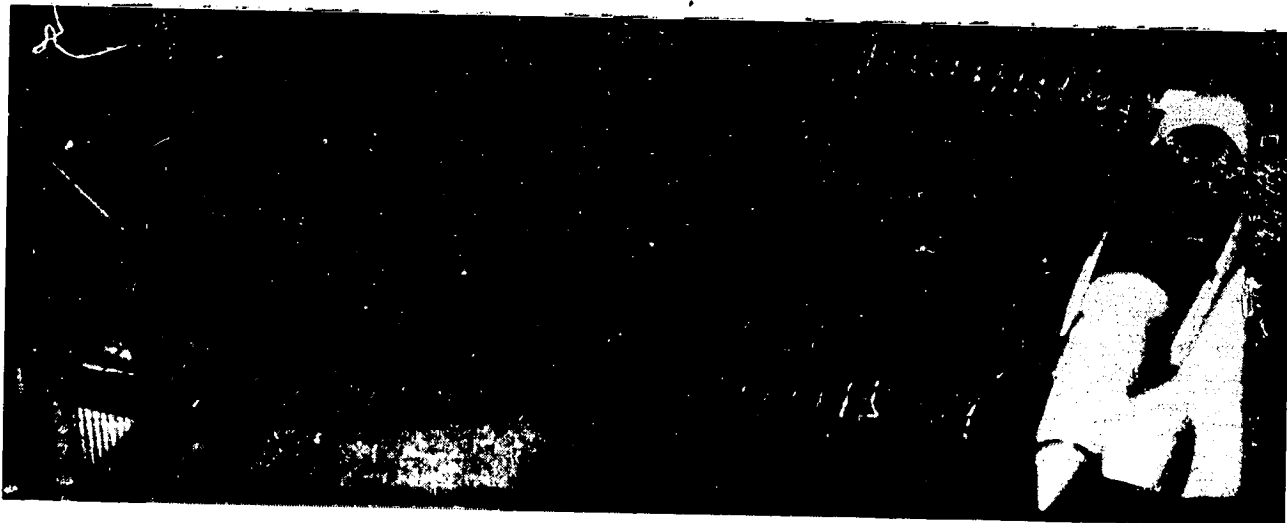
L-84-10,672

(b) $\alpha = -2.5°$.

Figure 8. Effect of angle of attack on wing surface flow patterns of basic configuration with leading-edge droop on.

36

Canard vortex impingement

L-84-10,673

(c) $\alpha = -0.5°$.
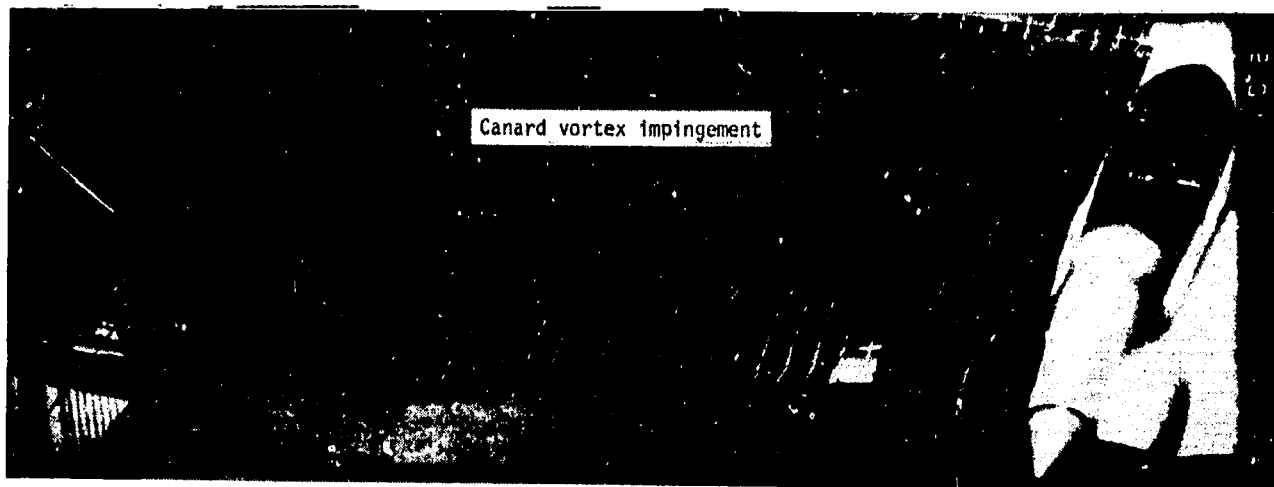
L-84-10,674

(d) $\alpha = 1.5°$.

Figure 8. Continued.

L-84-10,675

(e) $\alpha = 3.5°$.
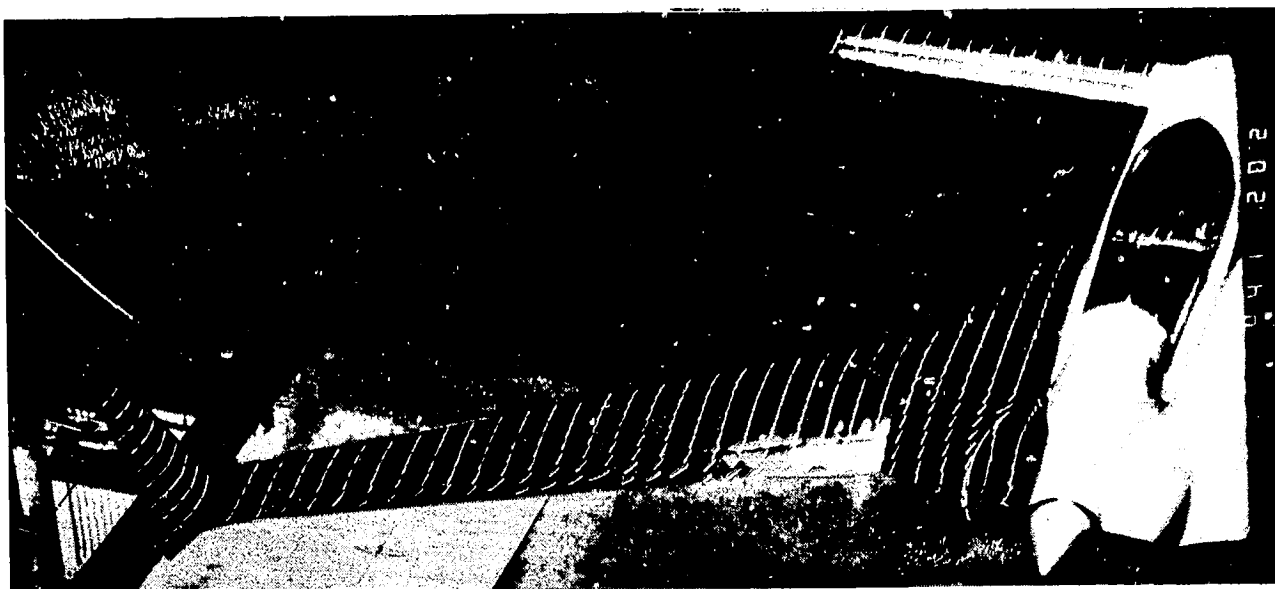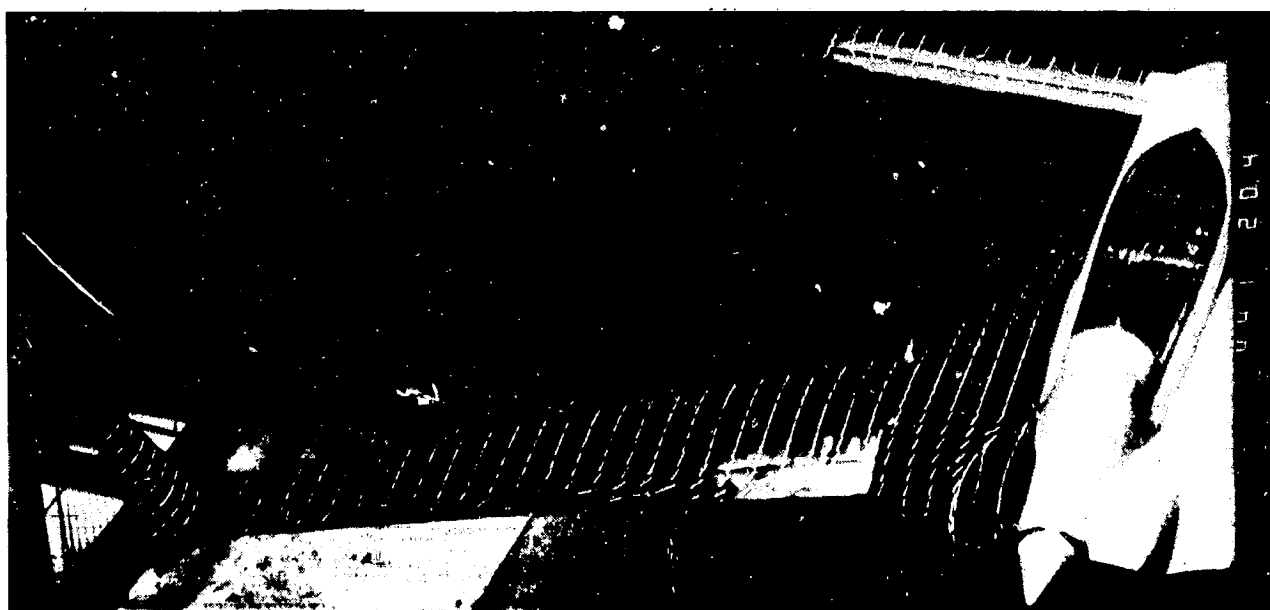
L-84-10,676

(f) $\alpha = 5.5°$.

Figure 8. Continued.
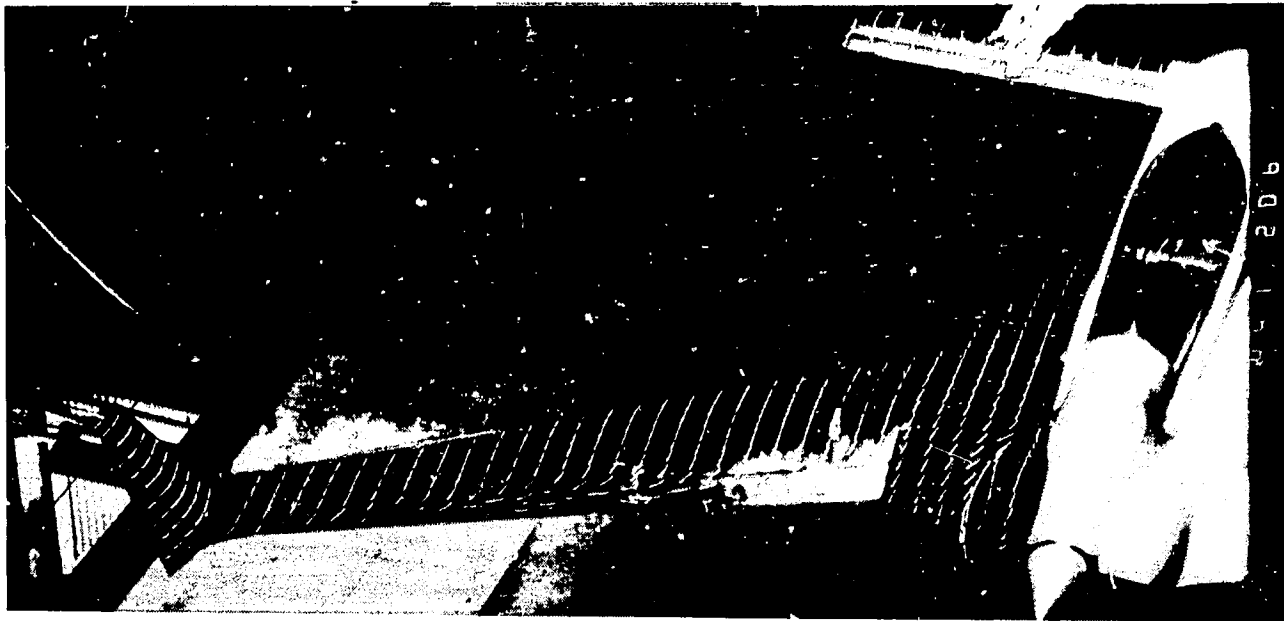
L-84-10,677

(g) $\alpha = 7.5°$.
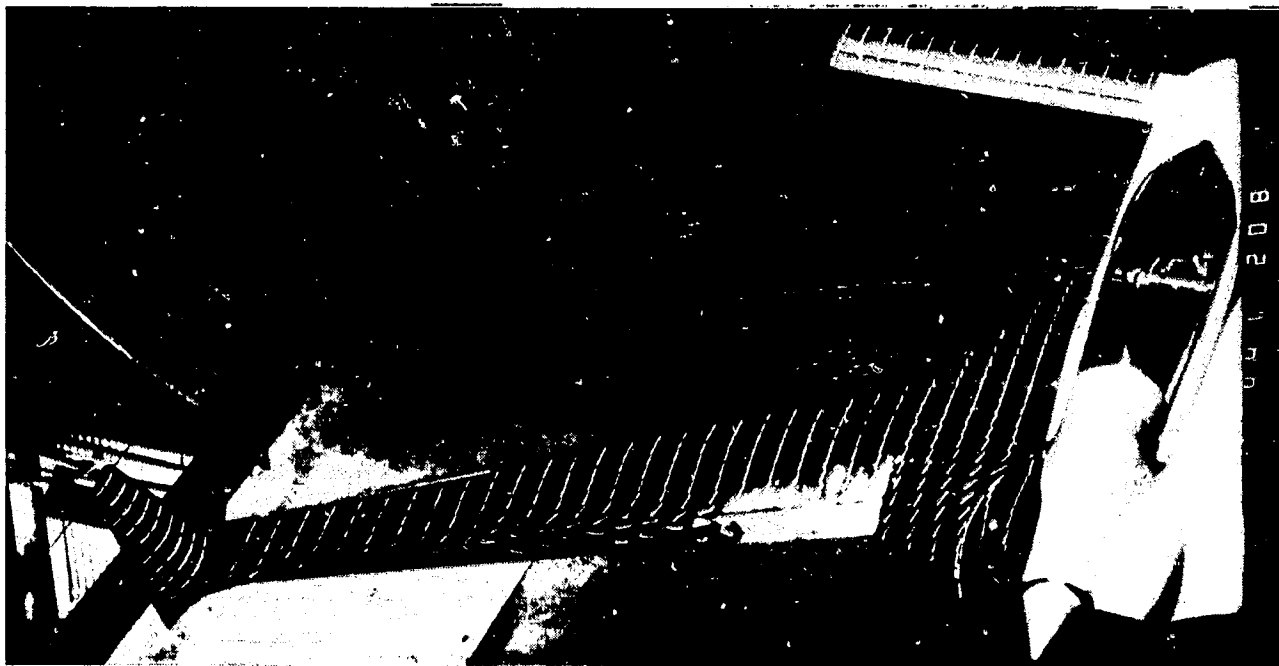
L-84-10,678

(h) $\alpha = 9.5°$.

Figure 8. Continued.
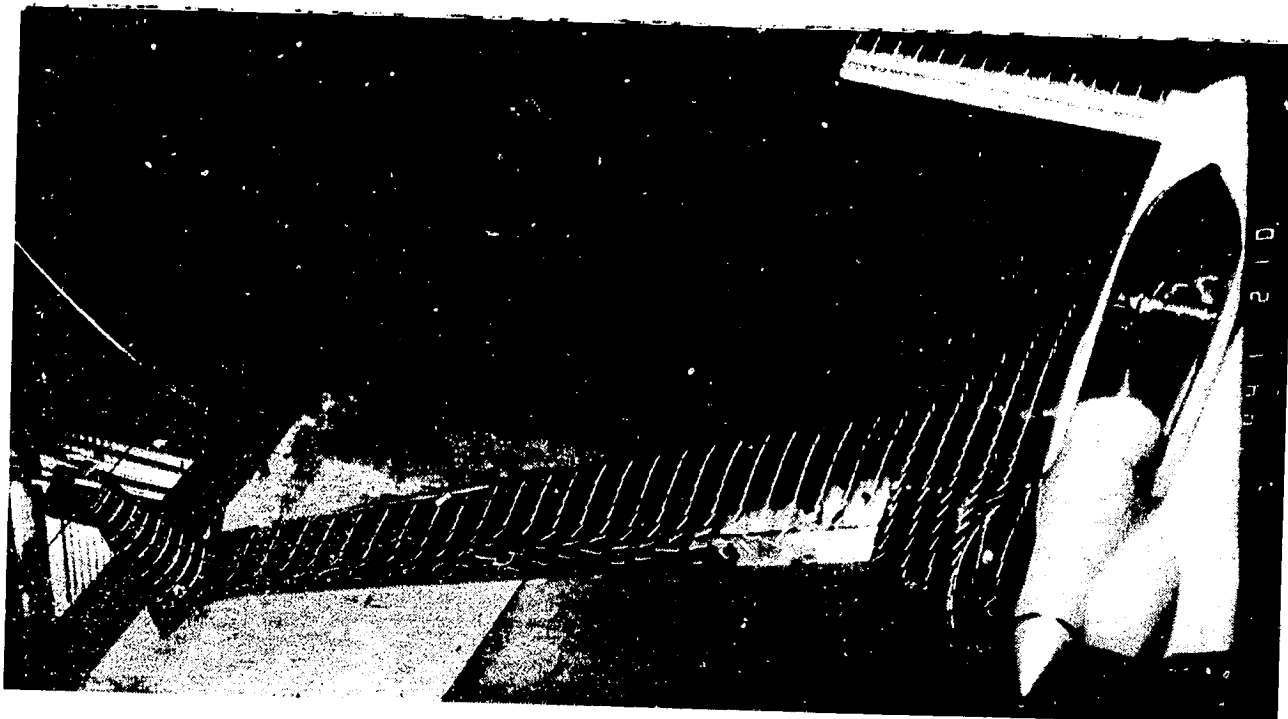
39

L-84-10,679

(i) $\alpha = 11.5°$.

L-84-10,680

(j) $\alpha = 13.5°$.

Figure 8. Continued.

40
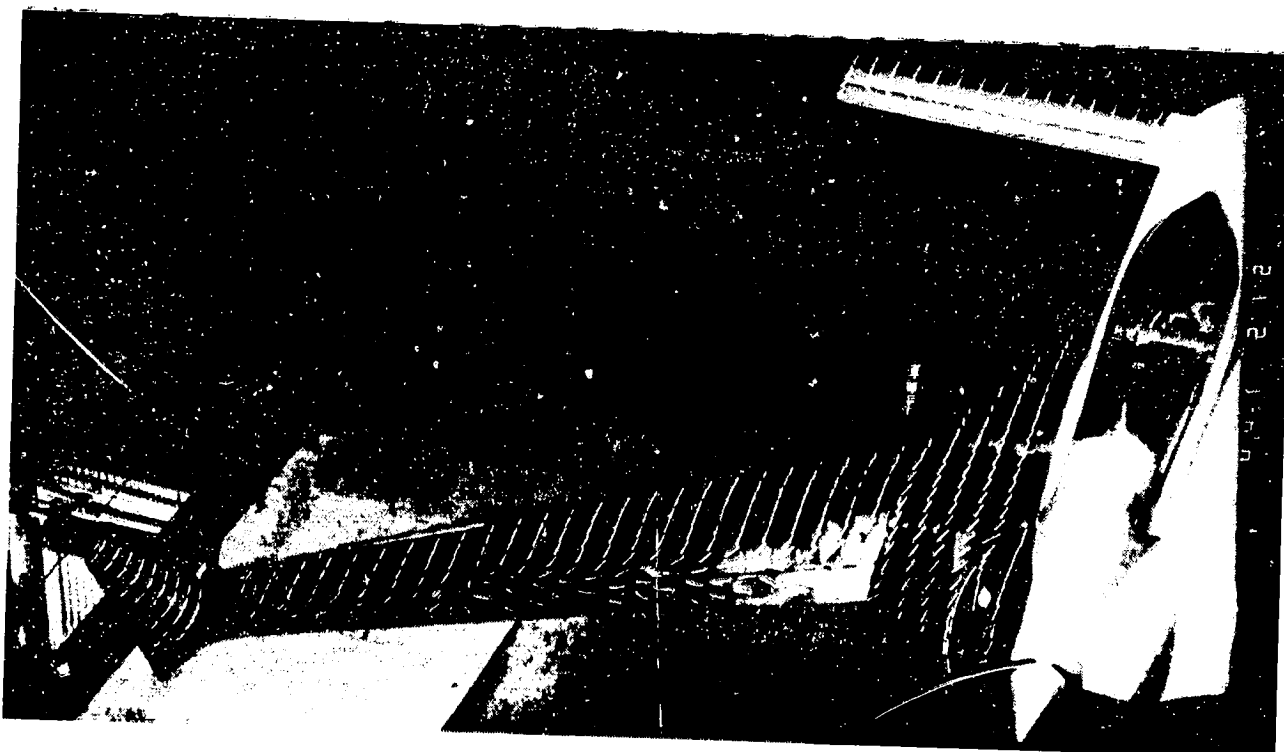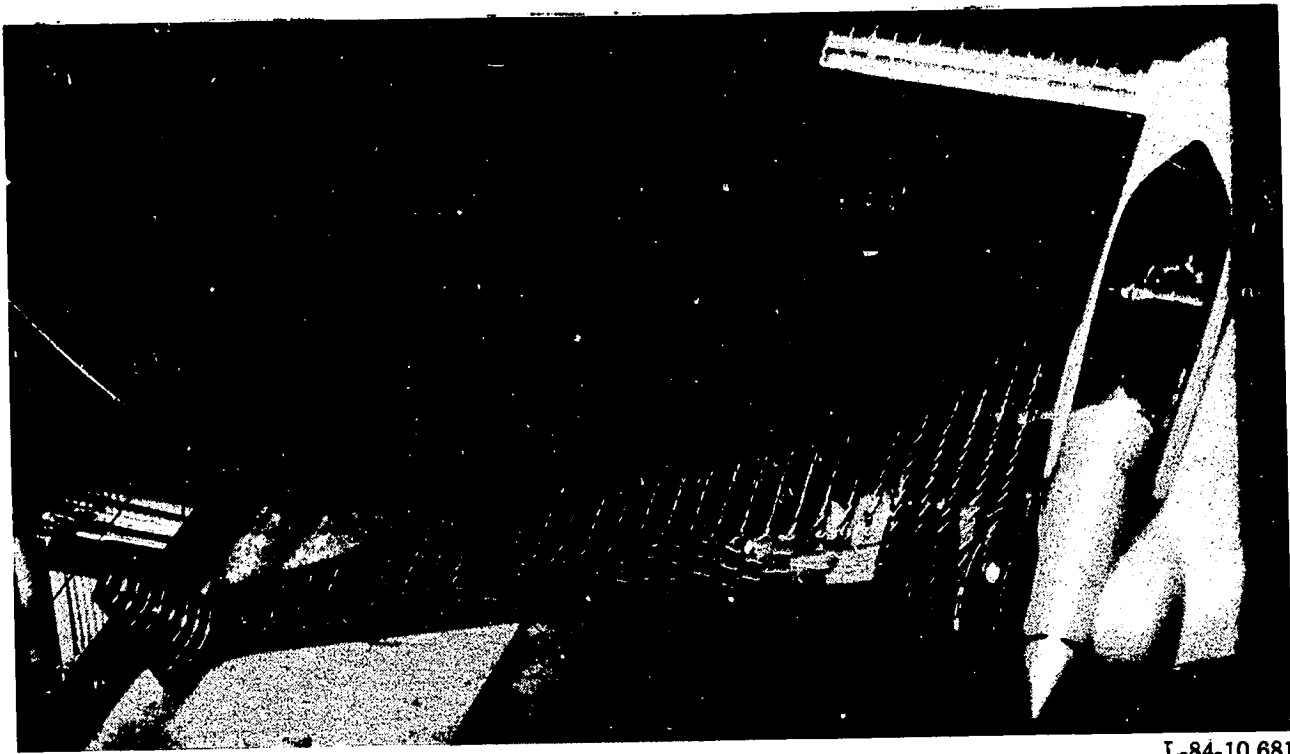
L-84-10,681

(k) $\alpha = 15.5°$.
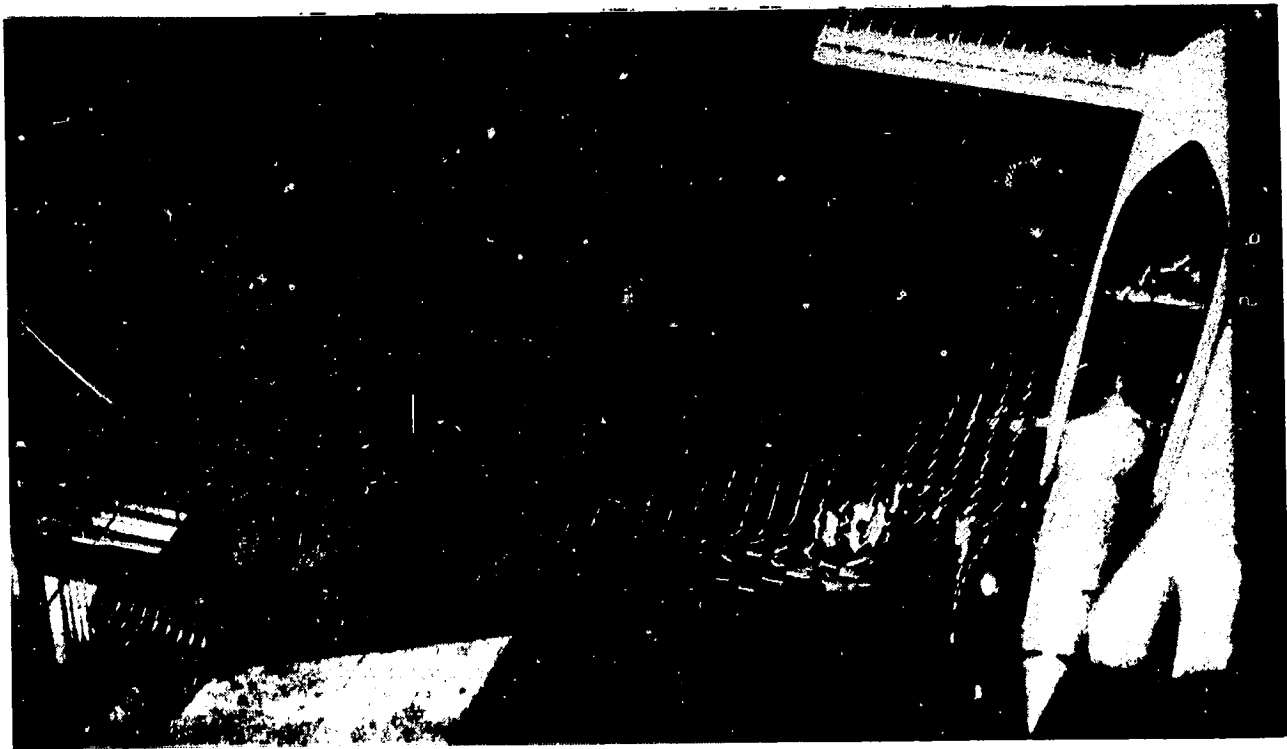
L-84-10,682

(l) $\alpha = 17.5°$.

Figure 8. Continued.

41
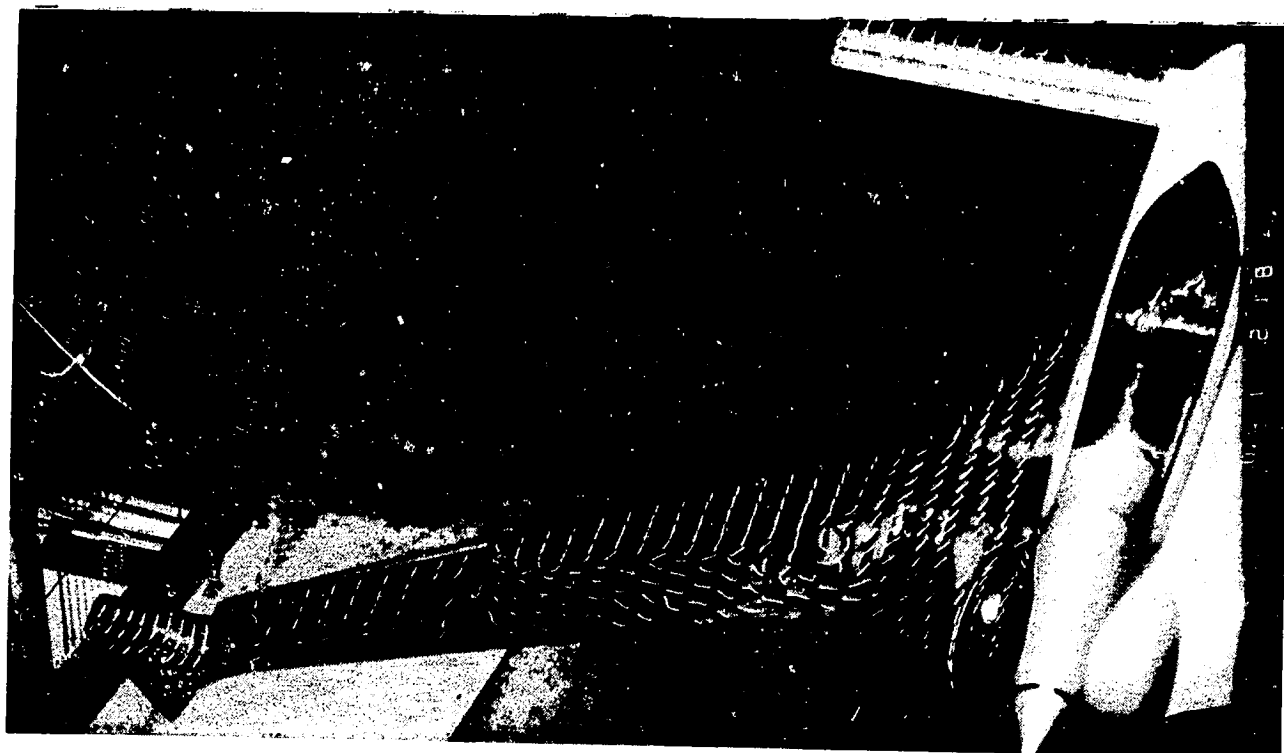
L-84-10,683

(m) $\alpha = 19.5°$.
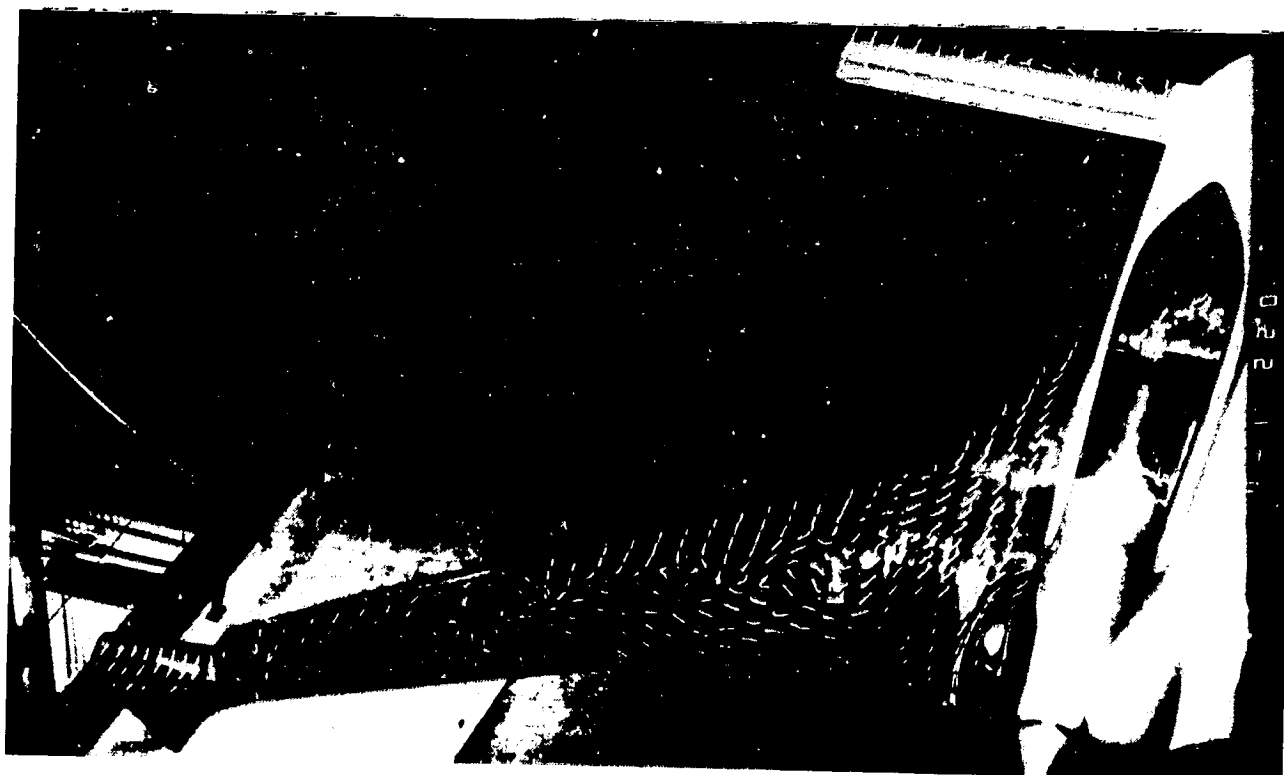
L-84-10,684

(n) $\alpha = 21.5°$.

Figure 8. Continued.

(o) $\alpha = 23.5°$.

L-84-10,685

(p) $\alpha = 25.5°$.

L-84-10,686

Figure 8. Concluded.

43
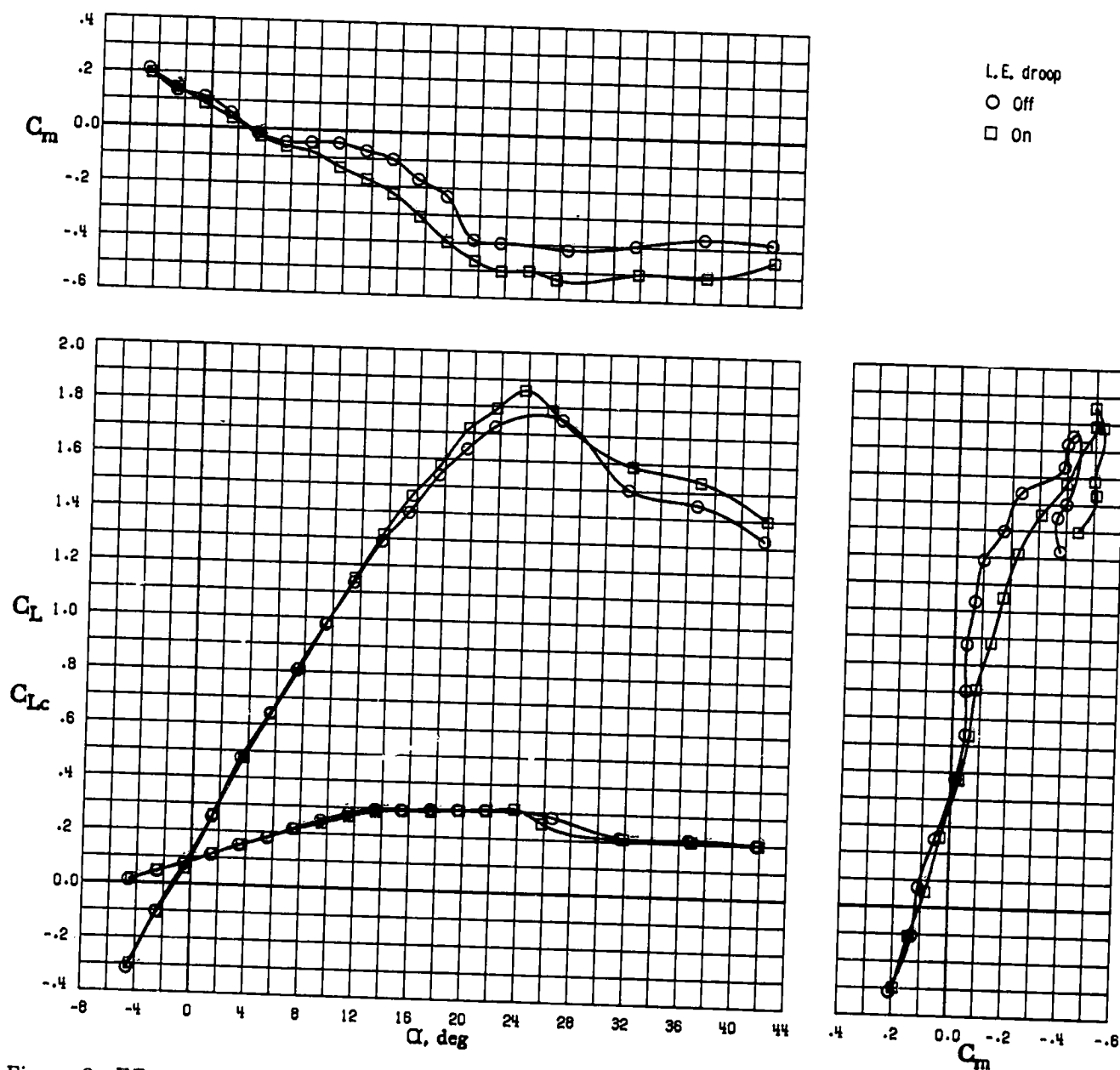
Figure 9. Effect of wing outboard leading-edge droop on longitudinal aerodynamic characteristics of basic configuration.

44
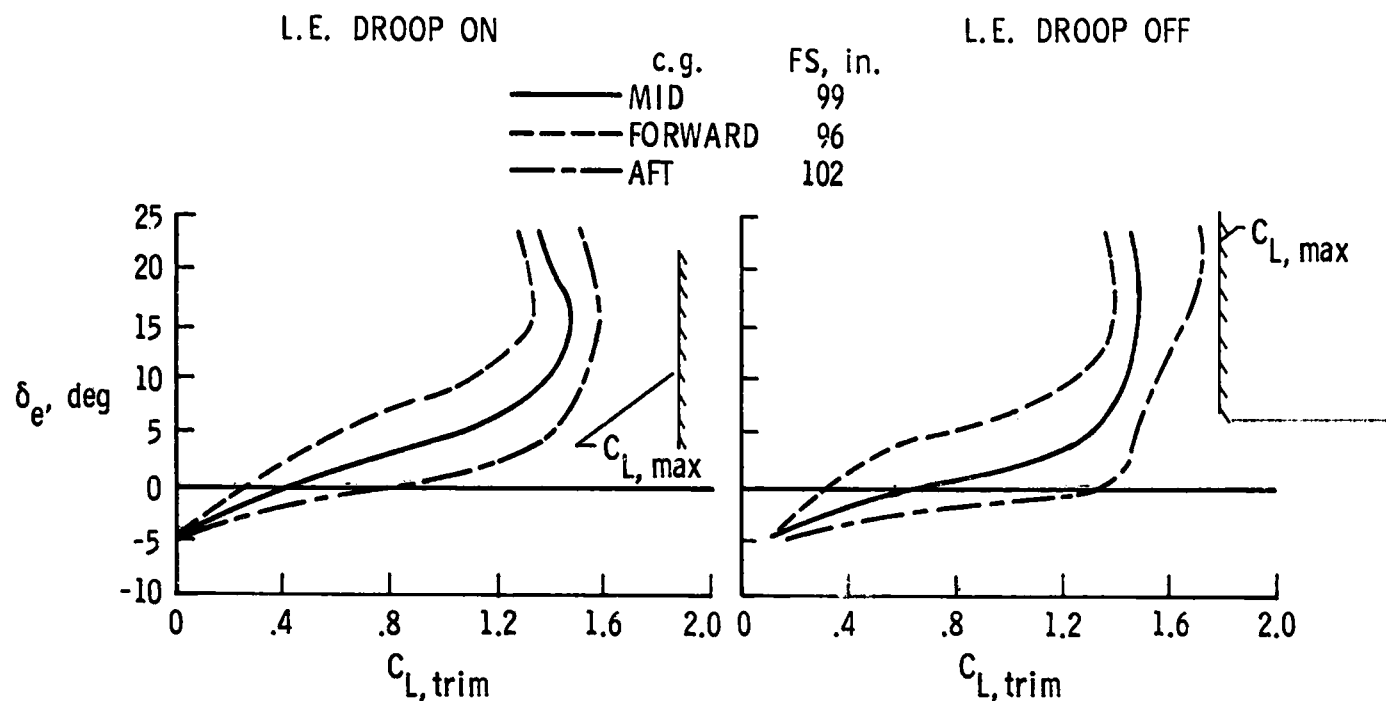
L.E. DROOP ON

Figure 10. Effect of leading-edge droop on elevator deflection required for trim.
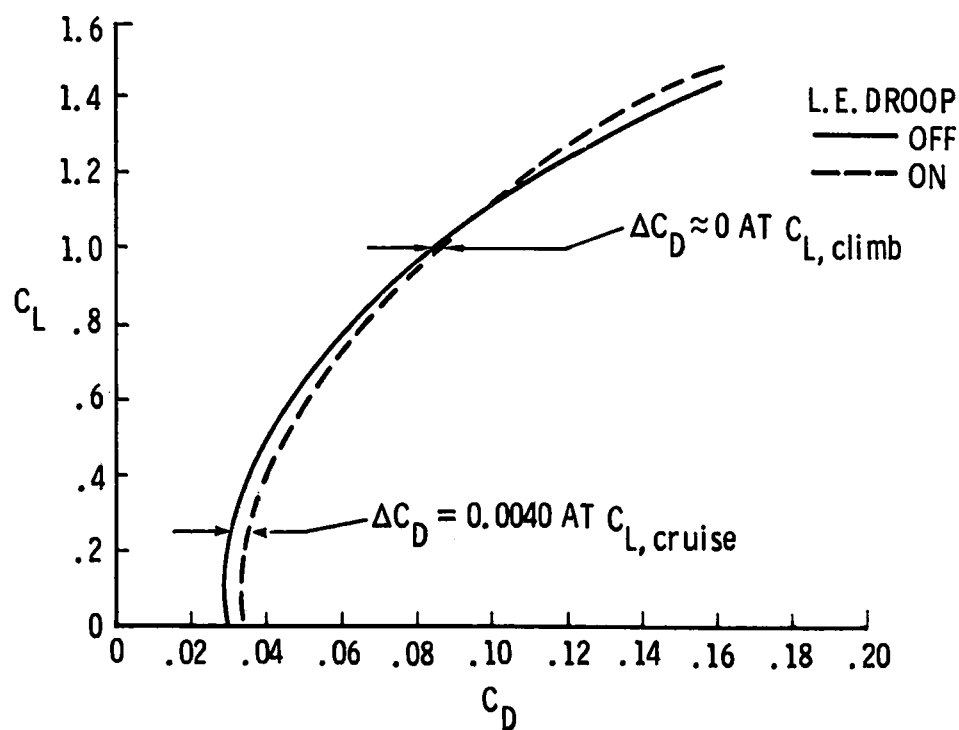
Figure 11. Effect of leading-edge droop on drag. Configuration trimmed at mid c.g. location (FS 99).
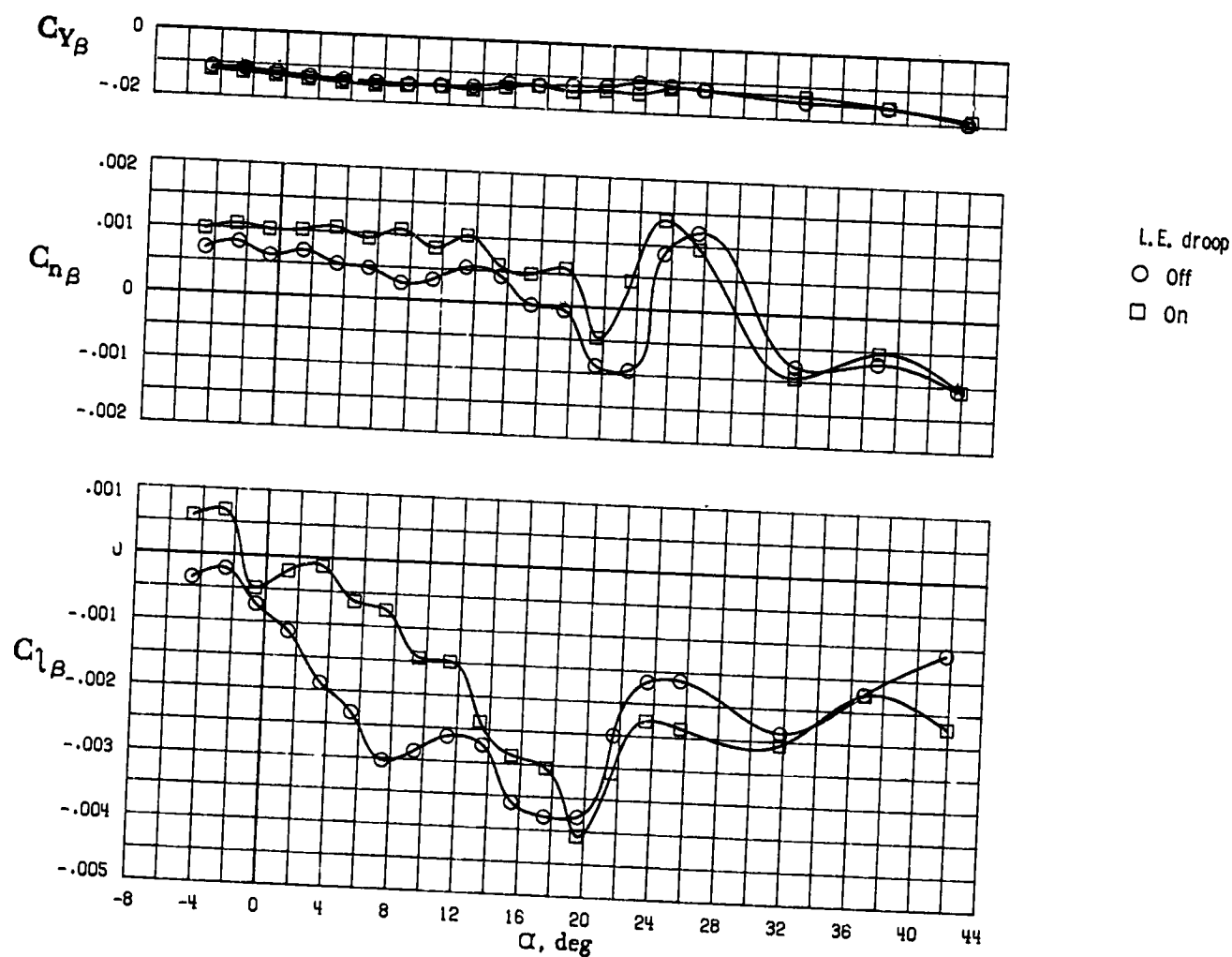
Figure 12. Effect of leading-edge droop on lateral-directional stability of basic configuration.
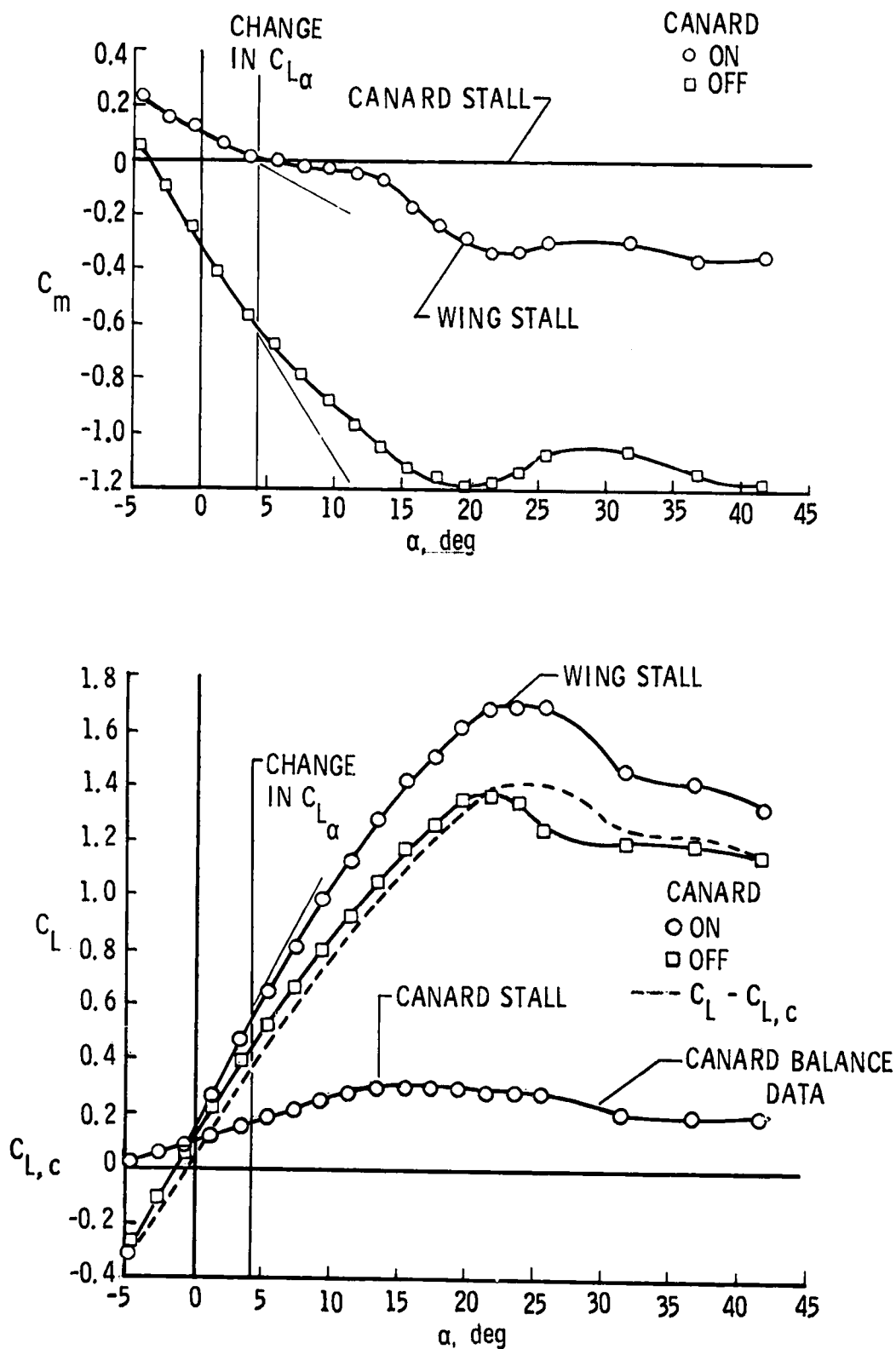
Figure 13. Effect of canard on lift and pitching-moment characteristics of basic configuration. Controls neutral; L.E. droop off; $R = 1.60 \times 10^6$.
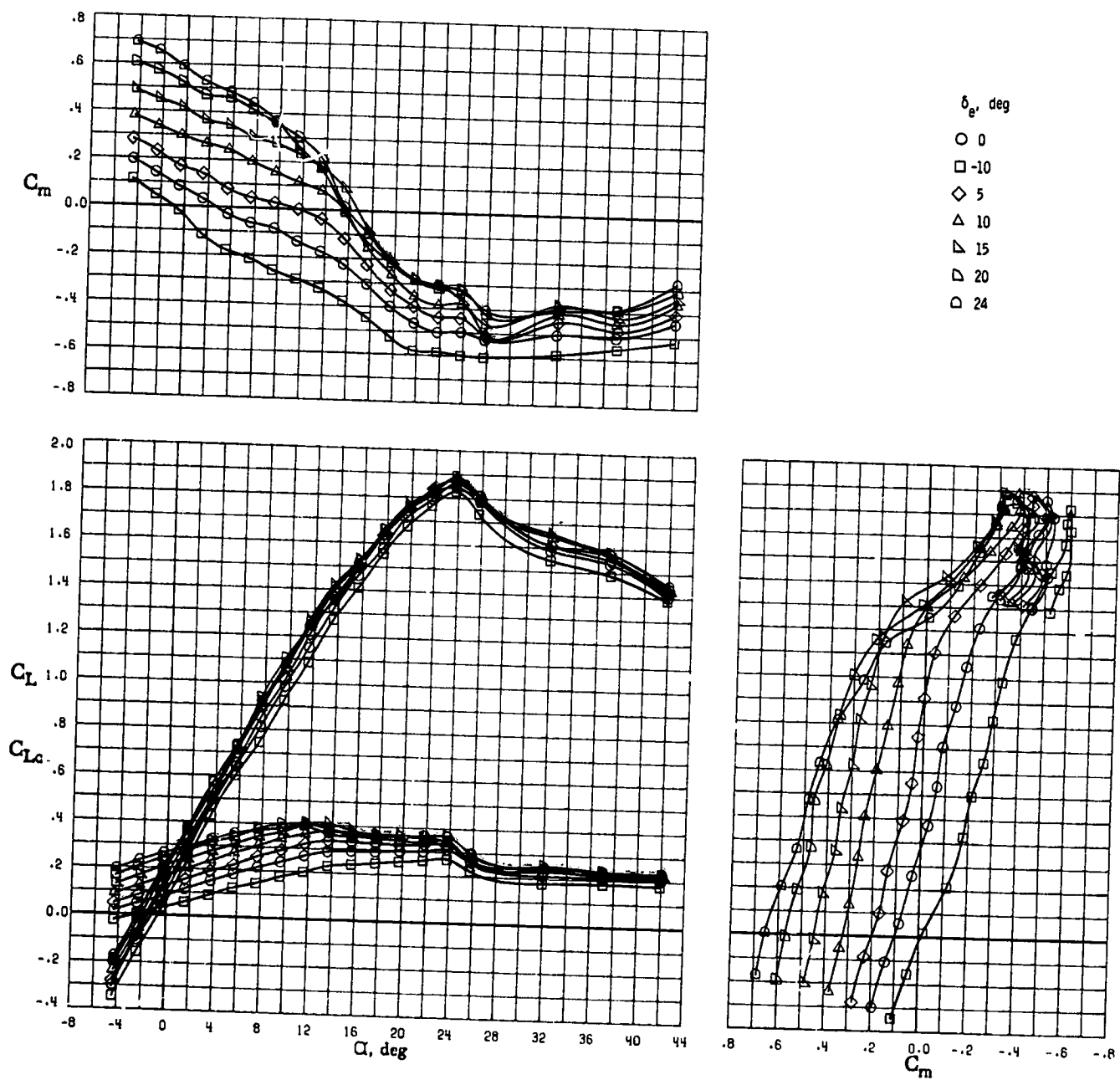
(a) Mid c.g. location (FS 99).

Figure 14. Effect of elevator deflection on longitudinal aerodynamic characteristics of basic configuration. L.E. droop on.
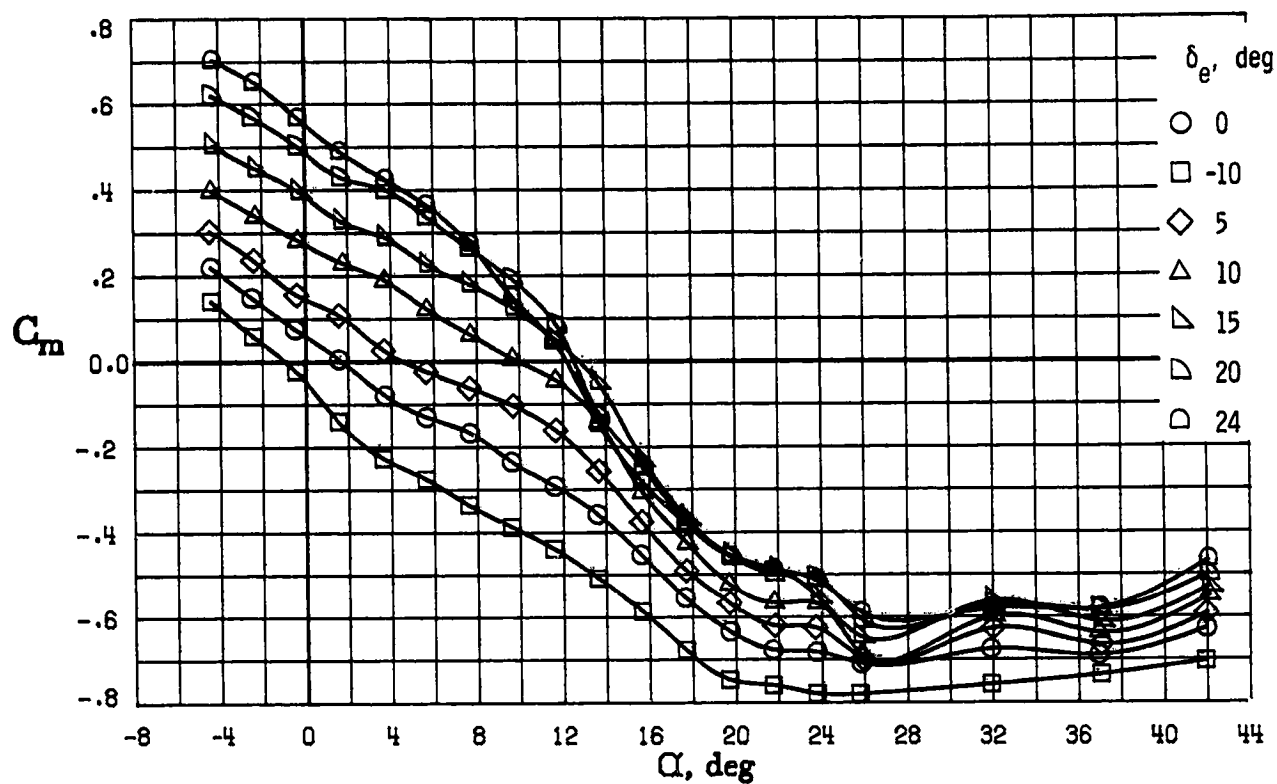
(b) Forward c.g. location (FS 96).
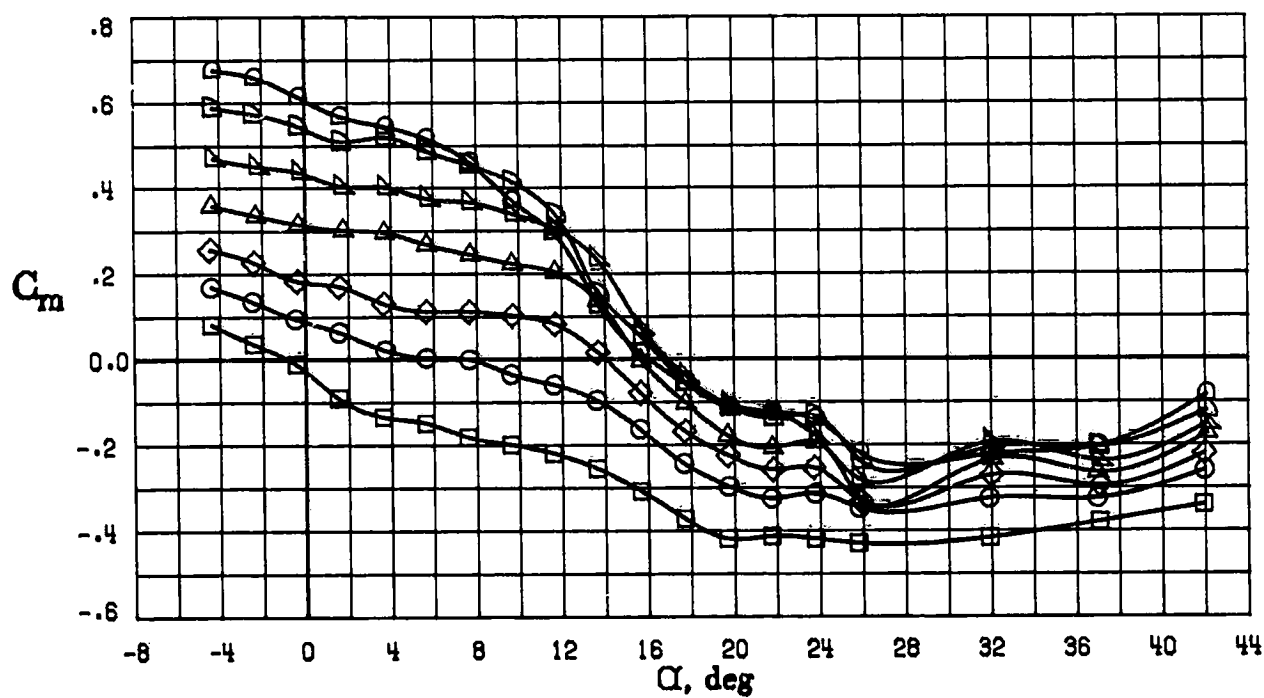
(c) Aft c.g. location (FS 102).

Figure 14. Concluded.
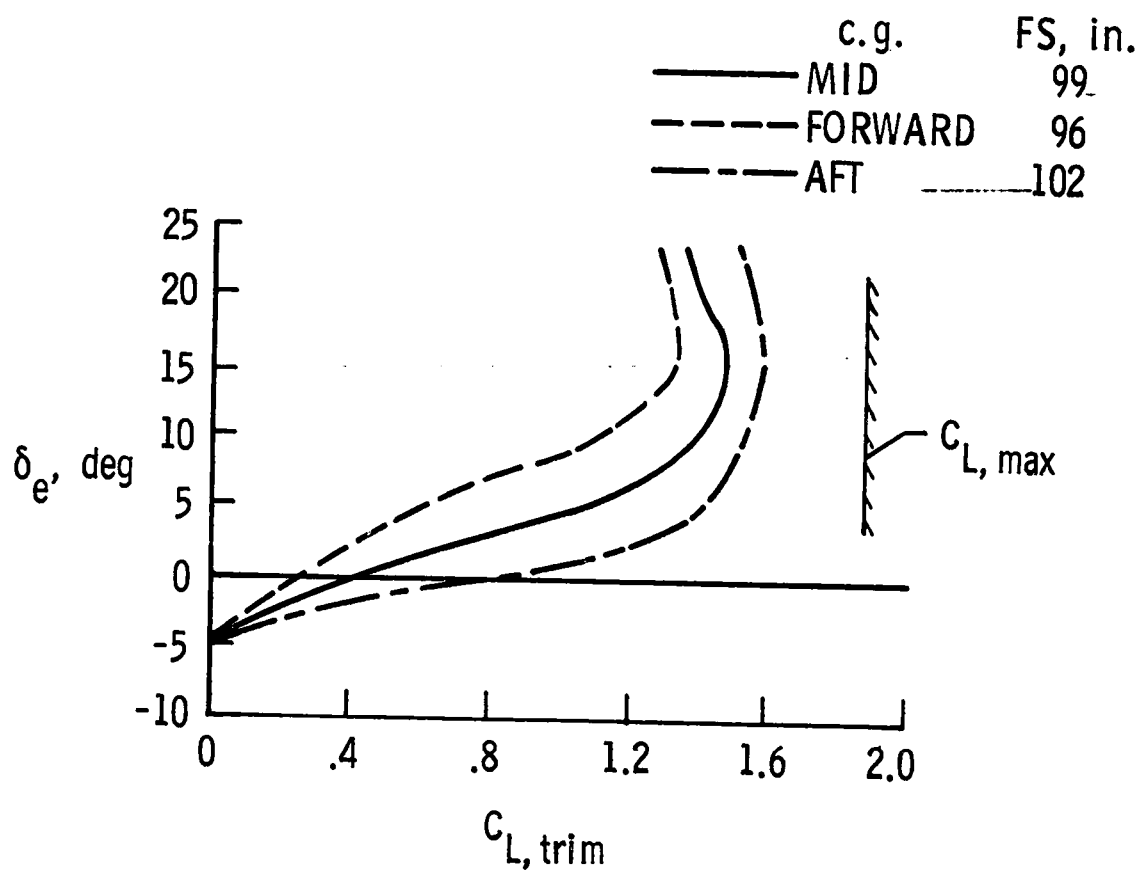
Figure 15. Effect of center-of-gravity location on elevator deflection required for trim. L.E. droop on.
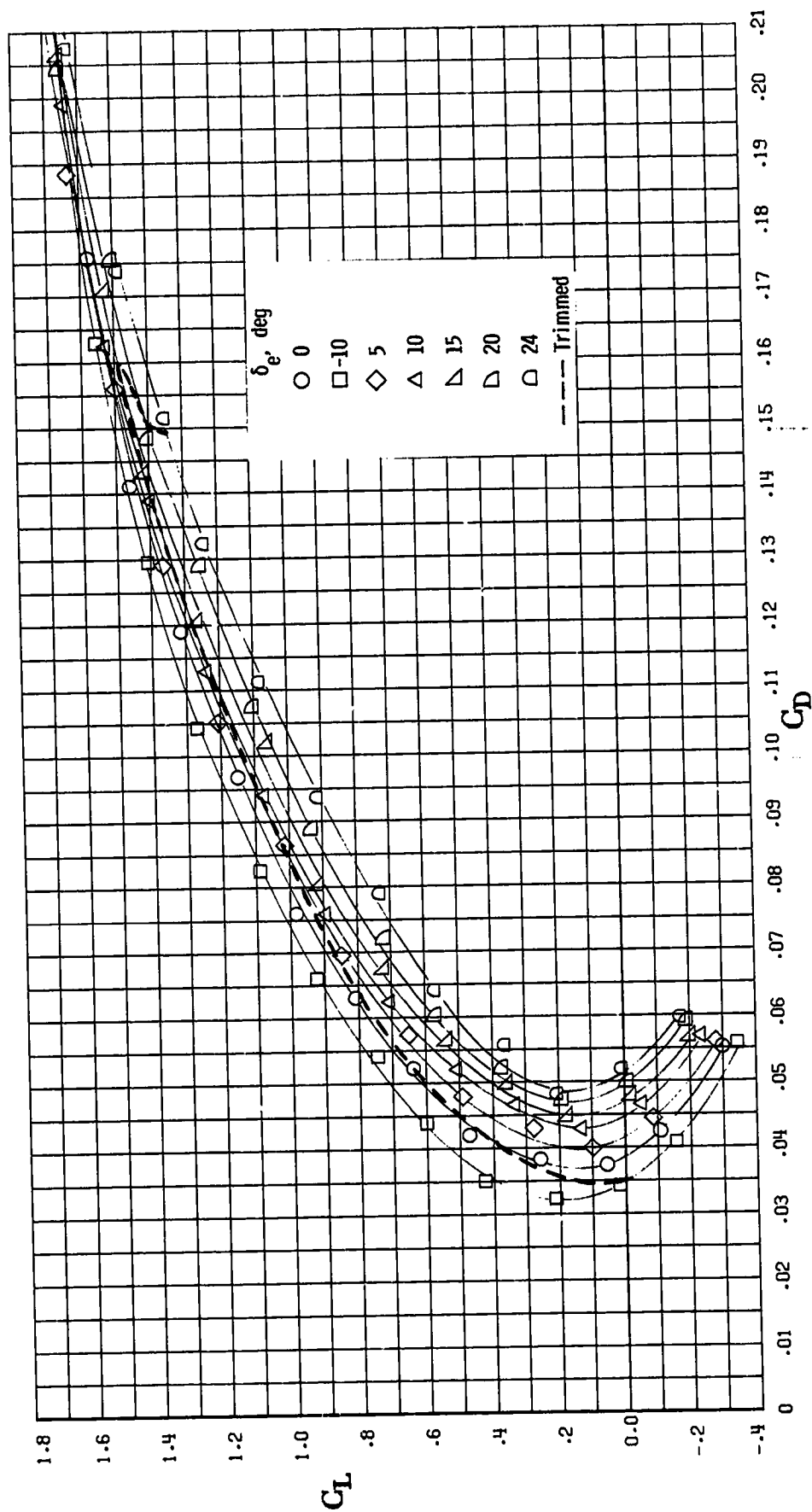
Figure 16. Effect of elevator deflection on drag characteristics of basic configuration. Trimmed drag curve indicated for mid c.g. location (FS 99); L.E. droop on.
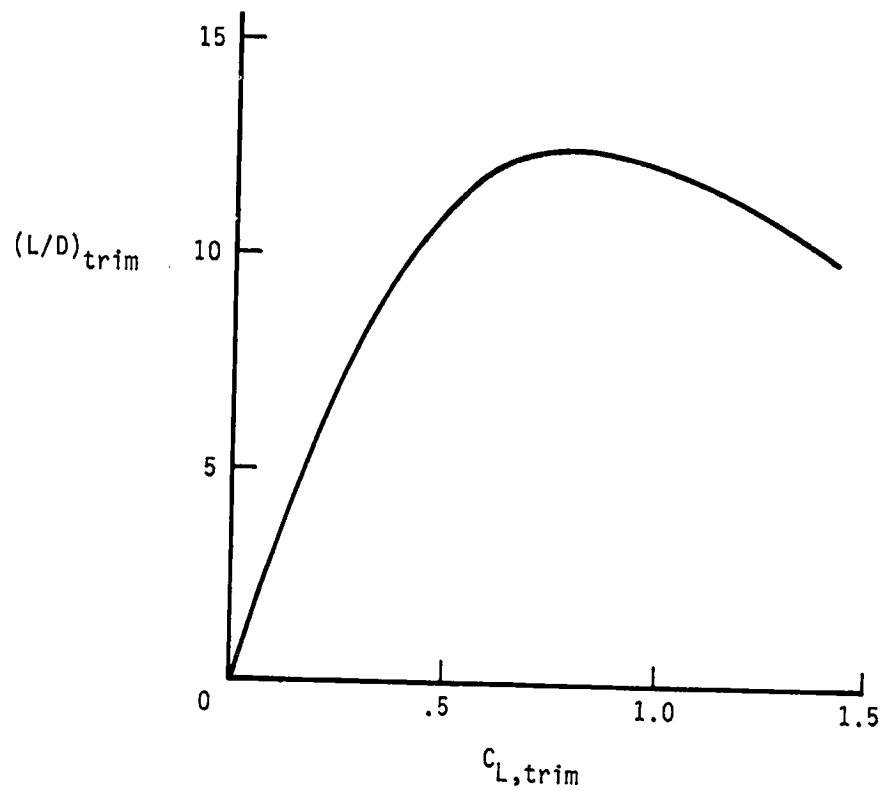
Figure 17. Trimmed lift-drag ratio of basic configuration. Mid c.g. location.
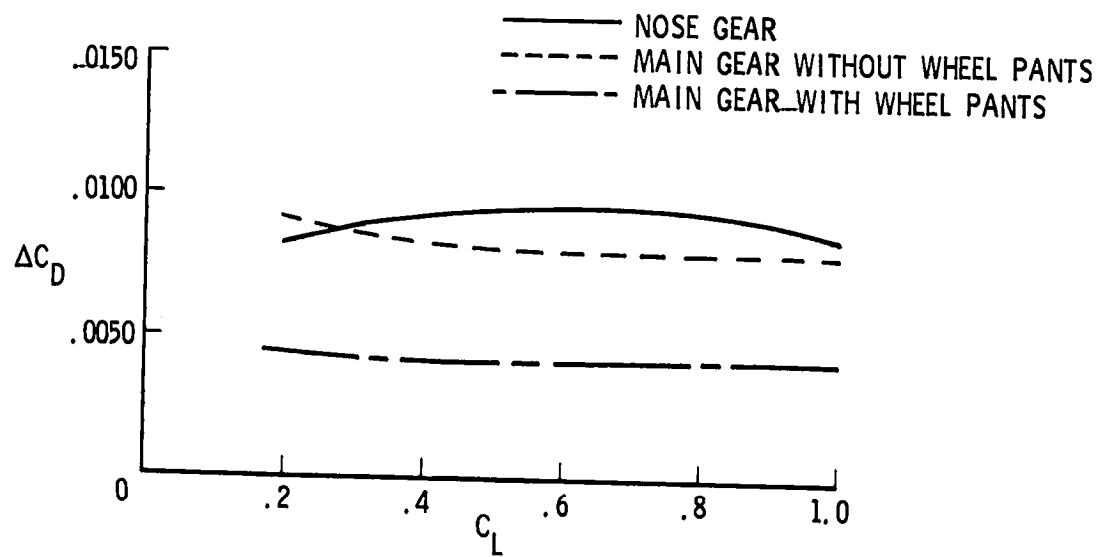
Figure 18. Drag increments of various landing-gear components.

$(L/D)_{max}$	Curve	c.g.	Wheel pants	L.E. droop	Main gear
12.6	————————	Mid	Off	On	On
13.1	— — — — —	Aft	Off	On	On
14.1	——— ——	Aft	On	On	On
15.4	——— ———	Aft	On	Off	On
17.1	—— ———	Aft	On	Off	Off
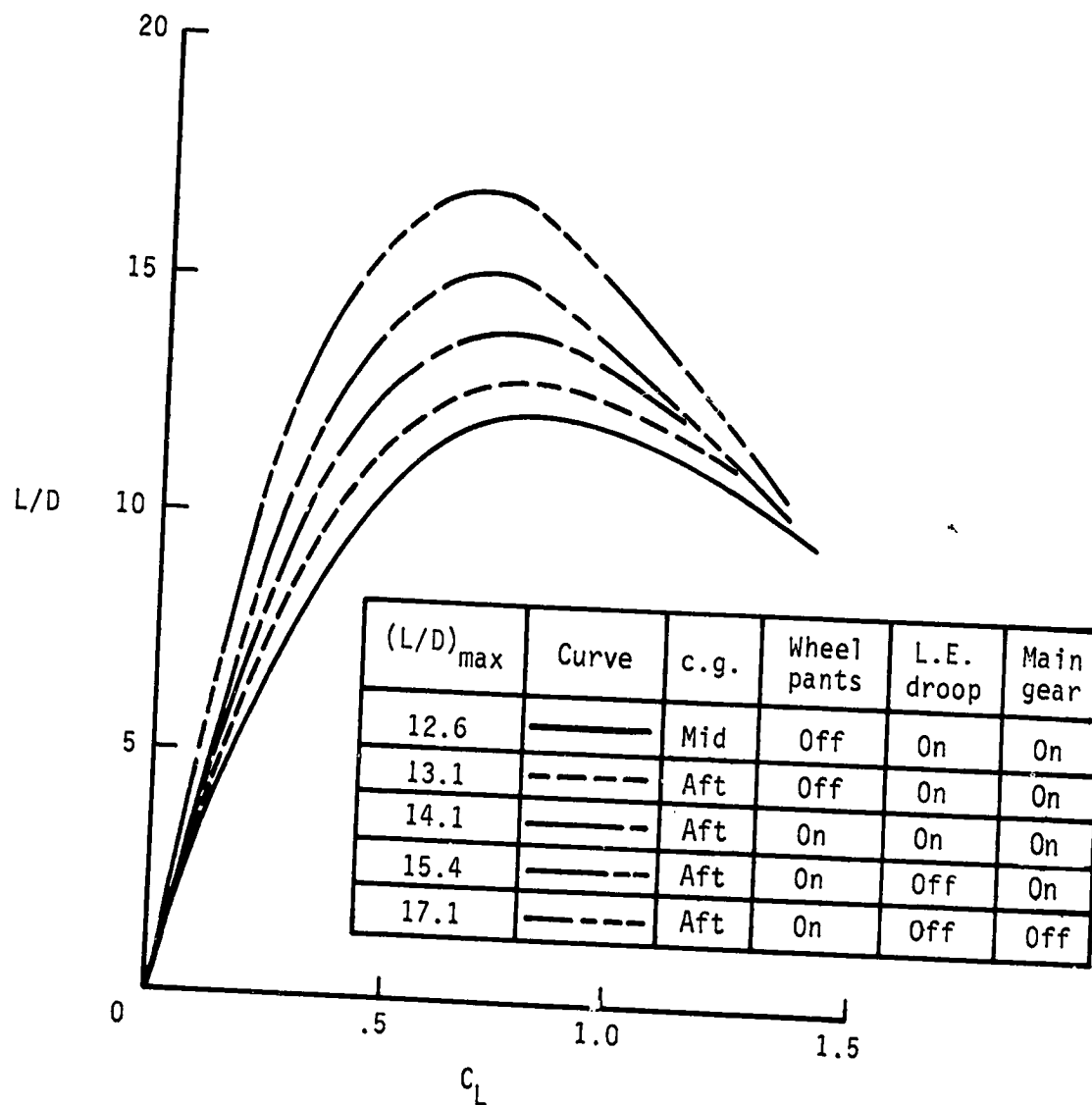
Figure 19. Trimmed lift-drag characteristics for various configuration changes.
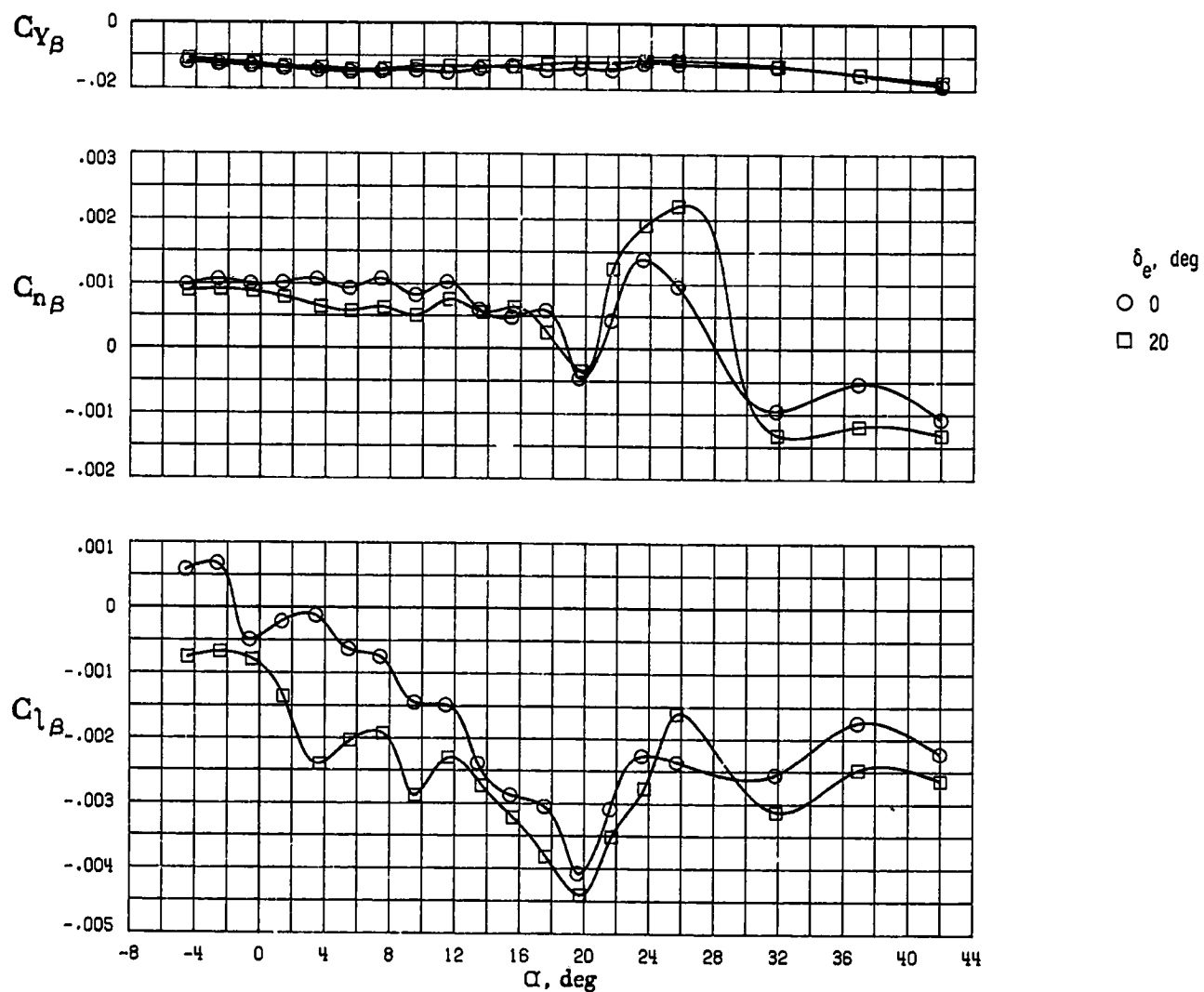
Figure 20. Effect of elevator deflection on lateral-directional stability characteristics of basic configuration. L.E. droop on.

54
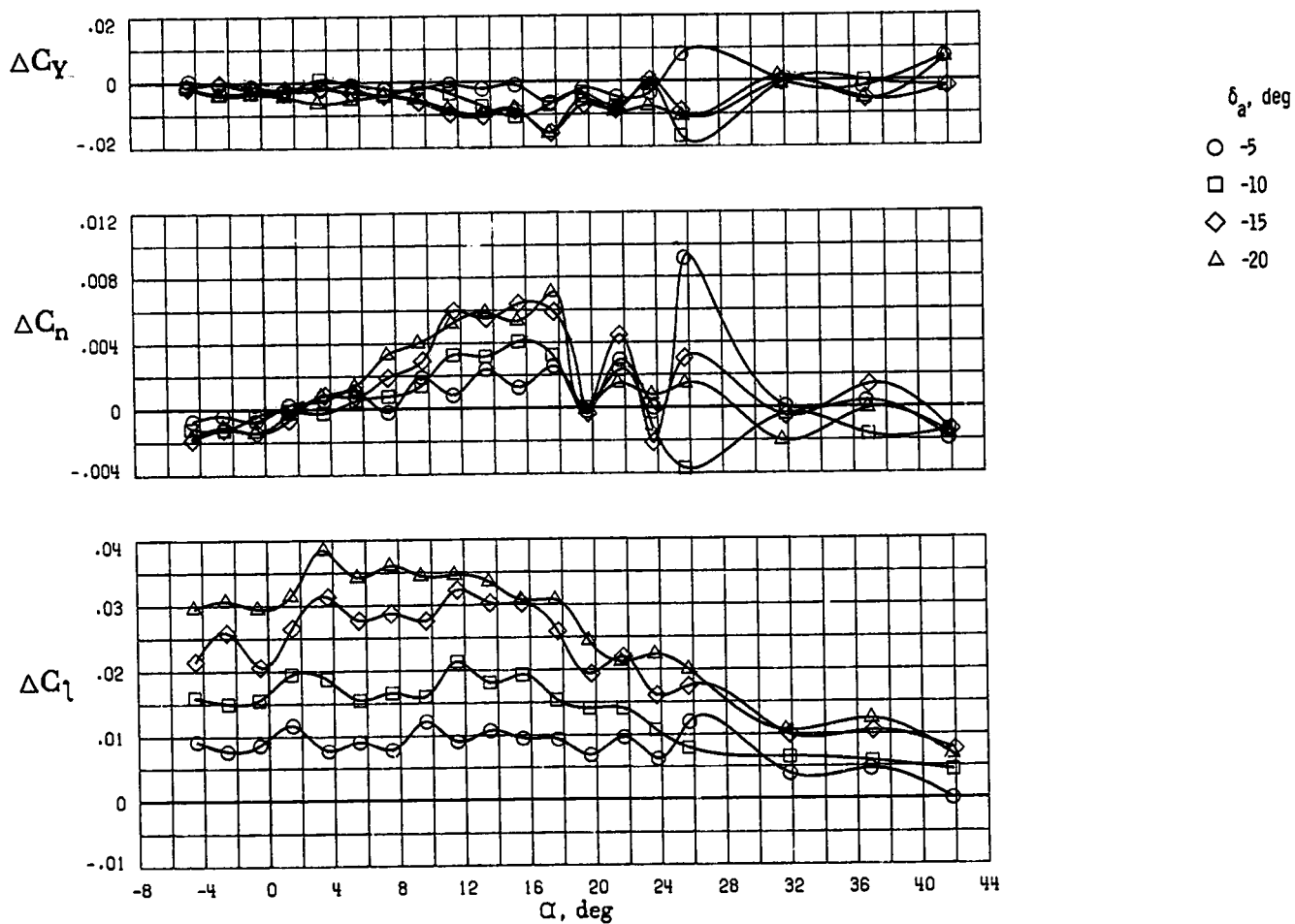
Figure 21. Aileron control authority of basic configuration. L.E. droop on.
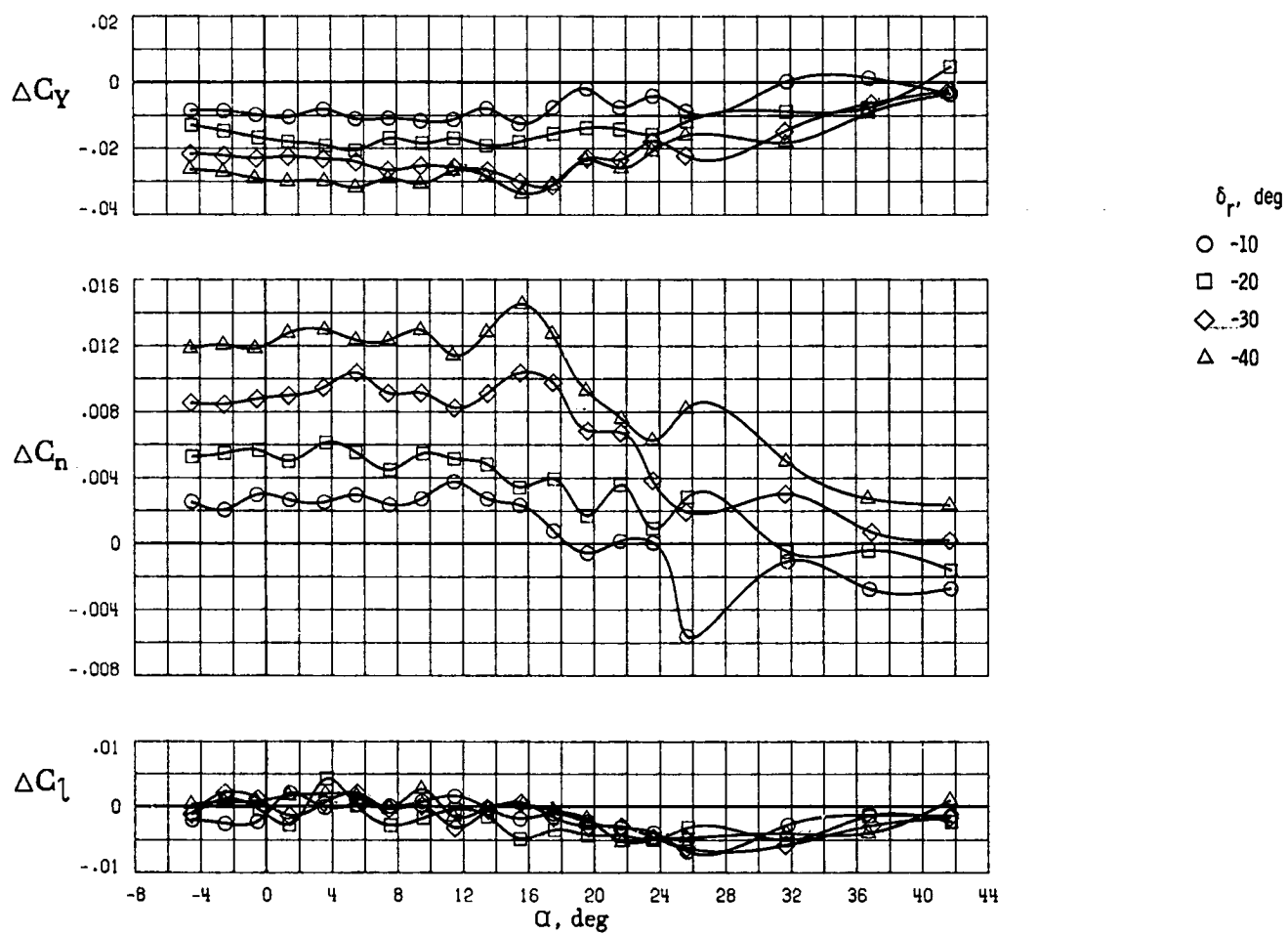
Figure 22. Rudder control authority of basic configuration. L.E. droop on.
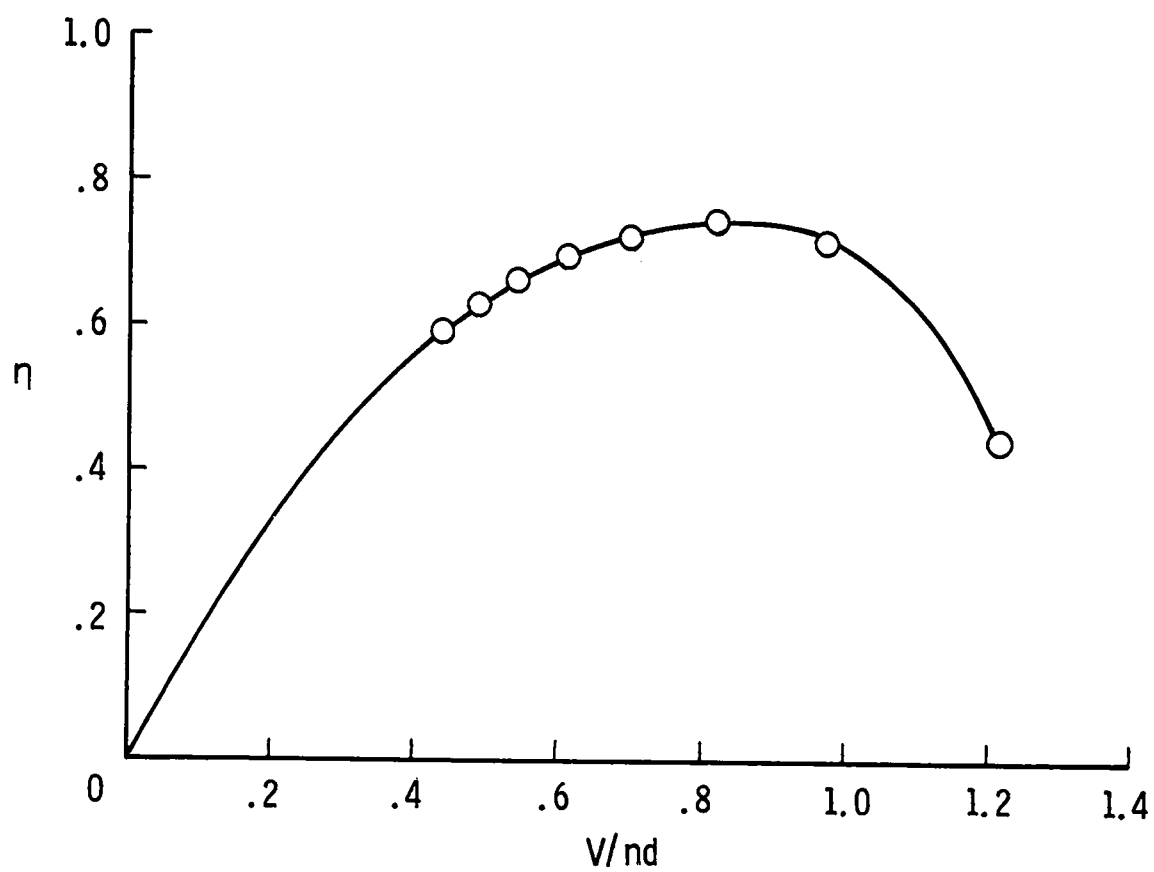
Figure 23. Measured propeller efficiency.
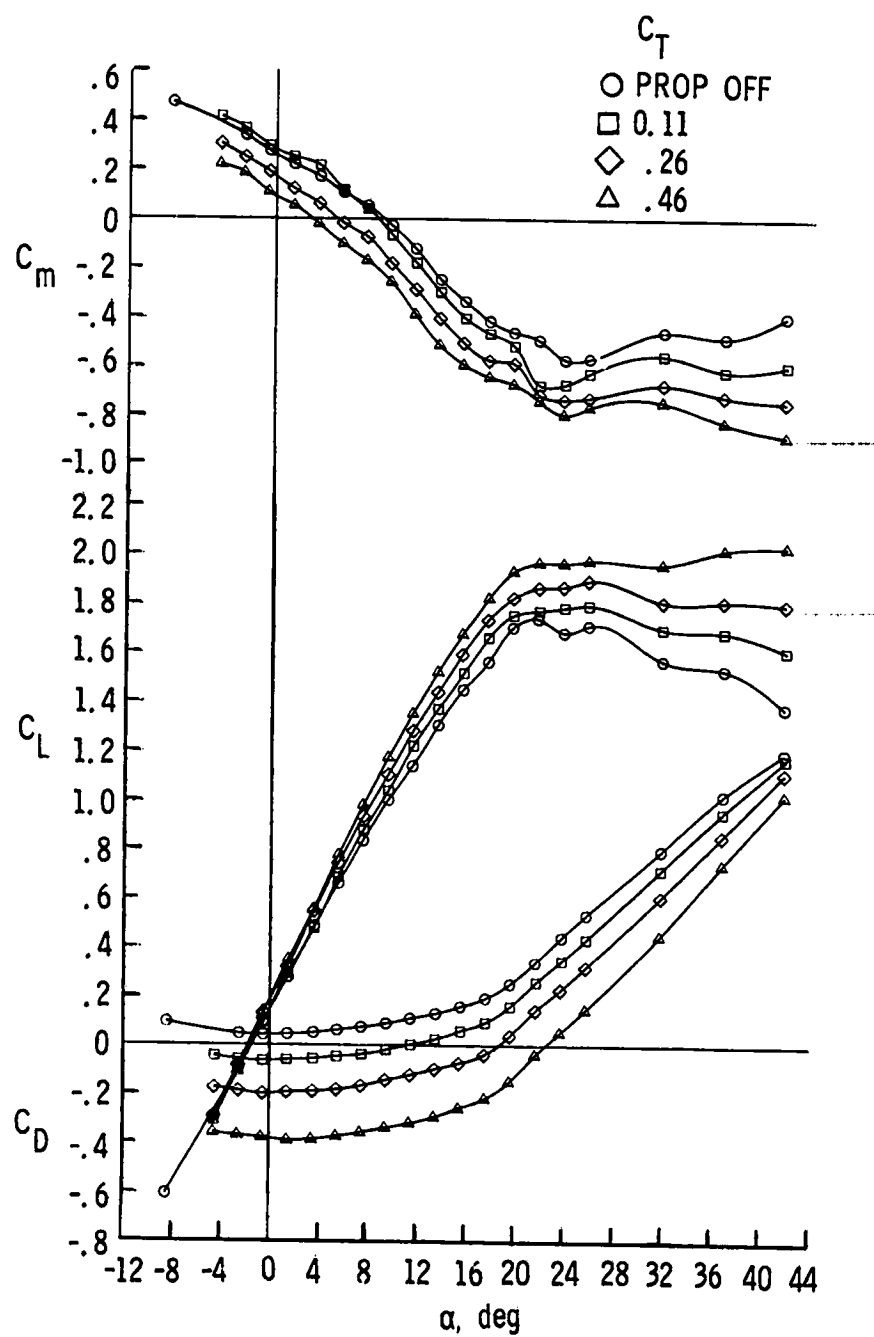
Figure 24. Effect of propeller thrust on longitudinal aerodynamic characteristics of basic configuration. L.E. droop on.
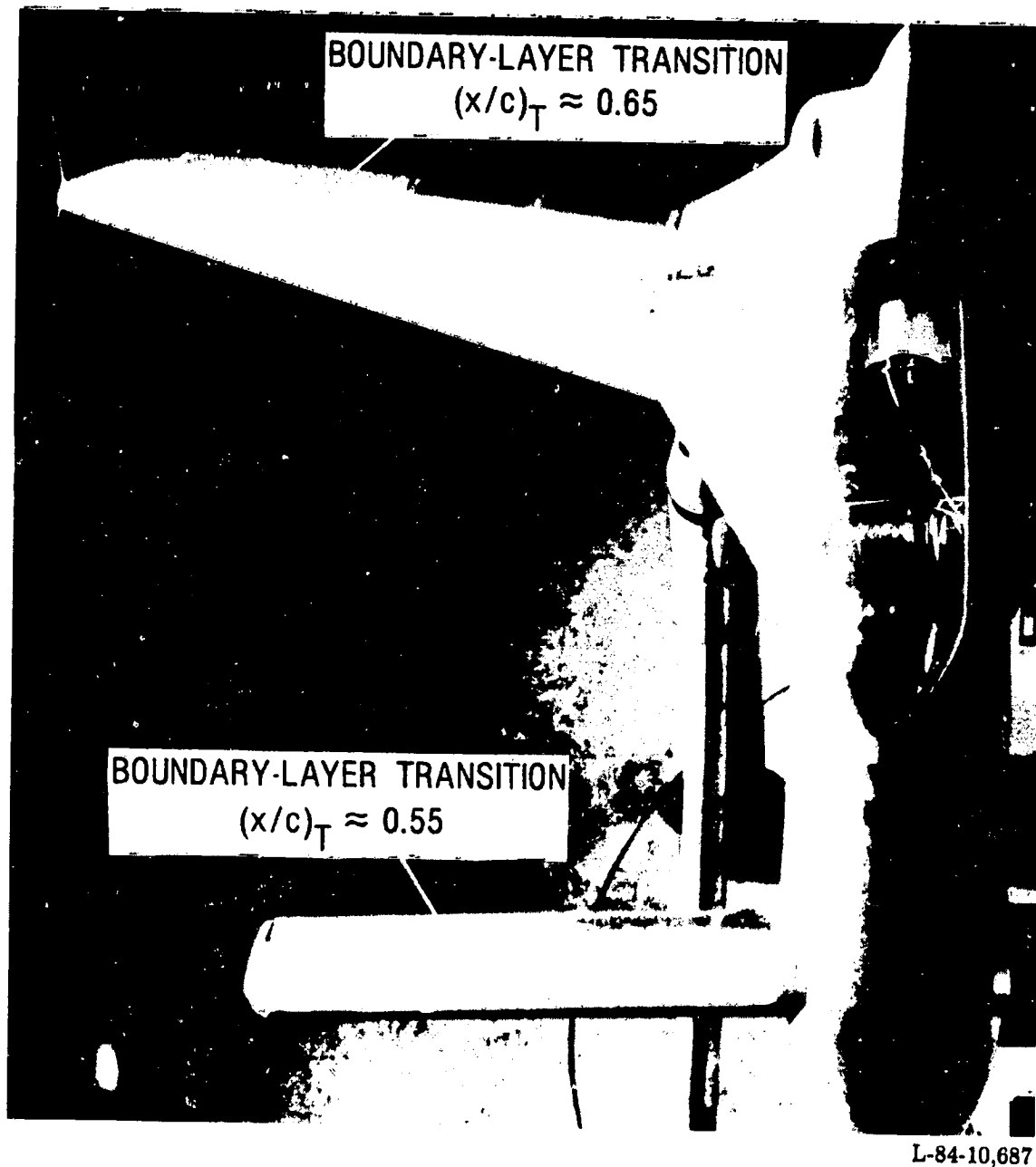
L-84-10,687

(a) Top view of wing and canard.

Figure 25. Flow visualization using sublimating chemicals to show natural boundary-layer transition. $\alpha = 1.5°$.

BOUNDARY-LAYER TRANSITION
$(x/c)_T \approx 0.55$
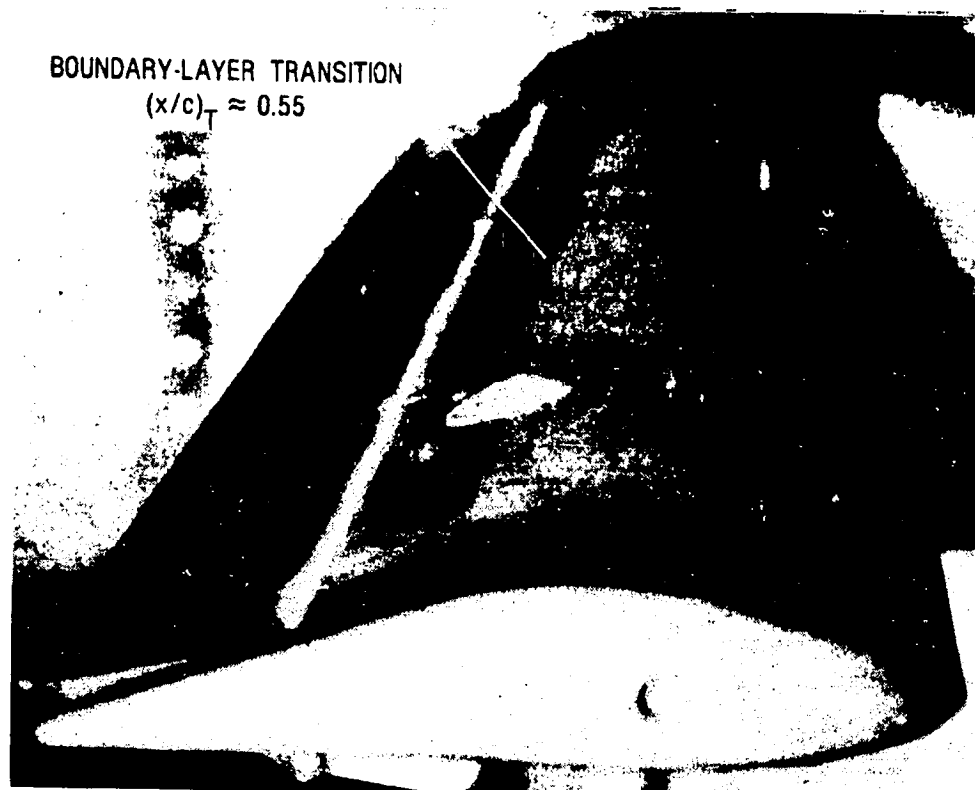
L-84-10,688

(b) Side view of canard.

Figure 25. Continued.

BOUNDARY-LAYER TRANSITION
$(x/c)_T \approx 0.6$

L-84-10,689

(c) Side view of winglet.

Figure 25. Concluded.
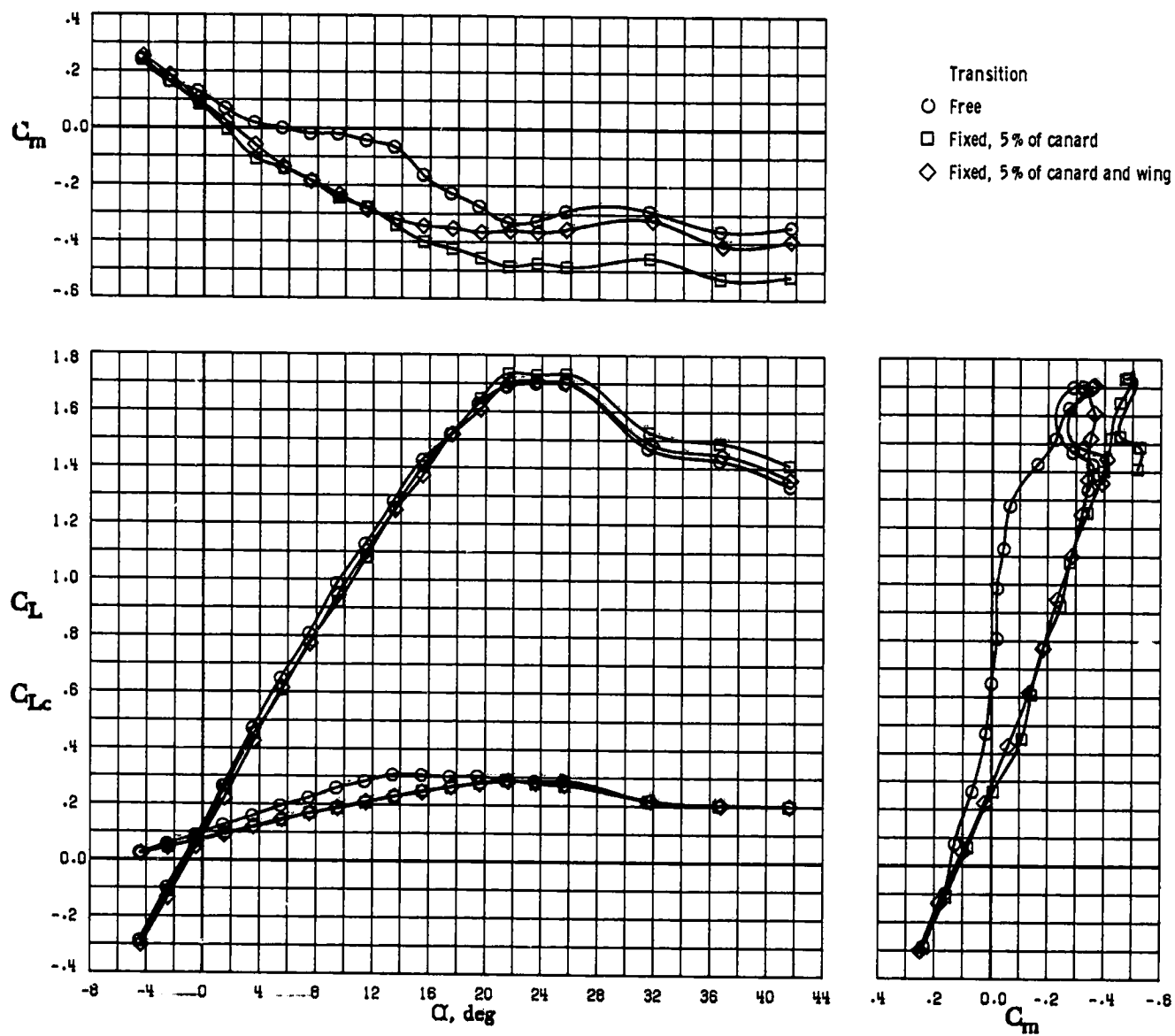
Figure 26. Effect of fixed transition on longitudinal aerodynamic characteristics of basic configuration. L.E. droop off.
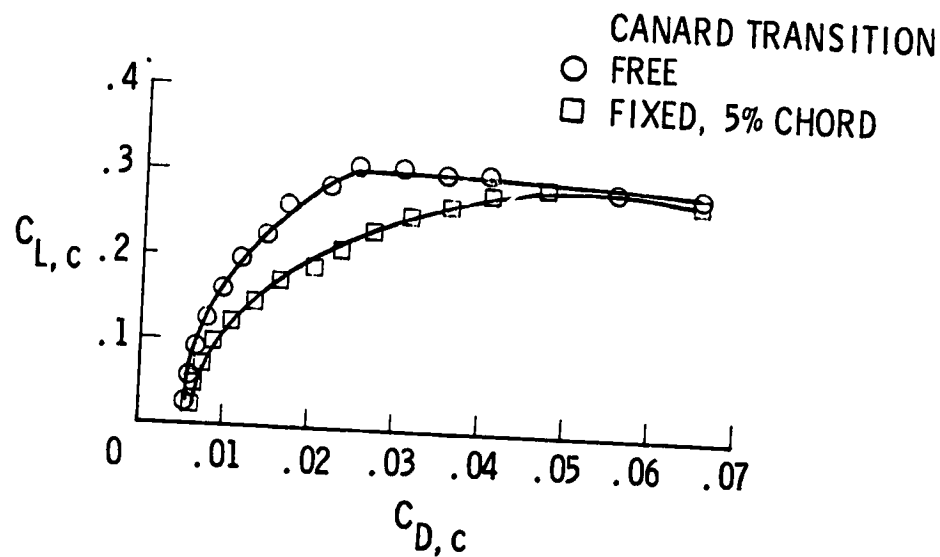
Figure 27. Effect of fixed transition on lift-drag characteristics of canard.
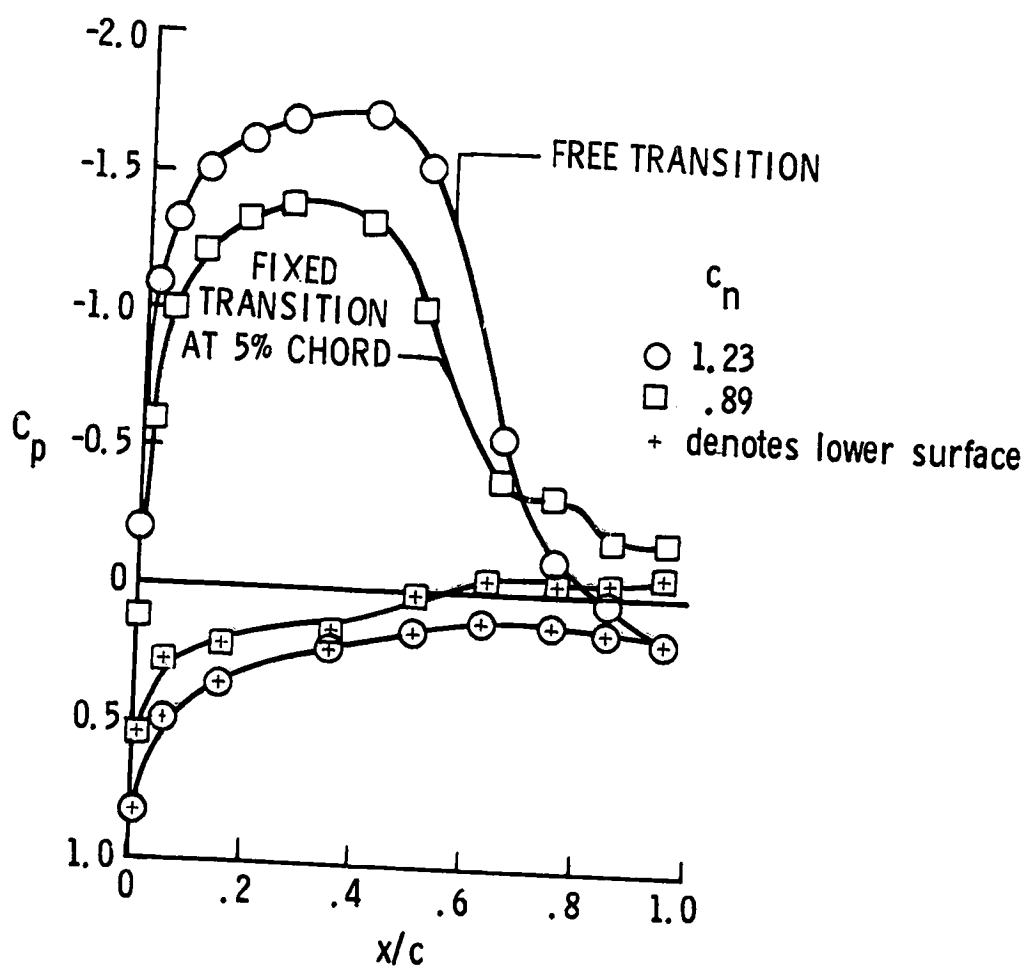
Figure 28. Effect of fixed transition on chordwise pressure distribution of canard. $\alpha = 8.0°$.
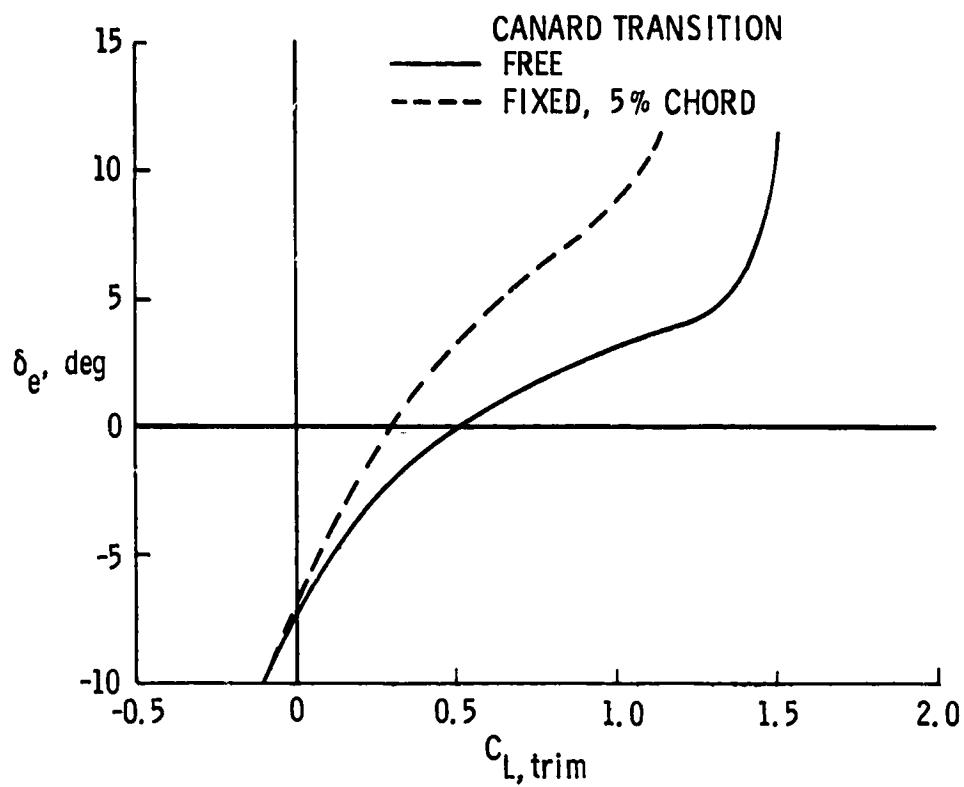
Figure 29. Effect of fixed transition on elevator deflection required for trim. L.E. droop off; mid c.g. location (FS 99).
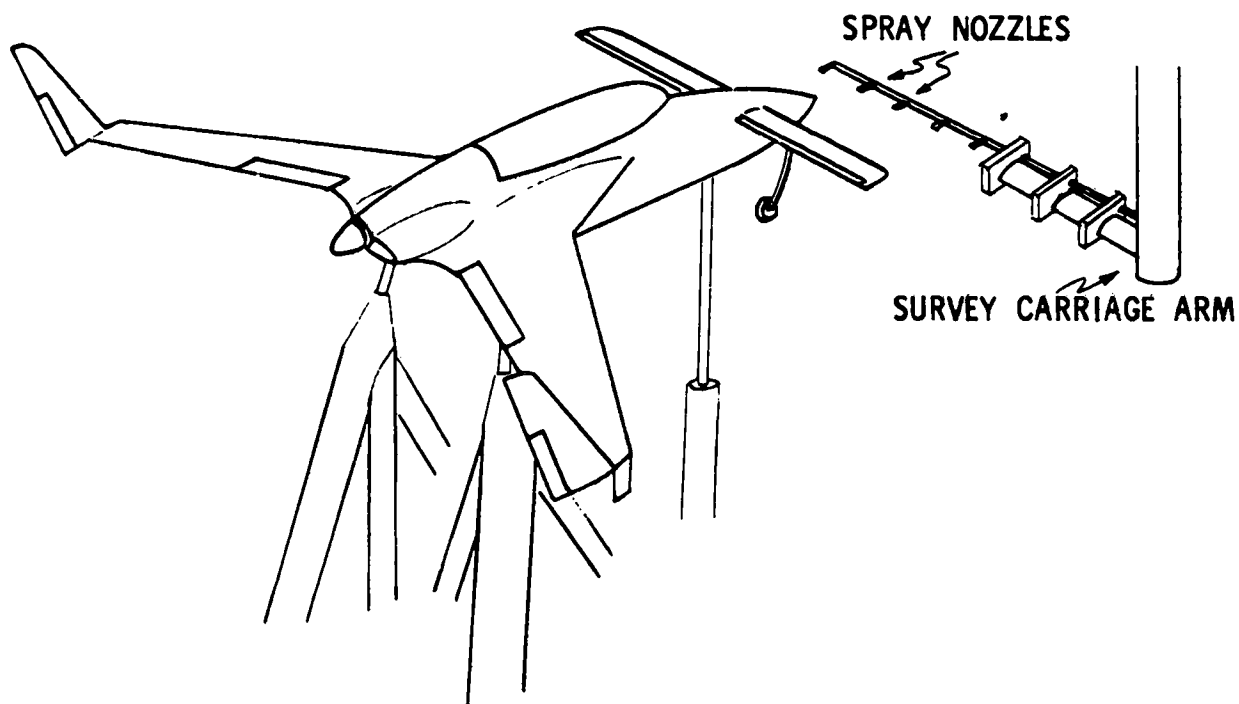
Figure 30. Water-spray boom.
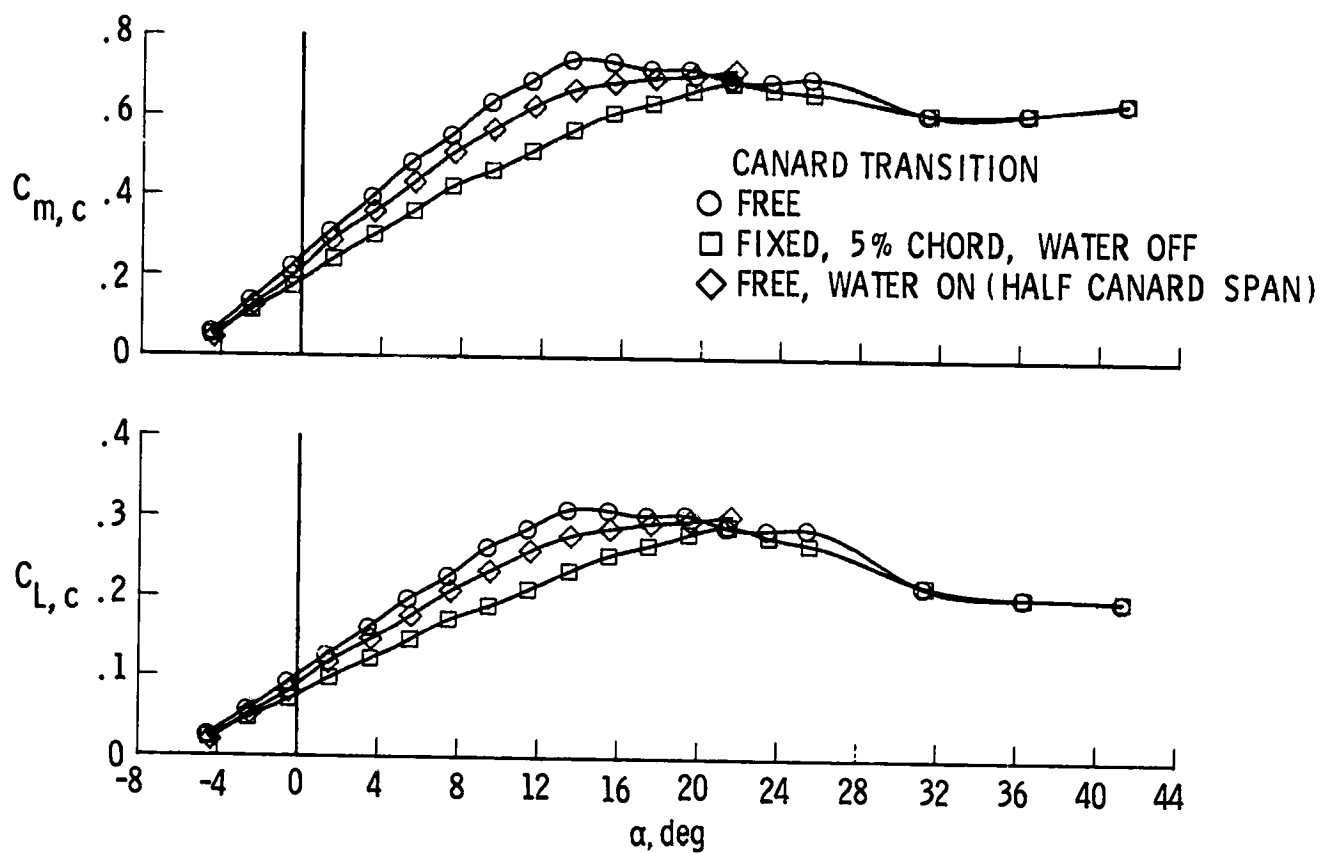
(a) Lift and pitching-moment characteristics.
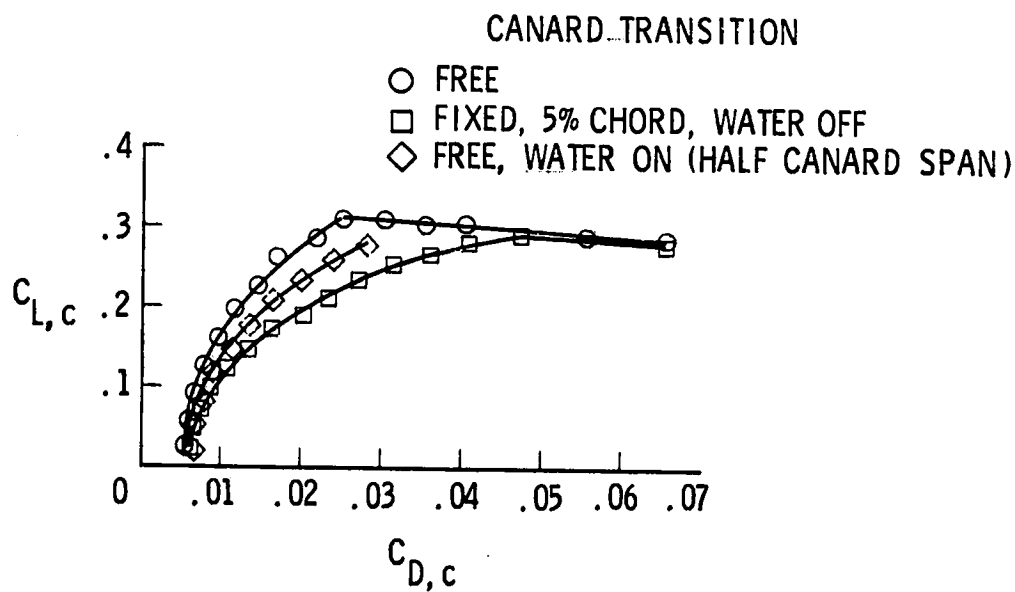
(b) Drag characteristics.

Figure 31. Effect of water spray on canard of basic configuration. Mid c.g. location (FS 99).
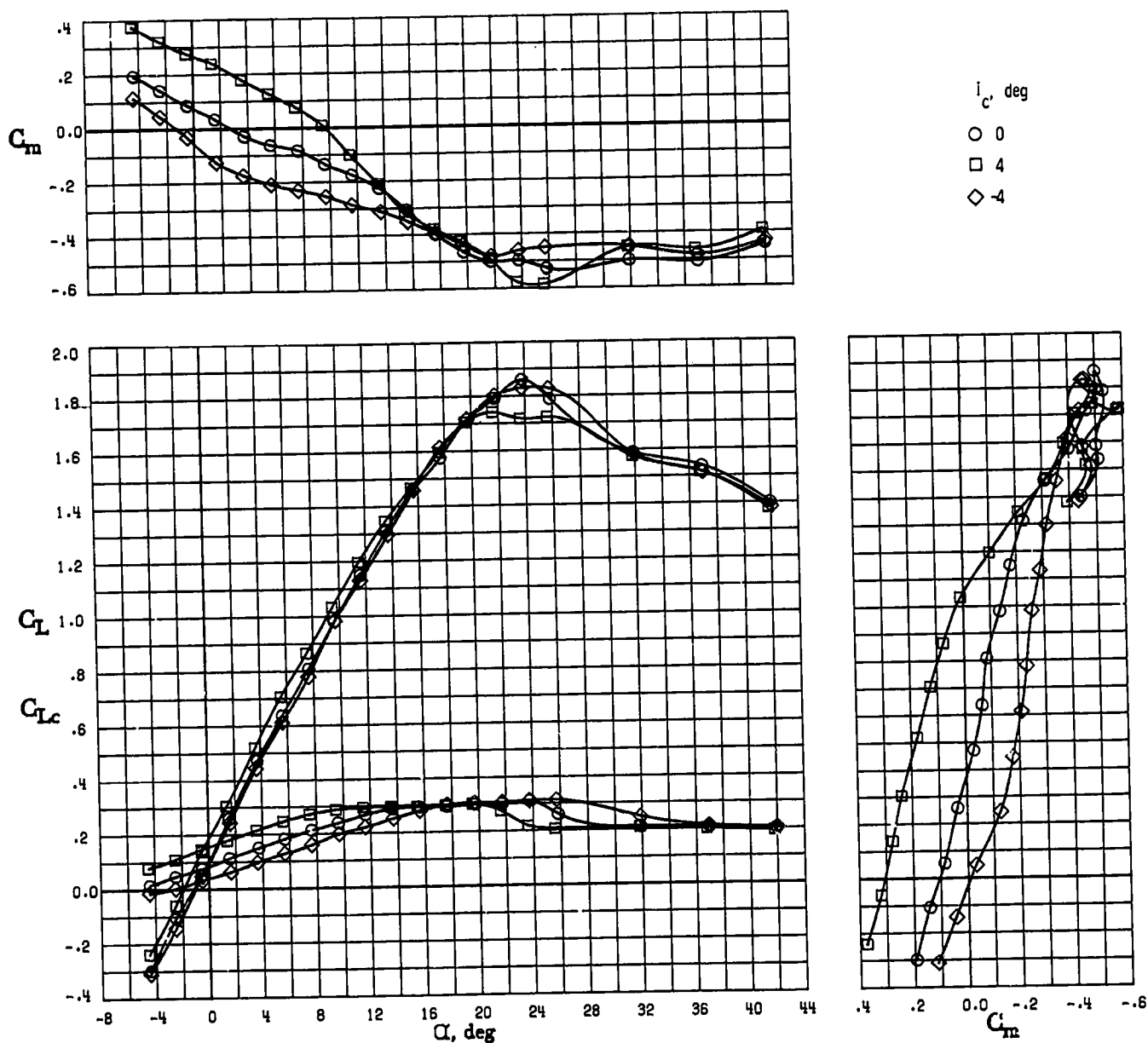
Figure 32. Effect of canard incidence on longitudinal aerodynamic characteristics of basic configuration. L.E. droop on; mid c.g. location (FS 99).
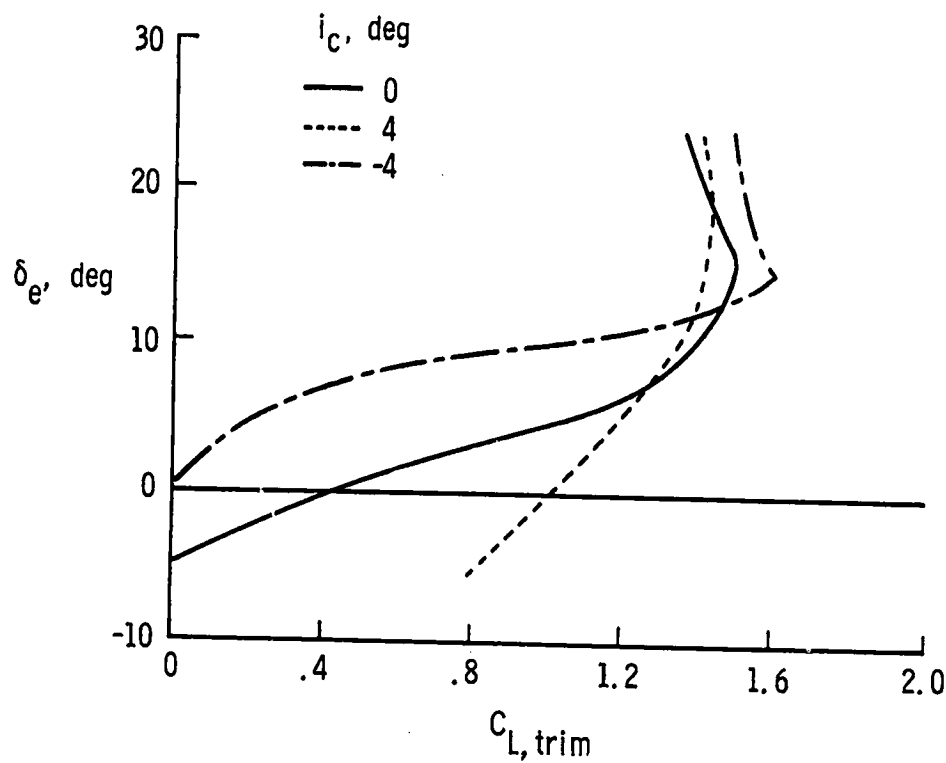
Figure 33. Effect of canard incidence on elevator deflection required for trim. L.E. droop on; mid c.g. location (FS 99).
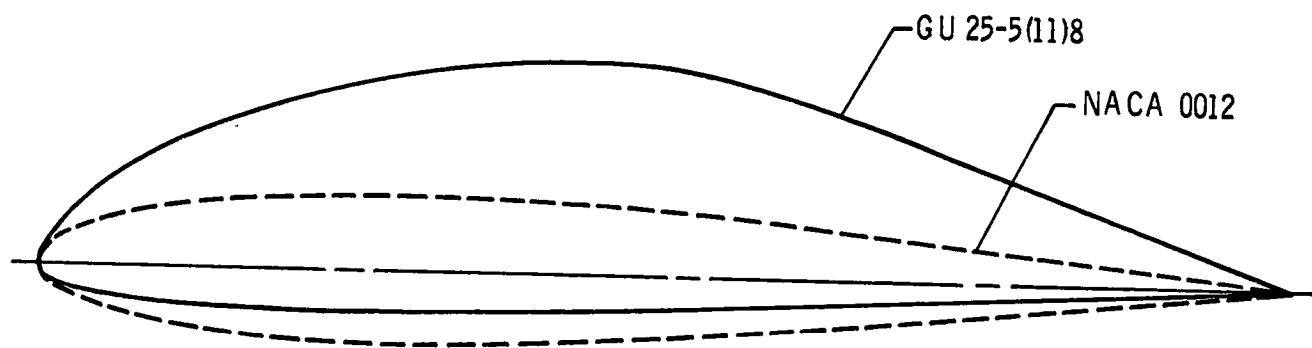
Figure 34. Comparison of canard airfoil-section contours.
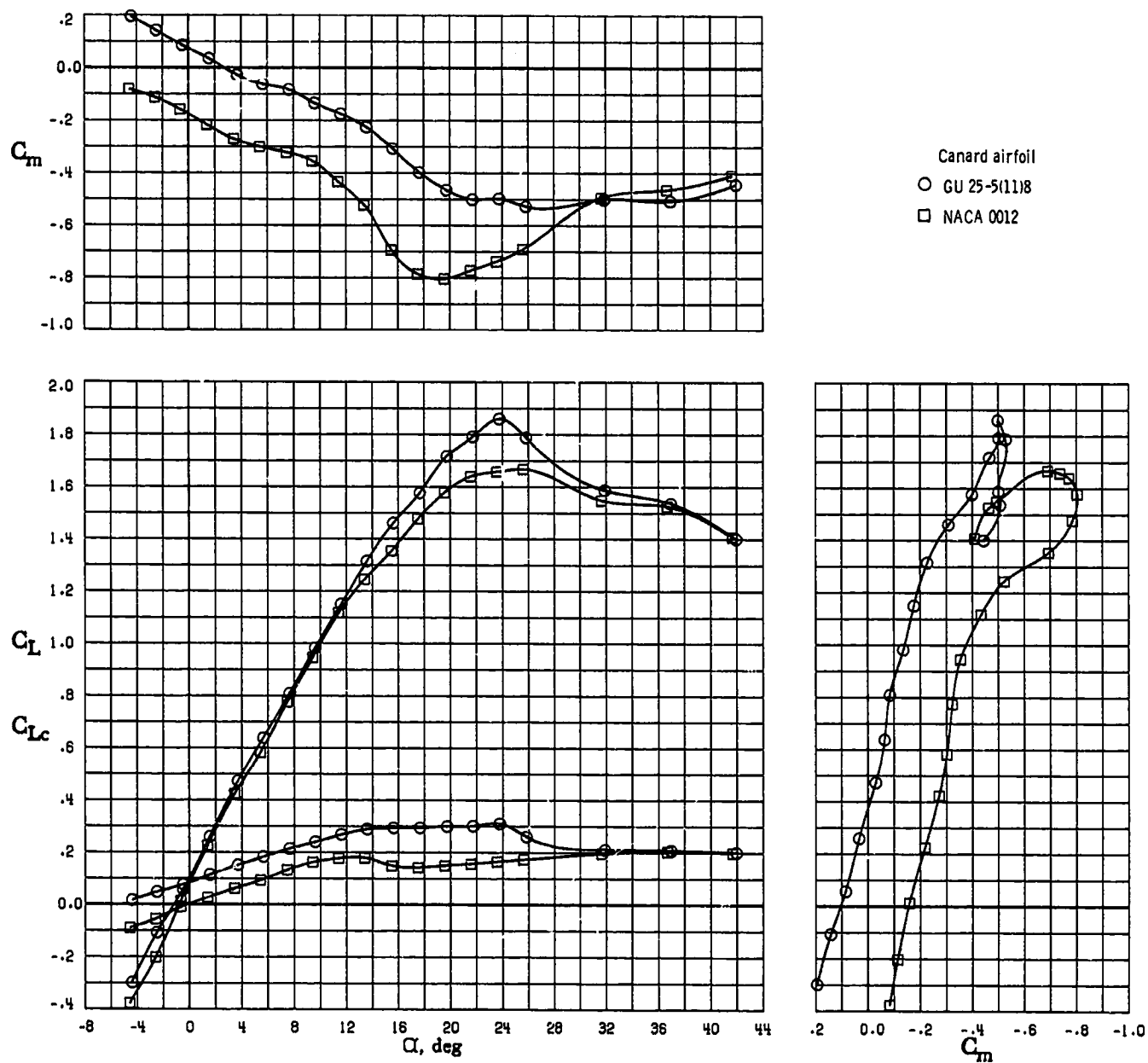
Figure 35. Effect of canard airfoil section on longitudinal aerodynamic characteristics of total airplane. $i_c = 0°$; mid c.g. location (FS 99); L.E. droop on.
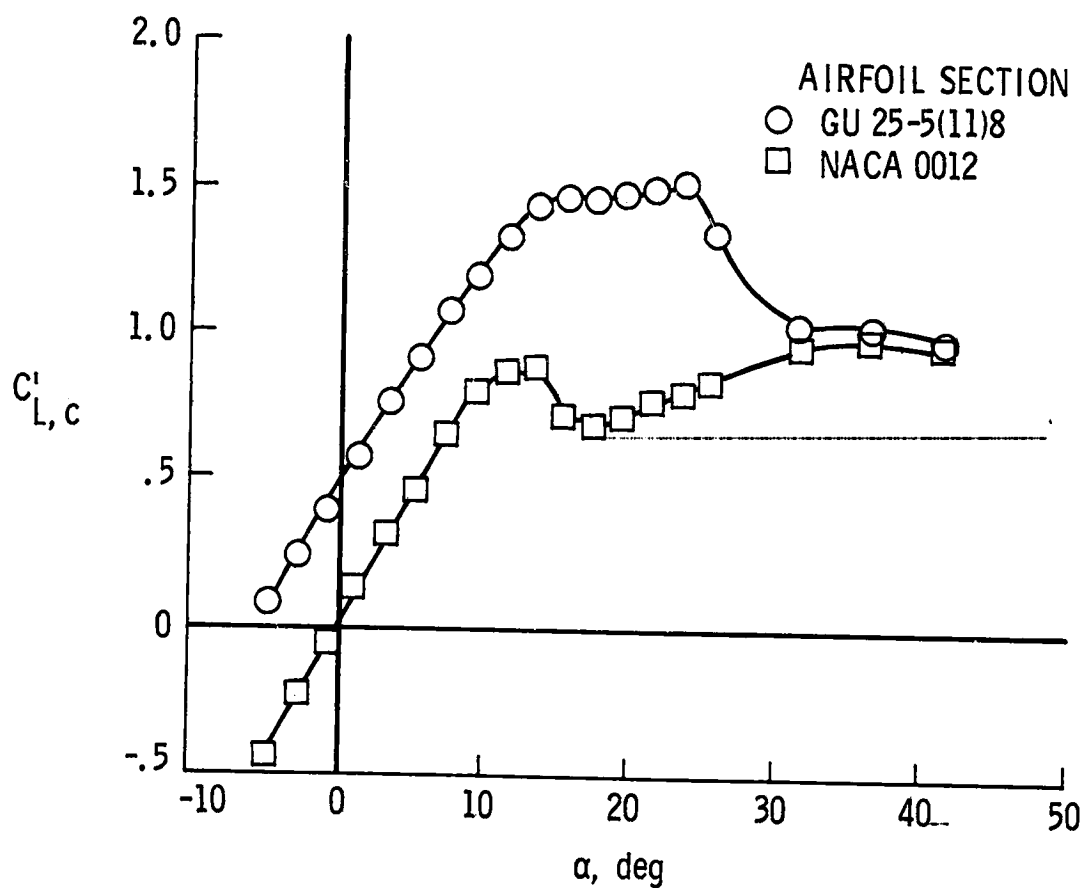
Figure 36. Comparison of lift characteristics of canard on model with GU 25-5(11)8 and NACA 0012 airfoil sections. $C'_{L,c}$ is based on canard area; $i_c = 0°$, $\delta_e = 0°$; $R = 1.60 \times 10^6$.
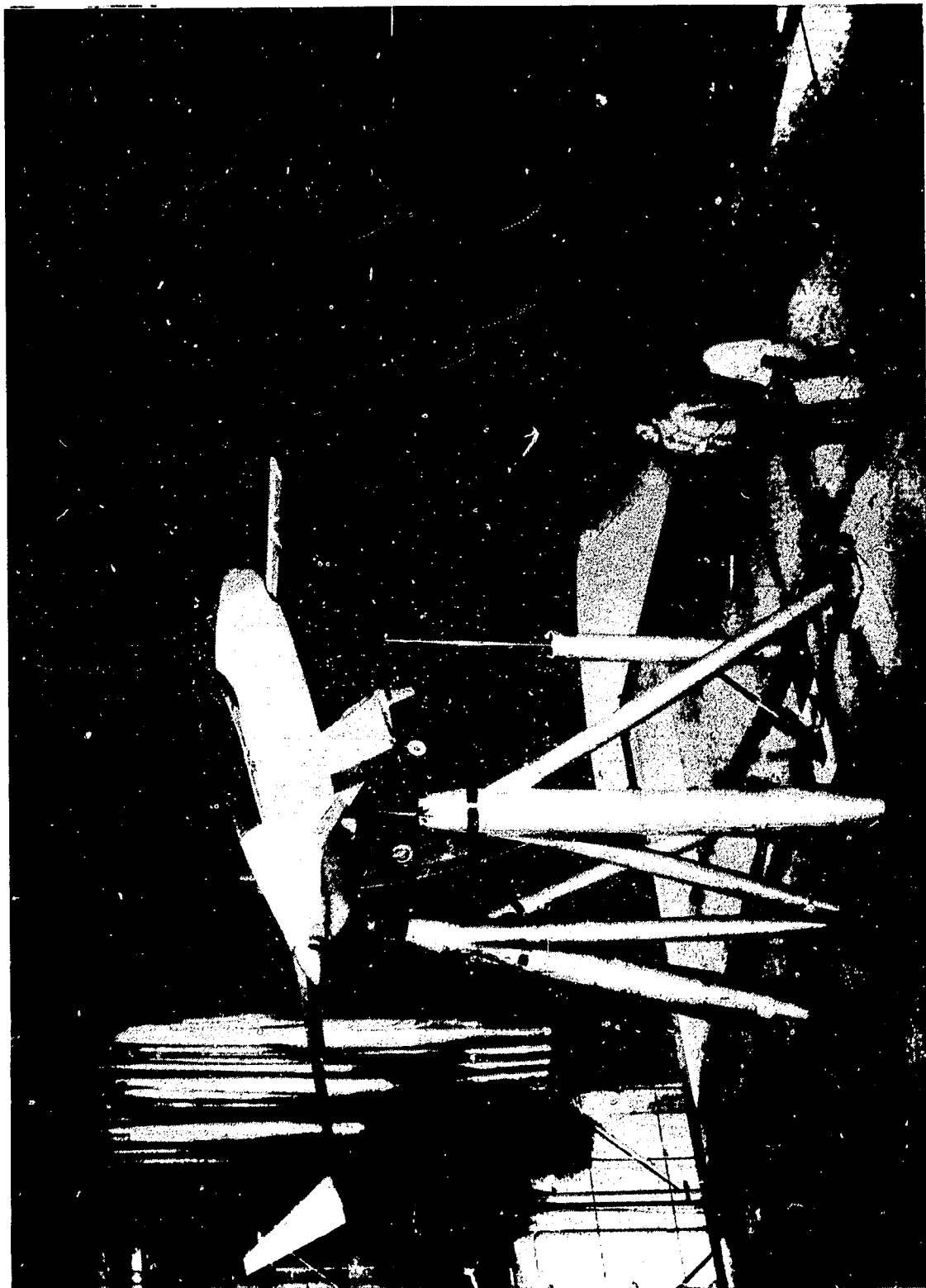
L-81-6940

Figure 37. Model with canard in low position.

L-84-10,690

(a) $\alpha = 3.5°$.

Canard vortex impingement
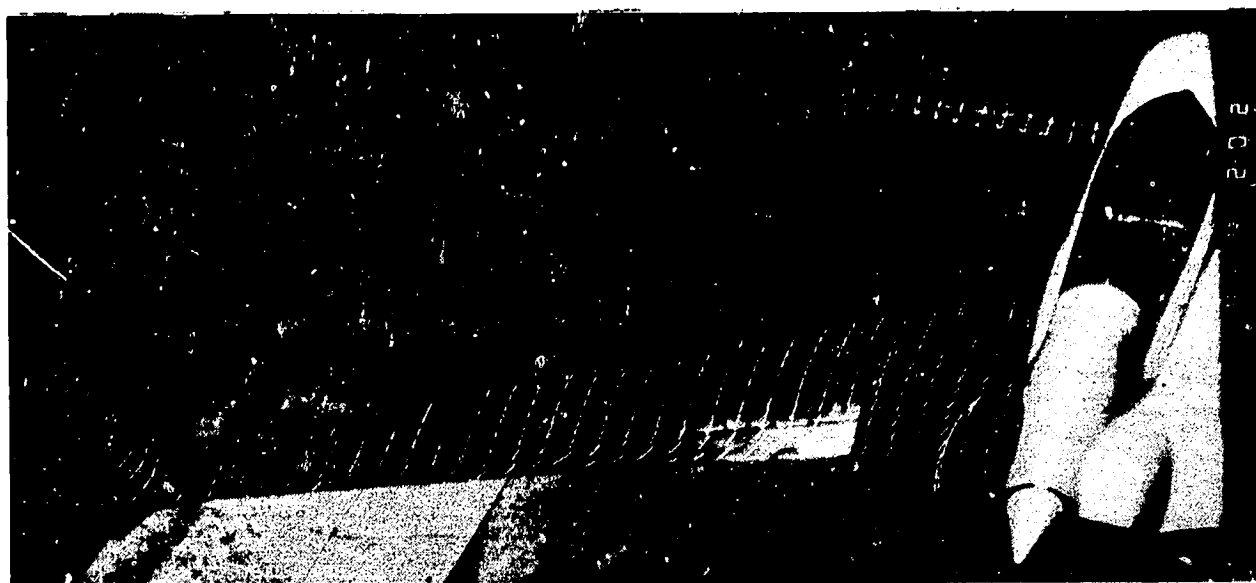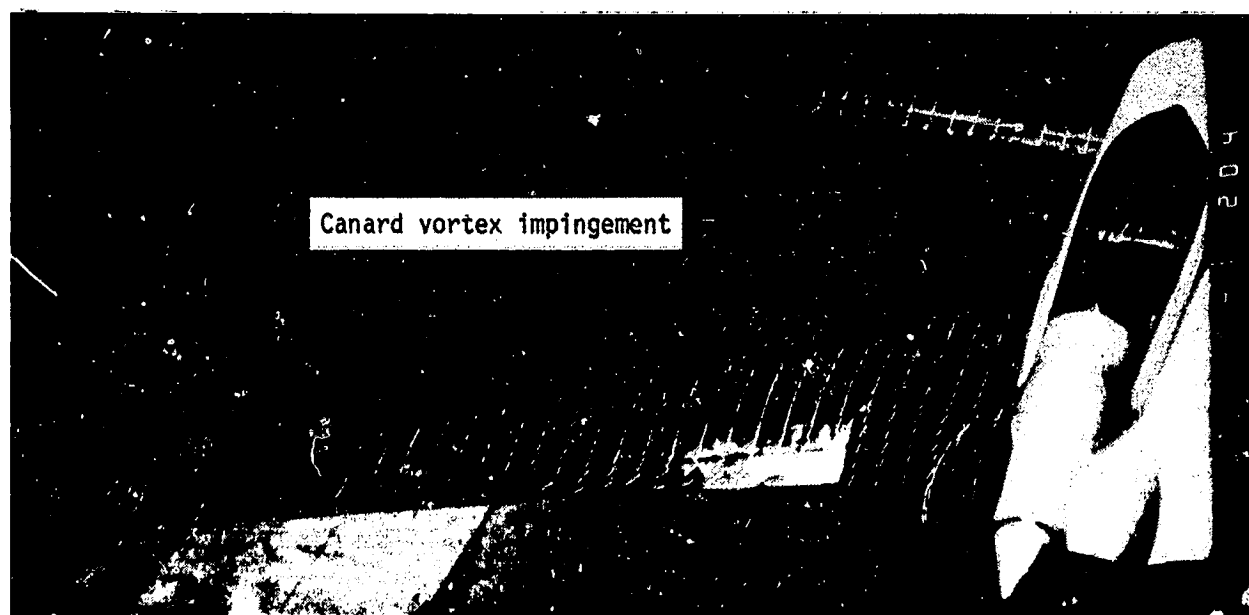
L-84-10,691

(b) $\alpha = 5.5°$.

Figure 38. Wing-surface flow patterns with canard in low position. L.E. droop on; $i_c = 0°$; $\delta_e = 0°$.

L-84-10,692

(c) $\alpha = 7.5°$.
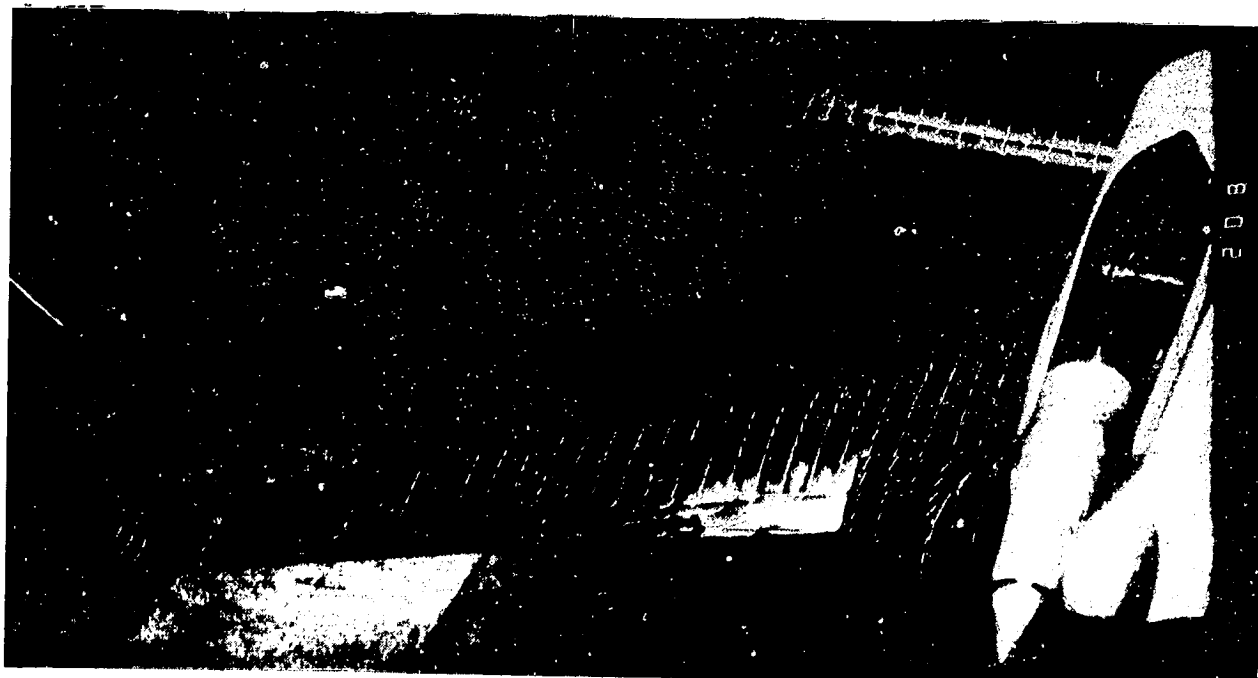
L-84-10,693

(d) $\alpha = 9.5°$.

Figure 38. Concluded.
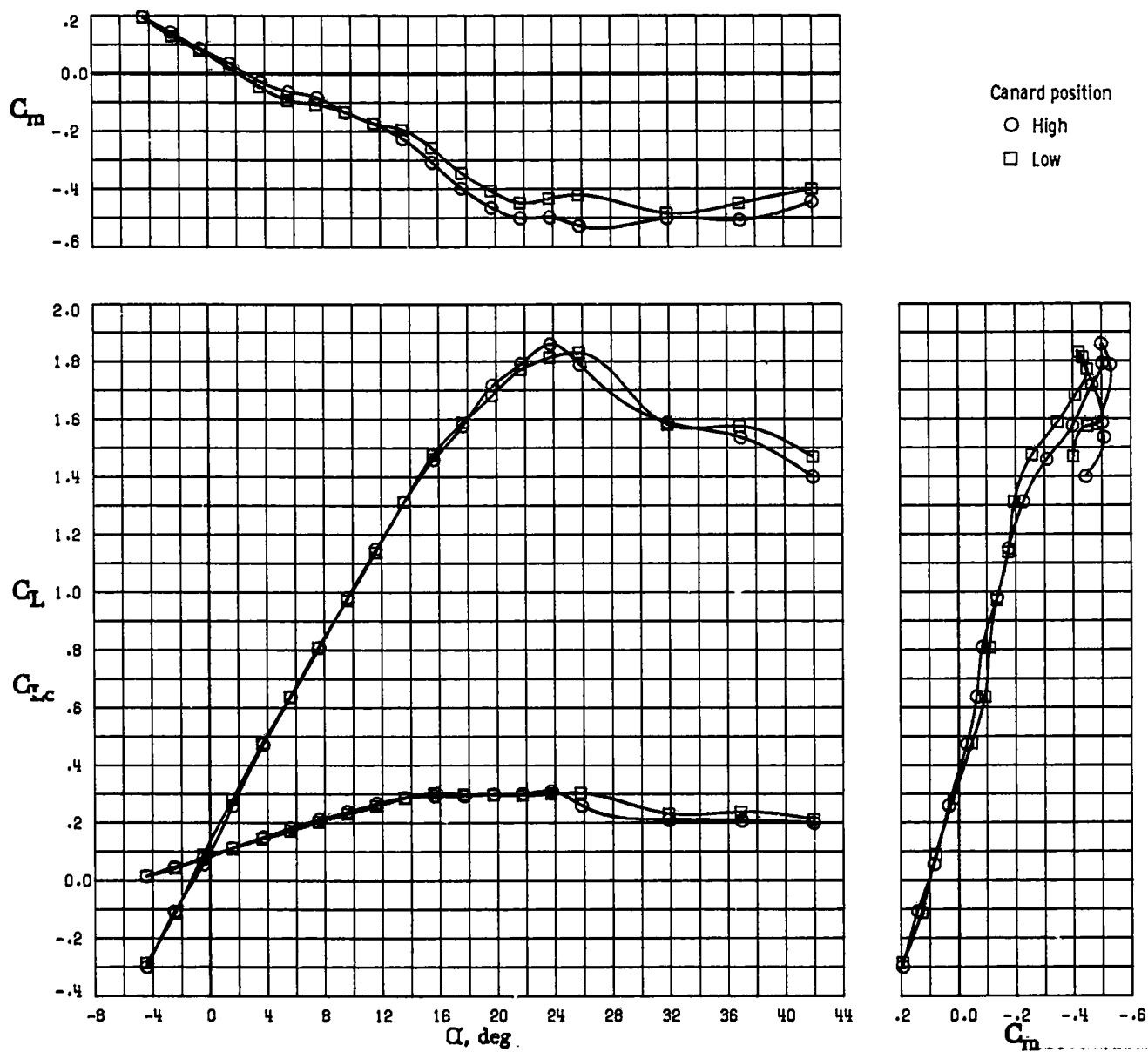
(a) Lift and pitching-moment characteristics.

Figure 39. Effect of canard position on longitudinal aerodynamic characteristics of basic configuration. L.E. droop on; mid c.g. location (FS 99).
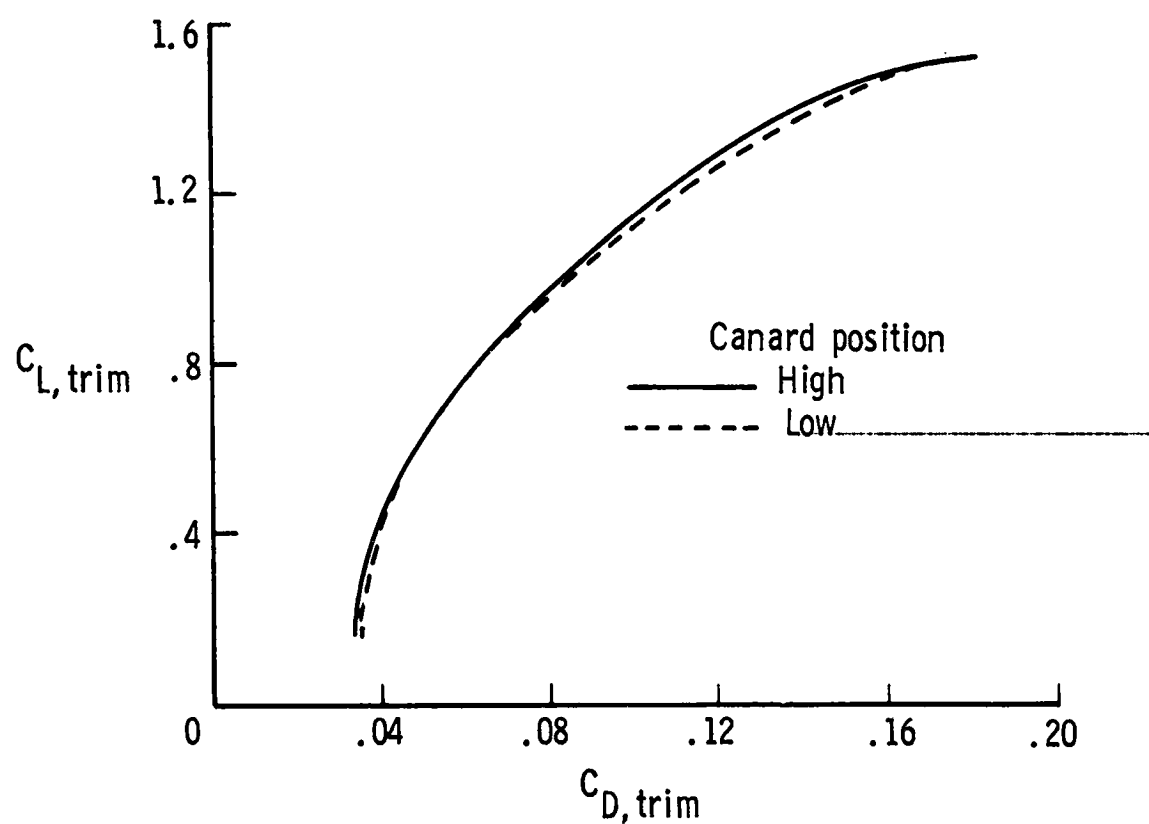
(b) Trimmed lift-drag polars.

Figure 39. Concluded.
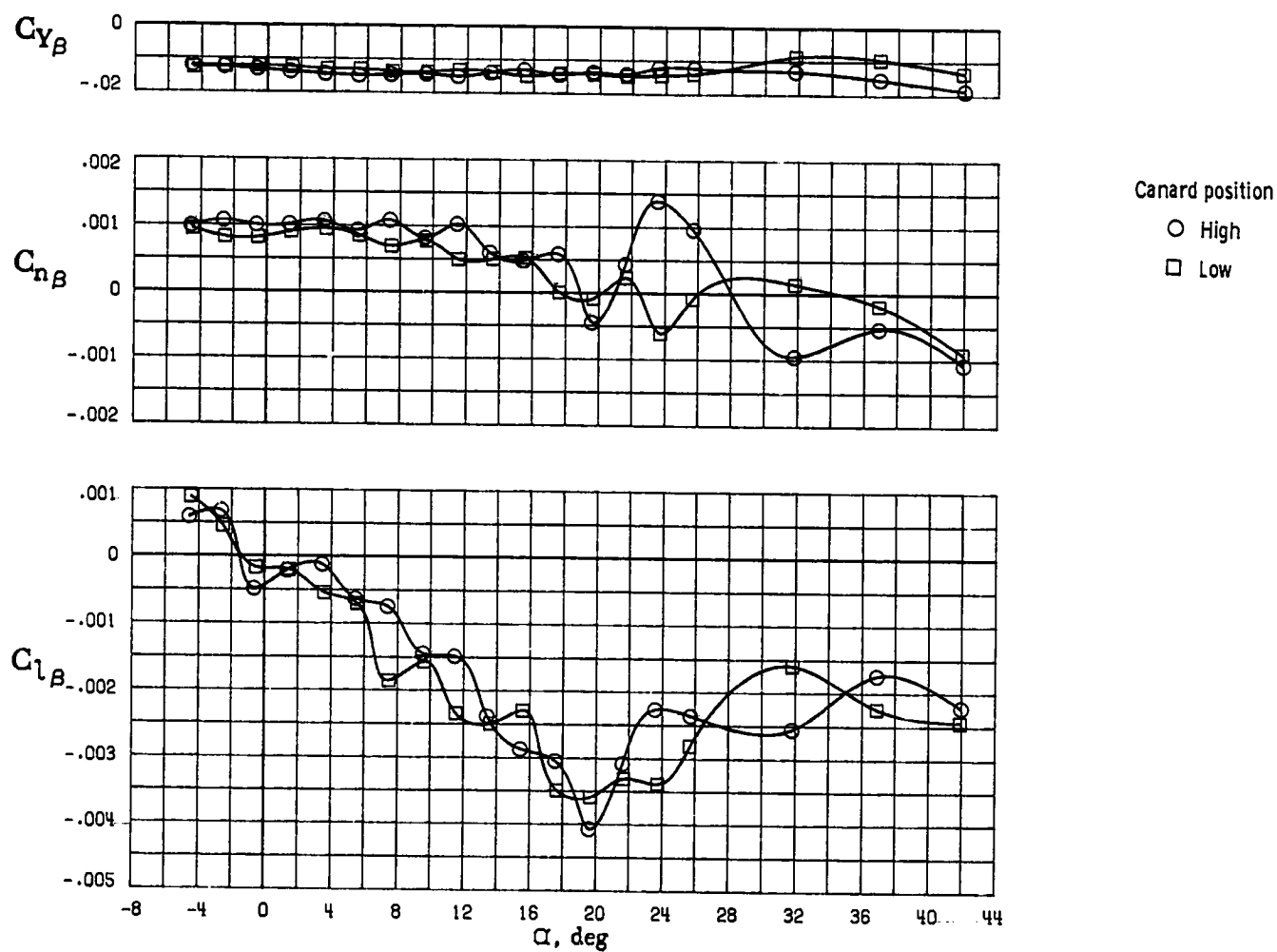
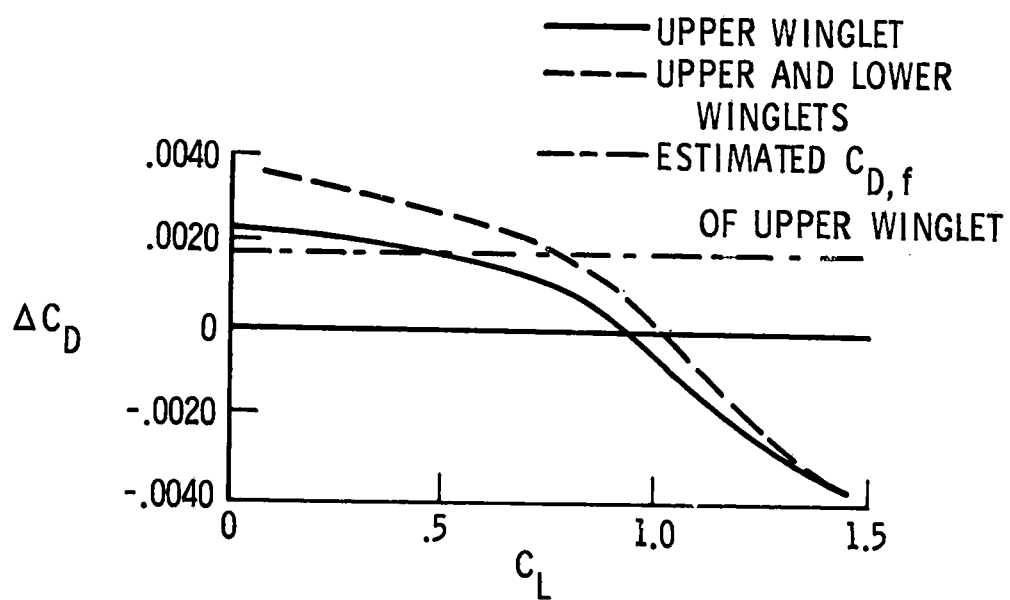Figure 40. Effect of canard position on lateral-directional stability of basic configuration. L.E. droop on.

Figure 41. Effect of winglets on drag characteristics. $\Delta C_D = (C_{D,w})_{\text{on}} - (C_{D,w})_{\text{off}}$.
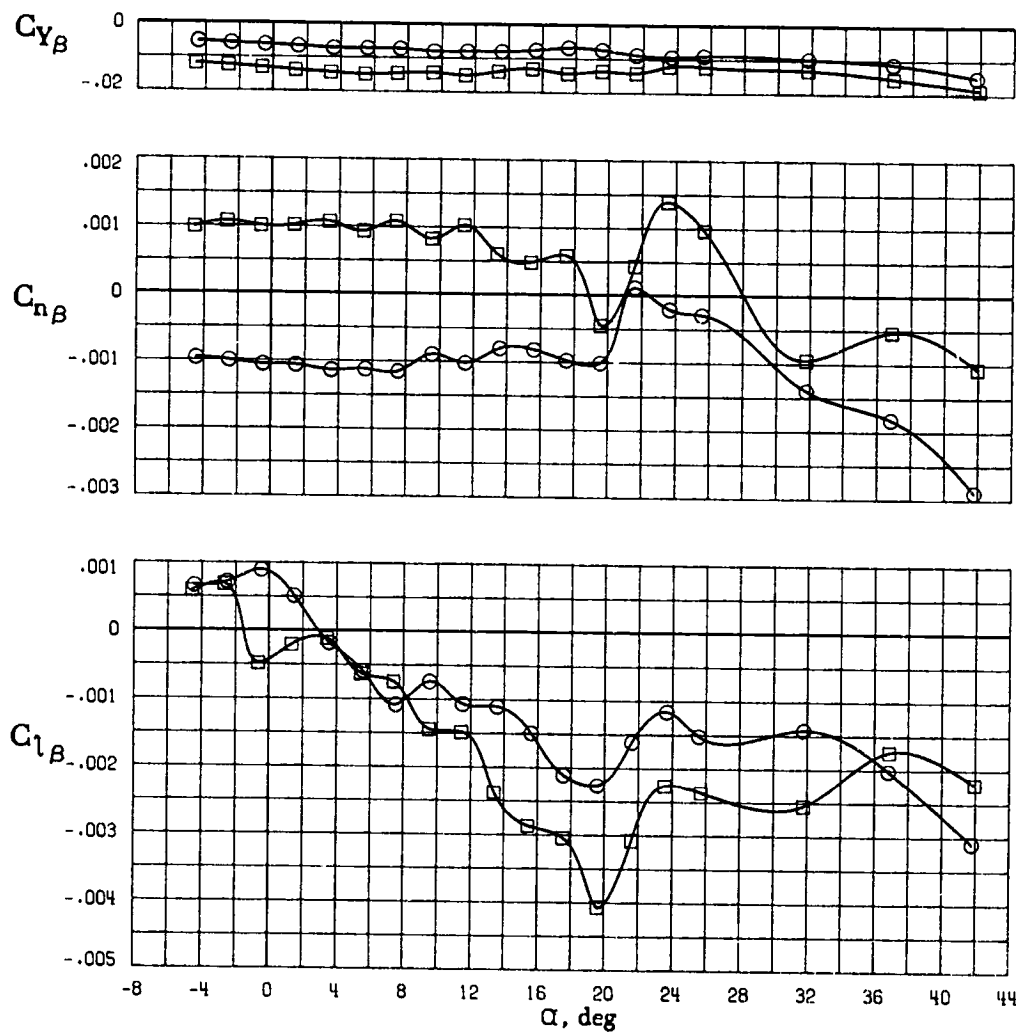
Figure 42. Effect of winglets on lateral-directional stability of basic configuration. L.E. droop on.
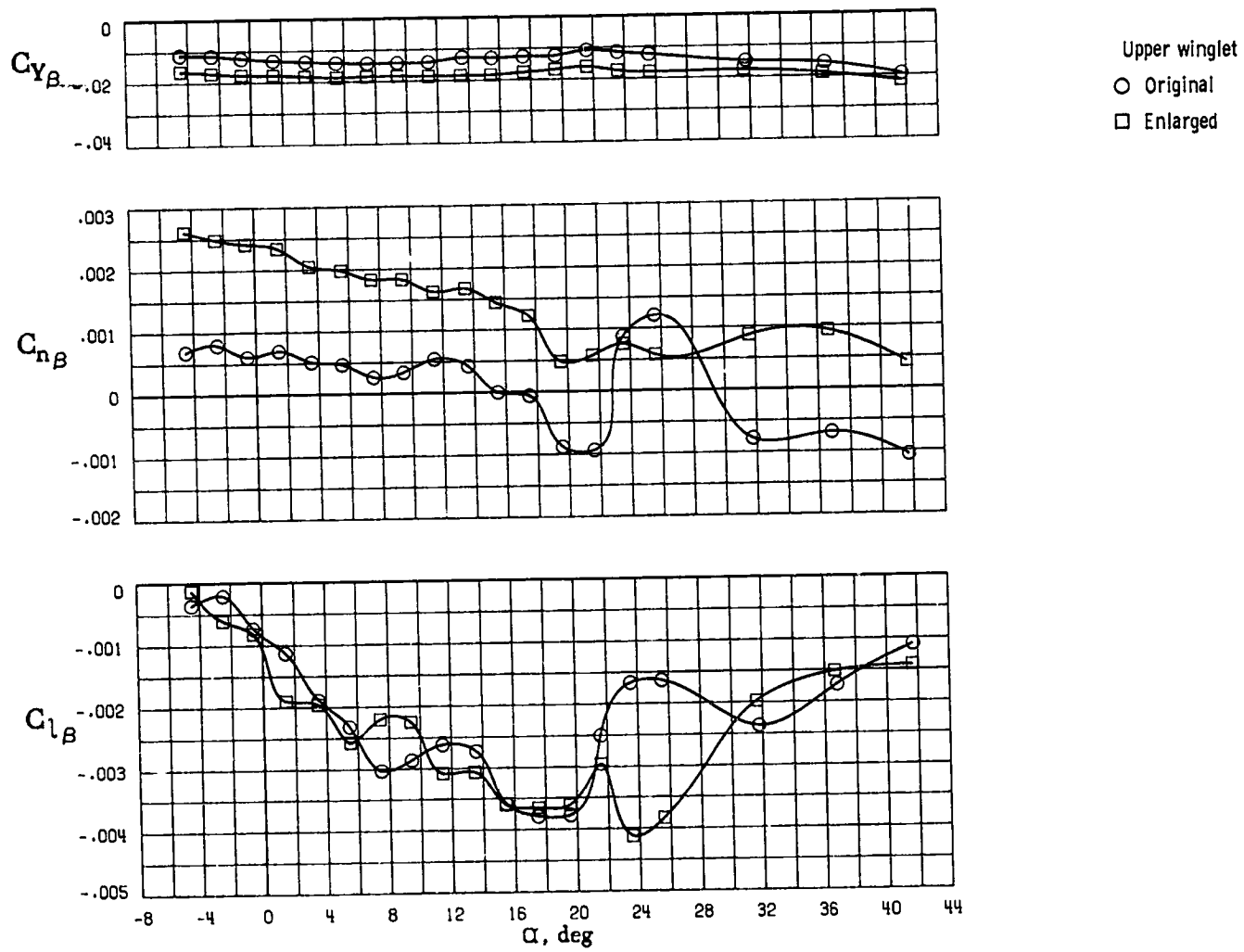
Figure 43. Effect of winglet size on lateral-directional stability of basic configuration. L.E. droop off.
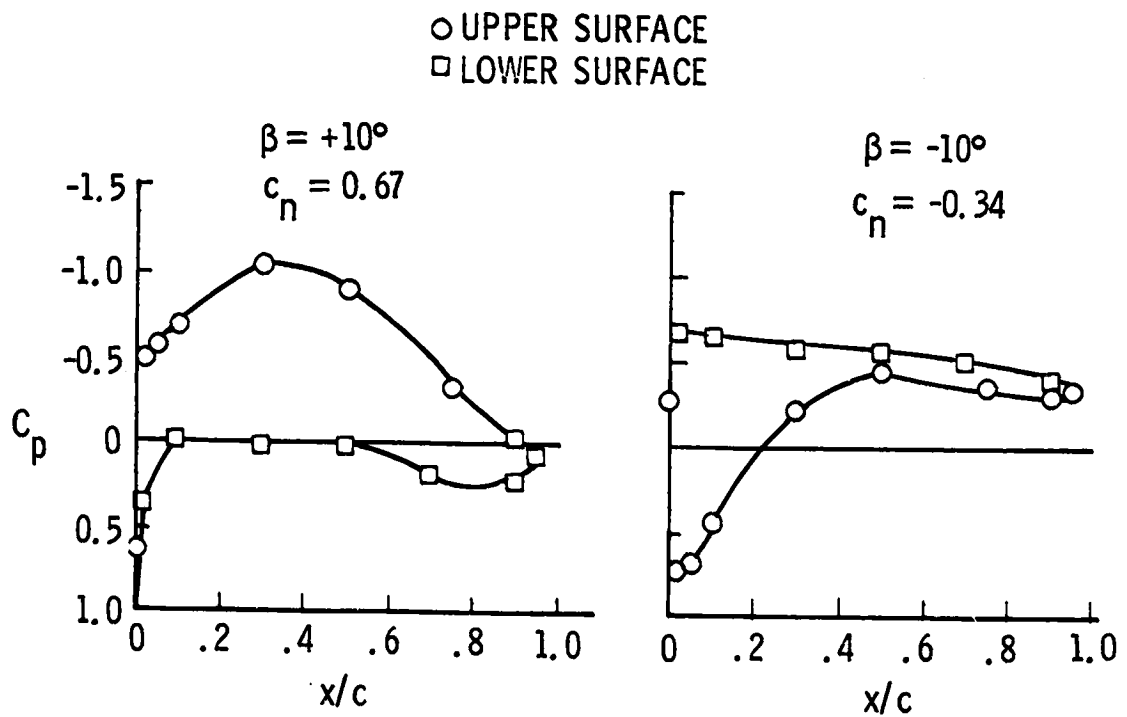
Figure 44. Effect of sideslip on chordwise pressure distribution of winglet at $y'/b_w = 0.60$. $\alpha = 1.5°$; L.E. droop on.